

DOCUMENT ROOM, DOCUMENT ROOM 36-412
RESEARCH LABORATORY OF ELECTRONICS
MASSACHUSETTS INSTITUTE OF TECHNOLOGY
CAMBRIDGE 89, MASSACHUSETTS, U.S.A.

3

THE MAGNETOHYDRODYNAMIC FLOW PAST A NONCONDUCTING
FLAT PLATE IN THE PRESENCE OF A TRANSVERSE MAGNETIC FIELD

DONALD M. DIX

Loan Copy Only

TECHNICAL REPORT 397

JULY 9, 1962

MASSACHUSETTS INSTITUTE OF TECHNOLOGY
RESEARCH LABORATORY OF ELECTRONICS
CAMBRIDGE, MASSACHUSETTS

The Research Laboratory of Electronics is an interdepartmental laboratory in which faculty members and graduate students from numerous academic departments conduct research.

The research reported in this document was made possible in part by support extended the Massachusetts Institute of Technology, Research Laboratory of Electronics, jointly by the U.S. Army (Signal Corps), the U.S. Navy (Office of Naval Research), and the U.S. Air Force (Office of Scientific Research) under Signal Corps Contract DA 36-039-sc-78108, Department of the Army Task 3-99-20-001 and Project 3-99-00-000; and in part by Signal Corps Contract DA-SIG-36-039-61-G14; additional support was furnished by the National Science Foundation under Grant G-9330.

Reproduction in whole or in part is permitted for any purpose of the United States Government.

MASSACHUSETTS INSTITUTE OF TECHNOLOGY
RESEARCH LABORATORY OF ELECTRONICS

Technical Report 397

July 9, 1962

THE MAGNETOHYDRODYNAMIC FLOW PAST A NONCONDUCTING FLAT
PLATE IN THE PRESENCE OF A TRANSVERSE MAGNETIC FIELD

Donald M. Dix

Submitted to the Department of Mechanical Engineering, M.I.T.,
August 25, 1961, in partial fulfillment of the requirements for
the degree of Doctor of Science.

(Manuscript received September 14, 1961)

Abstract

The general character of the magnetohydrodynamic flow past a nonconducting flat plate in the presence of transverse magnetic fields is analyzed in some detail. The appropriate extension of the Rayleigh problem to the magnetohydrodynamic case is shown to yield solutions that correctly predict some features of the steady flow past a semi-infinite flat plate. Also, it is shown that the knowledge of these significant features permits an easy evaluation of their magnitudes in other extensions of the Rayleigh problem. The flow past a semi-infinite flat plate is analyzed by two methods. First, by linearizing the governing equations and incorporating the assumption of a low ratio of viscous-to-magnetic diffusivity, the results for skin friction and the normal component of magnetic field at the plate are obtained, and are shown to be useful in interpreting the character of these low conductivity flows. Second, the complete set of governing equations is formulated as a finite difference problem and solved numerically on a digital computer. The results obtained show that the disturbance produced by the plate is no longer confined to a thin viscous layer if the ratio of viscous-to-magnetic diffusivity is greater than 10^{-2} ; but that an appreciable Alfvén type of disturbance is excited.

TABLE OF CONTENTS

| | |
|--|-----|
| Glossary | iv |
| I. INTRODUCTION | 1 |
| 1.1 Background of this Research | 1 |
| 1.2 Statement of the Problem | 5 |
| 1.3 General Summary | 6 |
| II. THE RAYLEIGH PROBLEM | 8 |
| 2.1 Formulation of the Problem | 8 |
| 2.2 Solutions and Discussion | 10 |
| 2.3 The Ultimate State | 16 |
| 2.4 Relation of the Rayleigh Problem to the Steady Flow Past a Semi-infinite Flat Plate | 19 |
| III. THE LINEARIZED PROBLEM | 23 |
| 3.1 Formulation of the General Problem | 23 |
| 3.2 Formulation of the Linearized Problem | 25 |
| 3.3 Solution of the Linearized Equations | 26 |
| 3.4 Discussion of Linearized Solution | 33 |
| IV. NUMERICAL SOLUTION OF COMPLETE PROBLEM | 37 |
| 4.1 Formulation of Numerical Problem | 37 |
| 4.2 Solution Technique | 56 |
| 4.3 Results | 59 |
| V. DISCUSSION OF RESULTS | 108 |
| 5.1 Discussion and Summary | 108 |
| 5.2 Conclusions and Recommendations | 119 |
| Appendix I Inversion of the Fourier Transform of Eq. 78 | 121 |
| Appendix II Perturbation Solution of Eq. 43 | 123 |
| Acknowledgement | 126 |
| References | 127 |

GLOSSARY

| <u>Symbol</u> | <u>Definition</u> |
|---|---|
| A | Magnetic vector potential |
| a | Alfvén-wave speed, $a = B/\sqrt{\mu_0 \rho}$ |
| B | Magnetic field intensity |
| c, d | Ratio of adjacent finite difference net spacings, x and y directions, defined in Fig. 12 |
| $\left. \begin{array}{l} C1Q, C2Q \\ C3Q, C4Q \\ C5Q, FFQ \end{array} \right\}$ | Coefficients in finite difference problem formulation; Q may be replaced by A, ψ , or ξ ; defined by (107) with (102), (103), (104), (105), and (106). |
| D | Larger of the two diffusivities ν or $1/\mu_0 \sigma$ |
| E | Electric field intensity |
| F | Coefficients in finite difference approximations to derivatives; defined by Eq. 99. |
| h | Half-channel width; or finite difference net spacing |
| i, j | Finite difference net point indices |
| J | Current density |
| K | Fraction of free stream velocity to be used as average velocity in linearized solution |
| L | Characteristic length; usually taken as $L = \nu/U_\infty$ |
| ℓ | Length from leading edge of plate to downstream boundary in numerical problem |
| NXL | Column coordinate of leading edge in numerical problem |
| p | Pressure |
| R | Reynolds number, $R = U_\infty L/\nu$ |
| Rm | Magnetic Reynolds number, $Rm = \sigma \mu_0 U_\infty L$ |
| t | Time |
| TOLQ | Convergence tolerance |
| V | Velocity vector |
| U | Reference velocity |
| u, v, w | Cartesian velocity components |
| x, y, z | Cartesian coordinates |

GLOSSARY

| <u>Symbol</u> | <u>Definition</u> |
|---------------|---|
| Δy | Width of Alfvén line |
| a | Dimensionless Alfvén speed = $B/\sqrt{\mu_0 \rho} U_\infty$ |
| δ | Boundary-layer thickness |
| ϵ | Ratio of viscous-to-magnetic diffusivity, $\epsilon = \sigma \mu_0 \nu$ |
| η | Viscosity |
| θ | Slope of Alfvén line |
| μ, μ_0 | Magnetic permeability |
| ν | Kinematic viscosity, $\nu = \mu/\rho$ |
| ξ | Vorticity |
| ρ | Fluid density |
| σ | Electrical conductivity |
| ψ | Stream function |

| <u>Subscripts</u> | <u>Reference</u> |
|-------------------|--|
| a | Conditions between Alfvén wave and plate or at Alfvén wave in Rayleigh problem |
| b | Boundary values in numerical problem (see Section IV) |
| g | Characteristic growth length of viscous layer |
| H | Viscous layer |
| p | Values at plate in Rayleigh problem |
| u | Values at upstream boundary in numerical problem |
| x, y, z | Cartesian vector components, or differentiation with respect to coordinate |
| ∞ | Free-stream conditions in semi-infinite plate problem (Sections III and IV) |
| 0 | Quiescent conditions in Rayleigh problem |
| 1 | Conditions upstream of Alfvén line |
| 2 | Conditions downstream of Alfvén line |
| \oplus | Function analytic in upper half-plane |
| \ominus | Function analytic in lower half-plane |

GLOSSARY

Notes:

1. Asterisk denotes dimensional quantity.
2. Bar and circumflex over symbol denotes Laplace or Fourier transforms of variable.
3. Primes denote perturbation from a specified value.
4. Bar placed below a letter denotes a vector quantity.
5. Numerical subscripts may also refer to net spacings, as defined in Figs. 12 and 13.

I. INTRODUCTION

1.1 BACKGROUND OF THIS RESEARCH

a. Practical Applications

The flow past obstacles and the flow adjacent to system boundaries are of fundamental importance in several magnetohydrodynamic devices that are in operation at the present time, or scheduled for development in the immediate future. The flow problems arising in these devices can be classified as either internal or external.

The primary interest in internal flows, at present, is related to magnetohydrodynamic accelerators, generators, shock tubes, and electromagnetic pumps or flowmeters. In accelerators, generators, pumps, and flowmeters, the flow at the wall is of interest to predict the friction and heat transfer (for accelerators and generators only) of the device. It is of further interest to determine the effect of the flow at walls on the main stream flow (current distribution, for example) with a view toward increasing the performance of such a device. In shock tubes, either electromagnetically driven or pressure-driven with an auxiliary magnetic field applied over the test region, the flow at the boundaries may be of importance in its effect on both the shock-propagation mechanism and conditions of the test gas behind the shock.

At present, there are two areas of interest in external flows. One area is that of employing electromagnetic means to control skin friction, heat transfer, or possibly the basic flow in high-speed flows of ionized gases. The second area involves flows about obstacles placed in experimental devices for diagnostic purposes. An example of such a device is a search coil placed in a moving stream of conducting fluid passing through a magnetic field in an attempt to detect magnetic-field changes caused by the flow.

There will undoubtedly be more practical interest in these flows as the field is developed further, but the few examples cited serve to illustrate a more than academic need for investigation of these flows.

b. Survey of Published Works

Previous investigations relevant to the flow at system boundaries or past obstacles can be classified in three main areas: (a) extensions of the Rayleigh problem to the magnetohydrodynamic case; (b) boundary-layer flows; and (c) flow about obstacles, including stagnation-point flow. Work by previous investigators will now be discussed briefly.

The Rayleigh Problem

In the fluid-mechanic sense, the classical Rayleigh problem is one in which an infinite plate is started impulsively from rest in a viscous medium. The usefulness of such a problem is that it exhibits qualitative boundary-layer characteristics and in this

respect yields insight into the behavior of the steady two-dimensional flow past a semi-infinite flat plate. Specifically, if one compares time in the Rayleigh problem to a velocity/length ratio in the latter problem, there is a distinct analogy. The primary advantage in studying this problem is that it is simple; the convective inertial terms vanish identically from the equations of motion and, as a consequence, the relevant forms of these equations are linear.

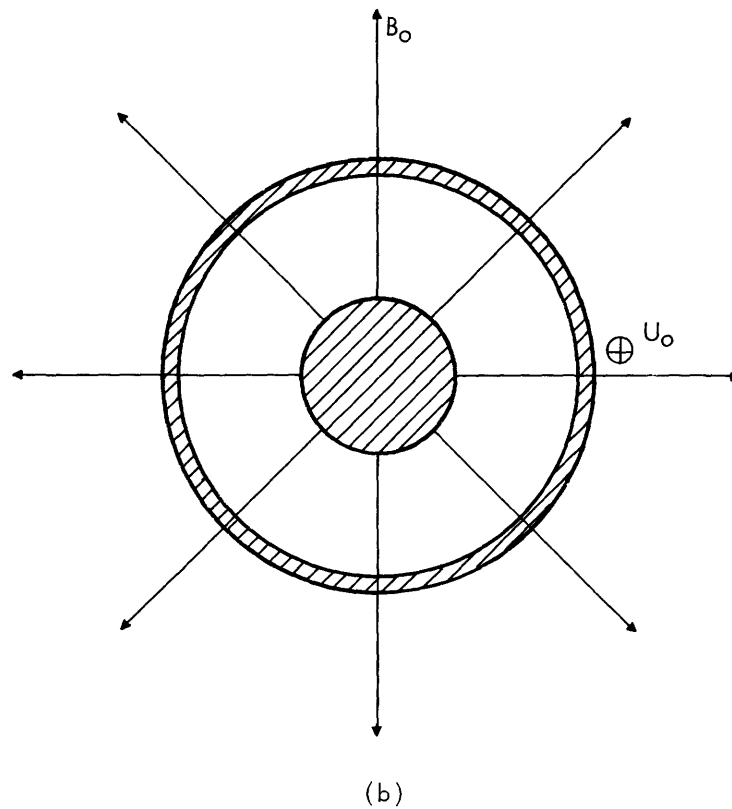
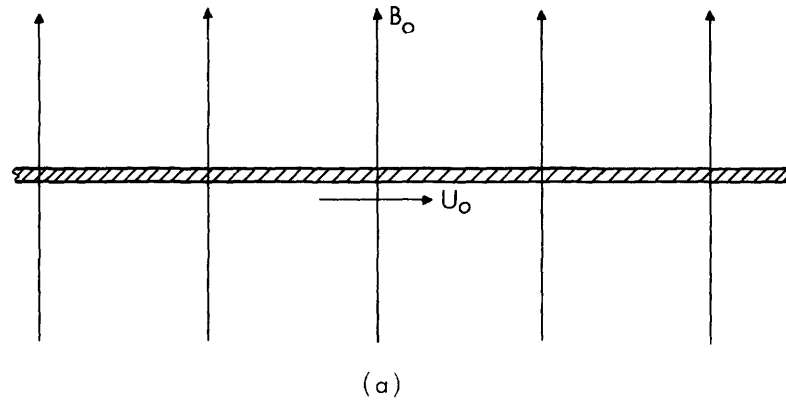


Fig. 1. (a) Plane Rayleigh problem.
(b) Annular Rayleigh problem.

There are obviously many magnetohydrodynamic extensions of this problem. With the introduction of electromagnetic effects, considerable latitude exists in the choice of electromagnetic properties of the plate, orientation of the applied magnetic field, form of the electromagnetic boundary conditions, and excitation methods. As it happens, the governing equations of the various extensions of fundamental interest in the incompressible problem retain the linearity of the classical problem.

Four authors have attacked different extensions of this problem. Rossow^{19, 21} attacked the problem of a nonconducting plate started impulsively from rest with velocity U_0 in a viscous, electrically conducting, incompressible medium with an applied magnetic field B_0 perpendicular to the plate (see Fig. 1a). He distinguished between two cases: "field fixed relative to fluid" which is for $E = 0$ far from the plate, and "field fixed relative to plate" which refers to application of an electric field $E = -U_0 B_0$ at time $t = 0$. The latter case is physically unrealistic and in his formulation of the former case, the boundary conditions employed are generally unrealistic. Because of these deficiencies, the only solution that is of significant physical interest is that for $E = 0$, where the electrical conductivity is sufficiently small so that the induced magnetic field is negligible. This solution yields a nontrivial steady-state solution (contrary to the ordinary Rayleigh problem) in which the magnetic forces balance the viscous forces, and suggests that in the analogy to steady flow past a semi-infinite plate, the boundary-layer thickness will approach a finite thickness.

Carrier and Greenspan⁴ presented an elaborate discussion of the corresponding annular problem (see Fig. 1b), correctly pointing out that the impulsive motion will generate an Alfvén wave whose strength depends upon the properties of the fluid. However, they are somewhat inaccurate in their interpretation of the plane problem, and, as a consequence, their discussion of the essential features of the flow is incomplete.

Chang and Yen⁵ and Ludford¹⁴ attacked the problem of the infinite conducting plate. Their results indicate that in this case the viscous layer is eventually diffused completely, and therefore indicates that in the two-dimensional steady flow past a semi-infinite plate, the boundary layer will grow indefinitely.

It should be emphasized that in all of these papers the physical interpretation of the results obtained is incomplete, and no specific relation to the two-dimensional flow past a flat plate is attempted.

Boundary-Layer Flows

Rossow¹⁹ has investigated the incompressible boundary-layer type of flow over a semi-infinite, nonconducting flat plate in the presence of an applied magnetic field perpendicular to the plate (see Fig. 2). He considers his two cases of "field fixed with respect to fluid" which in the frame of reference of Fig. 2 implies the presence of an applied electric field of $E = -U_\infty B_\infty$, and "field fixed with respect to plate," implying $E = 0$. In both cases he assumes that the magnetic Reynold's number is sufficiently small so that distortion of the applied magnetic field is negligible. By applying the

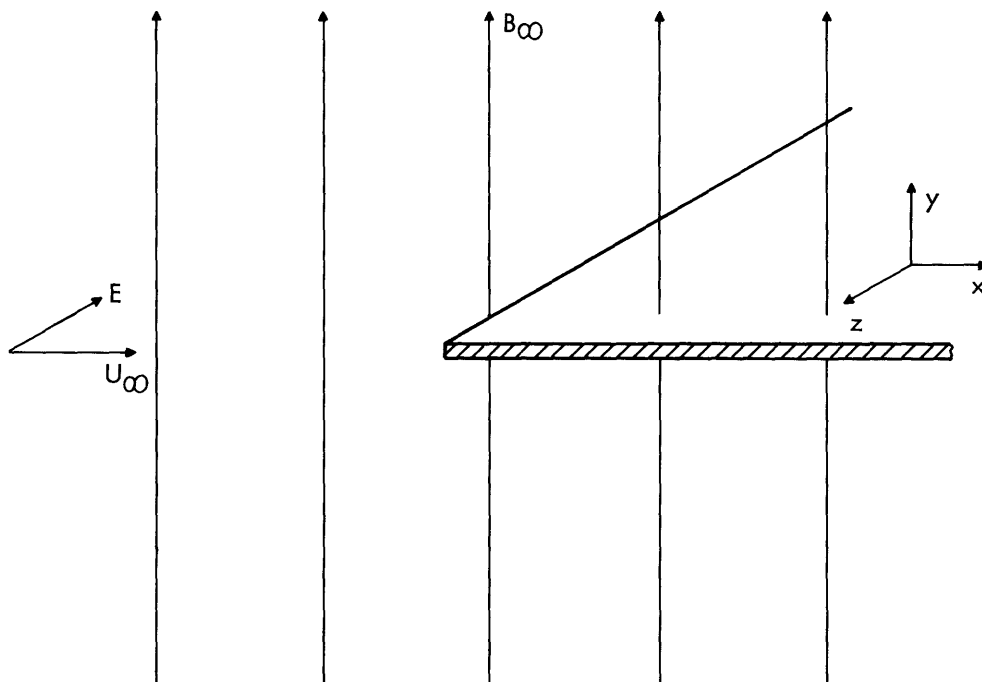


Fig. 2. Steady two-dimensional flow past a flat plate.

usual boundary-layer assumptions, and expanding in a perturbation series in terms of an interaction parameter (indicative of the ratio of magnetic forces to viscous forces) he obtained the first three terms in perturbation series solutions to both cases. The solutions obtained are unsatisfactory in that the convergence of the series is not ensured, the solutions are confined to a relatively small region downstream of the leading edge, and the qualitative behavior of the boundary layer is not portrayed.

Lykoudis¹⁵ and Bush¹ have examined the compressible problem analogous to the $E = 0$ case of Rossow. In addition to making the assumptions of Rossow, they further assumed that the applied magnetic field is proportional to the inverse square root of the distance from the leading edge. Under these assumptions, similarity solutions are obtainable; Lykoudis obtains results for the constant-property case, while Bush obtains results for variable properties. In addition, Lykoudis obtains solutions for flows about wedges and stagnation-point flows.

Carrier and Greenspan^{4, 8} and Greenspan⁹ have examined in great detail the flow past a semi-infinite flat plate with an applied magnetic field parallel to the direction of flow. They treat both the boundary-layer formulation and a linearized formulation analogous to Oseen flow in fluid mechanics. Their essential result is that an upstream wake is formed by means of the Alfvén-wave mechanism, and, in fact, that for flow velocities less than the Alfvén velocity, steady flow cannot exist. It is mentioned that their method of solution employs the Wiener-Hopf technique, which will be used in this report. Lewellen¹² treated similar flows by assuming the presence of an inviscid magnetic boundary layer. Using integral methods, he reached essentially the same conclusion.

Flows about Obstacles

Chester⁶ has treated the Stokes flow past a sphere with an applied magnetic field parallel to the flow, neglecting distortion of the magnetic field. Numerous other authors have considered extensions of this flow to applied fields perpendicular to the flow, incorporating Chester's basic assumptions. Neuringer and McIlroy¹⁶ have treated the incompressible stagnation-point flow at a flat plate with an applied field perpendicular to the plate. Kemp¹¹ considers the hypersonic stagnation-point flow about a blunt body with an applied field perpendicular to the body surface, and neglects magnetic-field distortion. Sears and Resler²³ have considered the linearized, nonviscous flow of highly conduction fluids over slender bodies in the presence of transverse fields, thereby incorporating the assumption (of dubious validity) that the disturbances so produced will be small. They obtain the result that the Alfvén wave mechanism causes the disturbance to propagate into the free stream for greater distances than the no field case. Resler and McCune¹⁸ have considered the general problem of flows about obstacles in the compressible case, again assuming linearization to be valid.

We wish to point out that in all previous theoretical work in the area of flows about obstacles in the presence of transverse magnetic fields, all solutions have been some form of a limiting case, and in a majority of cases, incorporate the assumption of a very small magnetic Reynolds number. In consonance with this last assumption, which essentially eliminates the coupling between Maxwell's equations and the equations of fluid mechanics and thereby reduces the problem to a pure fluid-mechanic one with an additional body force, previous authors have employed the familiar concepts developed in fluid mechanics. Finally, note that as a result of the small magnetic Reynolds number assumption, very little study has been devoted to effects of the flow on the magnetic field.

1.2 STATEMENT OF THE PROBLEM

a. Objectives

The broad objective of this report is to investigate in a theoretical manner the significant features of magnetohydrodynamic flow about obstacles in the presence of transverse magnetic fields. This investigation will include both major effects: the effect of the magnetic field on the flow field and the converse.

The specific problem considered is the flow about a nonconducting flat plate with an applied magnetic field perpendicular to the plate. In the fluid-mechanic sense, a study of this problem, in addition to yielding qualitatively useful results, confirms the presence of the boundary layer to which the viscous effects are confined, and indicates also that the effect of this layer on the nonviscous free-stream flow is very small. These two facts represent the significant features of fluid flow past obstacles. It is believed that a study of the analogous magnetohydrodynamic problem will yield similar results; that is, both qualitatively useful results and the significant features of flows of this

general type (although it is not to be expected that the conclusions from both studies will be identical).

b. Assumptions

The primary assumptions employed throughout this work are those usually applied in magnetohydrodynamics:

(i) The fluid is treated as an incompressible, macroscopically neutral continuum, and is assumed to possess constant viscosity and electrical conductivity.

(ii) The conventional form of Ohm's Law is assumed to be applicable.

(iii) The characteristic velocities of the problem are assumed to be much less than the speed of light, thereby making displacement and convection currents negligible.

(iv) The permeability and permittivity of both fluid and plate are assumed to be that of free space.

These assumptions permit the use of the Navier-Stokes equations for the description of fluid processes. For conducting liquids, such as liquid metals, these four assumptions are quite valid. For extensions to ionized gases, however, they are subject to considerable error. The effects of compressibility and of variable transport properties can be expected to be of the same magnitude of importance as in the fluid-mechanic case. These effects should not affect the qualitative characteristics of the results. For an ionized gas to be treated as a macroscopically neutral continuum, it is essential that the mean-free path be much smaller than the characteristic dimension of the problem and the electron-cyclotron radius, and much larger than the Debye length. Finally, the conventional form of Ohm's Law is valid only for gases in which the mean-free time between collisions is much less than the electron-cyclotron frequency.

The following brief summary of the contents of this report will serve to amplify the statement of the problem and to demonstrate the method of attack employed.

1.3 GENERAL SUMMARY

Section II contains an analysis of the Rayleigh problem for the nonconducting plate. The emphasis here is placed upon three factors. The first factor is the formulation of the problem, particularly the nature and number of the boundary conditions, as there appears to be some confusion in the literature of this subject.²¹ The second factor is a discussion and physical explanation of the salient features of the resulting flow. Finally, the relation of this problem to the steady two-dimensional flow past a semi-infinite plate is discussed, with a view toward gaining insight to this problem.

Section III contains a linearized analysis of the steady two-dimensional flow past a semi-infinite flat plate. This includes, as a necessary prerequisite, the formulation of the general problem and a discussion of the assumptions involved in the linearization process. Solutions are presented for the skin friction at the plate and the transverse component of magnetic field at the plate. These results are compared with the results of the Rayleigh problem.

Section IV contains the numerical analysis of the general problem. The numerical problem corresponding to the full set of equations is formulated for solution on an IBM 709 digital computer. The technique of solution is discussed, as well as several effects that bear on the accuracy of the solution.

In Section V, the significant features of the numerical results are discussed, and compared with the previous results obtained for the Rayleigh problem and the linearized problem. Also included is a summary of the major conclusions of this work and recommendations for possible extensions and verifications.

II. THE RAYLEIGH PROBLEM

2.1 FORMULATION OF THE PROBLEM

The basic problem considered here is the motion caused by the impulsive start, in a direction parallel to itself (the x-axis), of an infinite flat plate (the $y = 0$ plane) immersed in an infinite extent of an incompressible, viscous, electrically conducting fluid initially at rest, with a magnetic field applied over space perpendicular to the plate (see Fig. 1a). As mentioned previously, the problem is of interest because it yields insight into the general character of the flow to be expected in many practical applications.

Before proceeding to the formulation of the problem, a qualitative physical picture is beneficial. Initially, after the plate is set in motion, the motion of the fluid induces a current in the positive z-direction. The Lorentz force is then acting to retard the fluid. However, the current tends to produce a longitudinal component of the magnetic field, which in turn produces an electric field that opposes the initial current. This induction is then responsible for an Alfvén wave, which propagates and diffuses from the plate.

The governing equations may be simplified by noting that since the plate is infinite in extent, no variable depends on either x or z. (To be precise, p^* may in general depend upon x; however, if the initial state is current-free, p^* will be a function of y only.) Then, from continuity, $v^* = 0$. From the divergenceless property of \underline{B}^* we obtain $B_y^* = B_o$, where B_o is the applied magnetic field. From $\nabla \cdot \underline{J}^* = 0$, we have $J_y^* = 0$. The values of E_x^* , E_y^* , w^* , J_x^* , and B_z^* can be determined by investigating the initiating mechanism of the problem. As the plate is moved, a current J_z^* is induced. This current results in an induced B_x^* , and consequently the induced E_z^* . Since no further coupling of the equations exists, it is evident that the values of E_x^* , w^* , and J_x^* and B_z^* are no different from their initial values of zero. The variables in the problem are therefore reduced to u^* , B_x^* , J_z^* , E_z^* , and p^* which are governed by

Faraday's Law:

$$\frac{\partial E_z^*}{\partial y^*} = - \frac{\partial B_x^*}{\partial t^*} \quad (1)$$

Ampère's Law:

$$\mu J_z^* = - \frac{\partial B_x^*}{\partial y^*} \quad (2)$$

Ohm's Law:

$$J_z^* = \sigma (E_z^* + u^* B_o) \quad (3)$$

Equations of Motion:

$$\frac{\partial u^*}{\partial t^*} = \nu \frac{\partial^2 u^*}{\partial y^{*2}} - J_z^* \frac{B_o^*}{\rho} \quad (4)$$

$$\frac{\partial p^*}{\partial y^*} = J_z^* B_x^* \quad (5)$$

As Eq. 5 represents an uncoupled equation for the pressure, it will not be considered further.

It is essential to examine the equations, before any further reduction, to determine the number and nature of the boundary conditions. It is seen that one boundary condition is required on E_z^* , one boundary and one initial condition on B_x^* , and one initial and two boundary conditions on u^* . It is also permissible to substitute a boundary condition on J_z^* in place of the boundary condition on either (but not both) E_z^* or B_x^* . The boundary conditions for the present problems are:

$$\begin{aligned} E_z^* &= 0 & \text{as } y^* \rightarrow \infty, t^* \geq 0 \\ B_x^* &= 0 & \text{at } y^* > 0, t^* = 0 \\ B_x^* &= 0 & \text{at } y^* = 0, t^* \geq 0 \\ u^* &= U_o^* & \text{at } y^* = 0, t^* > 0 \\ u^* &= 0 & \text{as } y^* \rightarrow \infty, t^* \geq 0 \end{aligned} \quad (6)$$

The first and last of these arise from the fact that the motion of the plate is the initiating mechanism and hence at distances far from the plate disturbances should diminish. The third condition arises from the symmetry of the problem and the fact that since B_x^* must be continuous across the plate, the slope of the lines of force is also continuous; hence the lines of force are perpendicular to the plate at the plate, and B_x^* is zero.

The problem may now be formulated in more convenient terms by first introducing the following dimensionless variables: $B = B_x^*/B_o^*$, $u = u^*/a$, $y = y^*a/\nu$, $t = a^2t^*/\nu$, $\epsilon = \sigma\mu\nu$, $U_o = U_o^*/a$, $J = J_z^*\nu\mu/B_o^*a$, $E = E_z^*/aB_o^*$. Eliminating J and E from (1)-(4) yields:

$$\left(\frac{\partial}{\partial t} - \frac{\partial^2}{\partial y^2} \right) u = \frac{\partial B}{\partial y} \quad (7)$$

$$\left(\frac{\partial}{\partial t} - \frac{1}{\epsilon} \frac{\partial^2}{\partial y^2} \right) B = \frac{\partial u}{\partial y} \quad (8)$$

Since this elimination involved differentiation of (3), the additional requirement that (3) must be satisfied at some boundary is necessary. Selecting $y \rightarrow \infty$ as the appropriate boundary, the first condition of (6) combined with (3) leads to the condition $\partial B / \partial y = 0$ as $y \rightarrow \infty$. This last condition and the last five conditions of (6) are the appropriate boundary conditions for (7) and (8). Finally, (7) and (8) can be combined to yield:

$$\left(\frac{\partial^4}{\partial y^4} - (1+\epsilon) \frac{\partial^3}{\partial y^2 \partial t} - \epsilon \frac{\partial^2}{\partial y^2} + \epsilon \frac{\partial^2}{\partial t^2} \right) \left(\frac{u}{B} \right) = 0. \quad (9)$$

These equations with the boundary conditions on B and u previously formulated, and the requirement that (7) and (8) be satisfied, are the complete mathematical formulation of the problem. These equations⁹ are identical to those of Chang and Yen,⁵ but, of course, the boundary conditions are different. Rossow,²¹ in his work, included initial conditions on $\partial u / \partial t$, J_z , E_z all of which are superfluous, and excluded a necessary boundary condition on u .

It is worth while to note that ϵ , the ratio of the two diffusivities ν and $1/\mu_0 \sigma$ (the ratio of the magnetic Reynolds number to the viscous Reynolds number, sometimes called the magnetic Prandtl number), is the only significant parameter of the problem.

Finally, we point out that cases with different initial states can be handled easily by superposition. For example, if we consider an initial state in which the fluid is stationary, but a nonzero electric field is applied, it is easily shown that if the variables E , J , u , and B refer to the difference in these variables from their initial values, then the formulation of the problem is identical to that just obtained. The pressure distribution of course will not be a linear superposition, but can be obtained without difficulty from the uncoupled equation.⁵

2.2 SOLUTIONS AND DISCUSSION

a. Solution Technique

The problem is solved by using a Laplace transform in time, solving the resulting ordinary differential equations for the transforms of u and B (denoted by \bar{u} and \bar{B} , respectively), and inverting the result.

The solutions for \bar{u} and \bar{B} which satisfy the given boundary and initial conditions are:

$$\begin{aligned} \bar{u} = & \frac{(p-D_2^2) D_1}{(p-D_2^2) D_1 - (p-D_1^2) D_1} \left(\frac{U}{p} \right) \exp(D_1 y) \\ & + \frac{(p-D_1^2) D_2}{(p-D_1^2) D_2 - (p-D_2^2) D_1} \left(\frac{U}{p} \right) \exp(D_2 y) \end{aligned} \quad (10)$$

$$\bar{B} = \frac{(p-D_2^2)(p-D_1^2)}{(p-D_2^2)D_1 - (p-D_1^2)D_2} \left(\frac{U}{p}\right) [\exp(D_1 y) - \exp(D_2 y)]. \quad (11)$$

where D_1 and D_2 are given by

$$D_{1,2} = -\frac{1}{2} \{ [\epsilon + (1 + \epsilon + 2\sqrt{\epsilon})p]^{1/2} \pm [\epsilon + (1 + \epsilon - 2\sqrt{\epsilon})p]^{1/2} \} \quad (12)$$

The general inversion of these equations for an exact solution involves an extremely large amount of manipulation; such solutions will not be dealt with here, as they are not readily interpretable. There does exist, however, a sufficient number of special cases for which solutions can be extracted to yield the significant features of the flow.

b. Exact Solution for $\epsilon = 1$

For this special case, the exact solution can be obtained with the aid of an inversion table.² The solutions for u , B , and J are given by

$$\begin{aligned} \frac{u}{U_o} = & \frac{1}{4} [1 + \exp(y)] \operatorname{erfc} \left(\frac{y}{2\sqrt{t}} + \frac{\sqrt{t}}{2} \right) \\ & + \frac{1}{4} [1 + \exp(-y)] \operatorname{erfc} \left(\frac{y}{2\sqrt{t}} - \frac{\sqrt{t}}{2} \right) \end{aligned} \quad (13)$$

$$\begin{aligned} \frac{B}{U_o} = & \frac{1}{4} [1 - \exp(y)] \operatorname{erfc} \left(\frac{y}{2\sqrt{t}} + \frac{\sqrt{t}}{2} \right) \\ & - \frac{1}{4} [1 - \exp(-y)] \operatorname{erfc} \left(\frac{y}{2\sqrt{t}} - \frac{\sqrt{t}}{2} \right) \end{aligned} \quad (14)$$

$$\begin{aligned} \frac{J}{U_o} = & \frac{1}{4\sqrt{\pi t}} \exp - \left(\frac{y}{2\sqrt{t}} + \frac{\sqrt{t}}{2} \right)^2 [\exp(y) - 1] \\ & - \frac{1}{4\sqrt{\pi t}} \exp - \left(\frac{y}{2\sqrt{t}} - \frac{\sqrt{t}}{2} \right)^2 [\exp(-y) - 1] \\ & + \frac{1}{4} \exp(y) \operatorname{erfc} \left(\frac{y}{2\sqrt{t}} + \frac{\sqrt{t}}{2} \right) + \frac{1}{4} \exp(-y) \operatorname{erfc} \left(\frac{y}{2\sqrt{t}} - \frac{\sqrt{t}}{2} \right). \end{aligned} \quad (15)$$

The solution for E can be obtained from Carrier,³ if desired.

These solutions for u , B , and J are plotted in Figs. 3, 4, and 5. The physical phenomena portrayed by these solutions is described as follows. At $t = 0$, a viscous

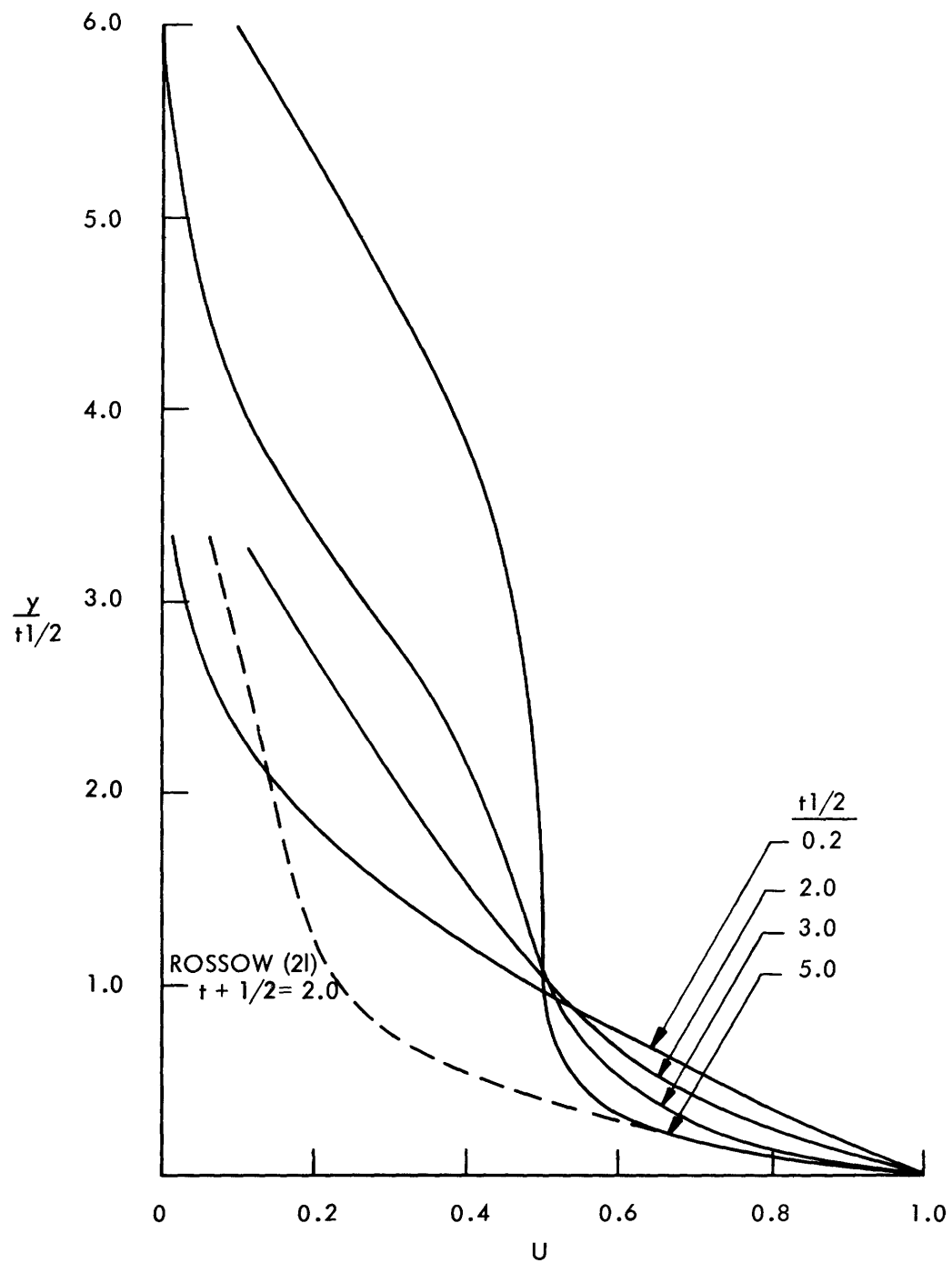


Fig. 3. Velocity profiles for Rayleigh problem, $\epsilon = 1$.

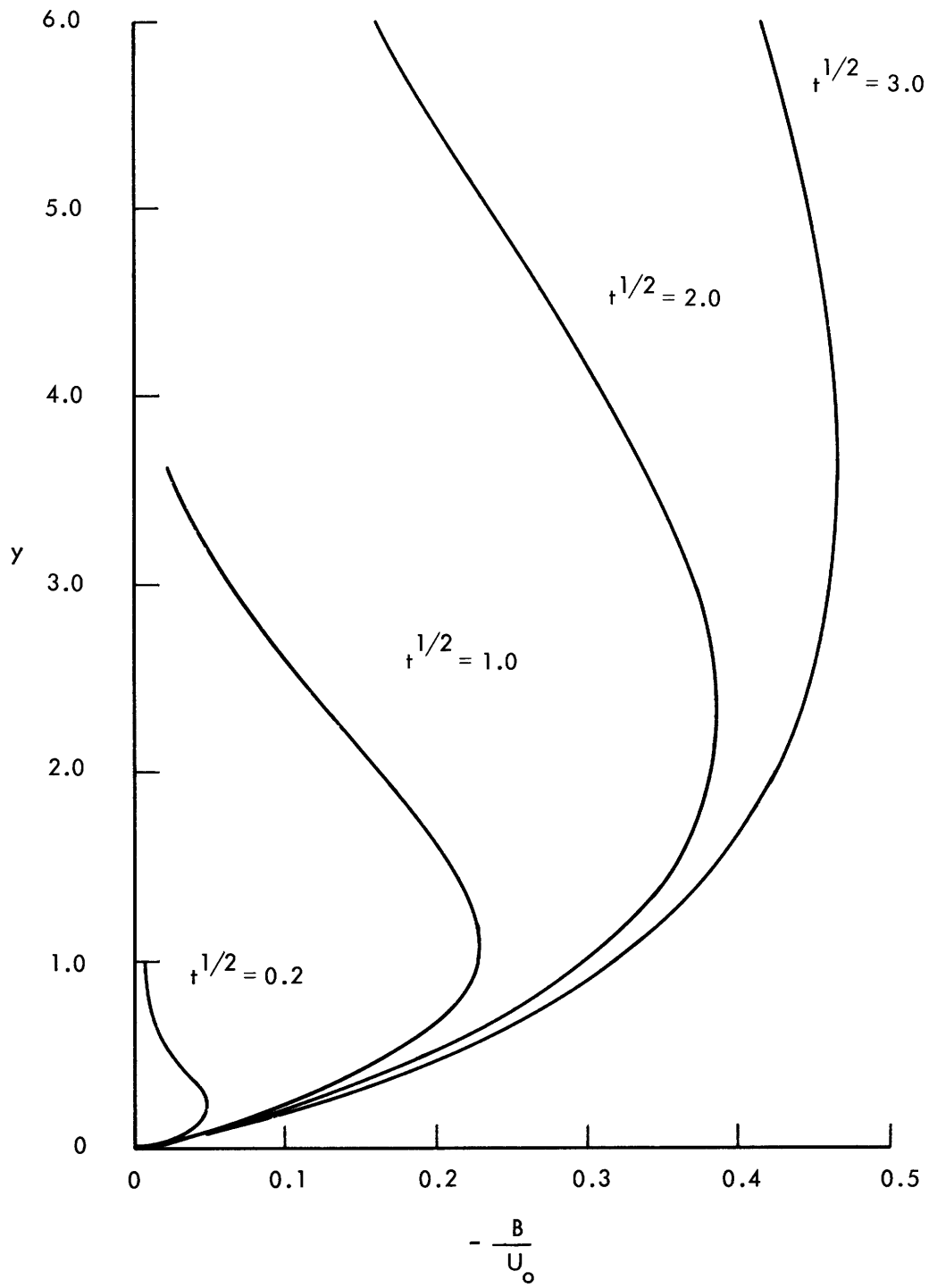


Fig. 4. Magnetic-field profiles for Rayleigh problem, $\epsilon = 1$.

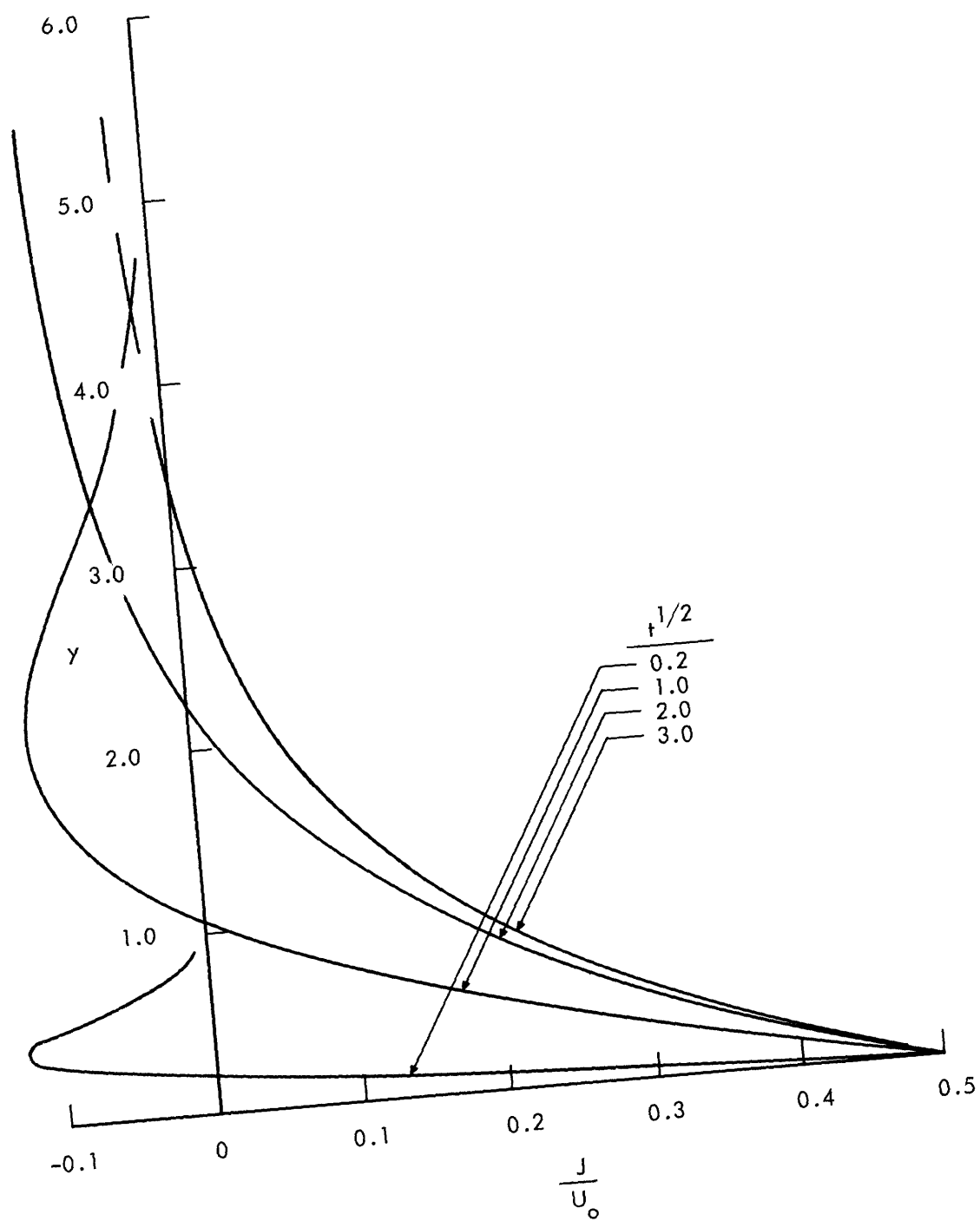


Fig. 5. Current-density distribution for Rayleigh problem, $\epsilon = 1$.

shear wave is generated by the motion of the plate. This shear wave in turn produces an Alfvén wave (actually a continuous succession of Alfvén waves), and by this action is itself diminished. The eventual magnitudes of two waves are dependent upon the ratio of the magnetic-to-viscous forces (ϵ), and are equal in this special case. The Alfvén wave propagates at a velocity $u = 1$, and diffuses, while the viscous wave remains stationary, and undergoes a finite diffusion that is limited by the electromagnetic forces not associated with the Alfvén wave. Thus, at large times, when the Alfvén wave is far from the plate, the velocity profile in the viscous layer next to the plate, which is of the Hartmann form, is time-independent (the thickness of the layer remains constant). These phenomena can be detected by observing the form of the solutions at various times. At $t \ll 1$, ($\sqrt{t} = 0.2$, for example) the Alfvén wave has not been fully generated, viscous forces predominate, and the solution differs but little from the classical Rayleigh solution. For $t \gg 1$, three regimes of flow are observed. For $y < 1$, the viscous wave dominates, and has essentially reached its maximum amount of dispersion; the inertial forces are zero. For $1 \ll y \ll t - \sqrt{t}$ the effect of diffusion of both waves is negligible, the region is current-free, and the resulting velocity is governed by the magnitude of the Alfvén wave. In this special case, since the waves are of equal strength, the velocity is $U_0/2$. The adjacent region, $y \sim t$, is dominated by the Alfvén wave. For $y \gg t + \sqrt{t}$ the effects of the diffusion of the Alfvén wave are negligible, and the fluid is essentially undisturbed.

As it is necessary to provide closed-current paths in all magnetohydrodynamic problems, it is natural to examine this phase of the present problem. It is easily seen that this constitutes no difficulty because the current in the viscous layer is equal and opposite to the current in the Alfvén wave.

c. Solution as $t \rightarrow \infty$

This solution is obtained by allowing $p \rightarrow 0$ in the transformed equations. The solutions for u and B are given by

$$\left. \begin{aligned} \frac{u}{U_0} &= (1+\sqrt{\epsilon})^{-1} \exp(-\sqrt{\epsilon} y) + \sqrt{\epsilon}/(1+\sqrt{\epsilon}) & y < t \\ \frac{u}{U_0} &= (1+\sqrt{\epsilon})^{-1} \exp(-\sqrt{\epsilon} y) & y > t \end{aligned} \right\} \quad (16)$$

$$\left. \begin{aligned} \frac{B}{U_0} &= -\sqrt{\epsilon} (1+\sqrt{\epsilon})^{-1} [1 - \exp(-\sqrt{\epsilon} y)] & y < t \\ \frac{B}{U_0} &= \sqrt{\epsilon} (1+\sqrt{\epsilon})^{-1} \exp(-\sqrt{\epsilon} y) & y > t \end{aligned} \right\} \quad (17)$$

Observe that the change in velocity associated with the Alfvén wave is given by $\sqrt{\epsilon}/(1+\sqrt{\epsilon})$. The mathematical formalism involved, unfortunately, completely suppresses the

diffusion of the Alfvén wave, and hence the solutions for $y > t$ are those attributed only to dispersion of the viscous wave.

At this point, an examination of the transverse electric field behind the Alfvén wave is warranted. It can be shown from the solution above for the Alfvén wave and Ohm's Law that there exists an electric field

$$E_z = -\frac{\sqrt{\epsilon}}{1 + \sqrt{\epsilon}} U_o. \quad (18)$$

This field is due to the continuous generation of the longitudinal component of the magnetic field by the Alfvén wave. That this is so can be easily verified from Faraday's Law:

$$E_z = \frac{d}{dt}(B_a y_a) = B_a = -\frac{\sqrt{\epsilon}}{1 + \sqrt{\epsilon}} U_o. \quad (19)$$

Here, y_a is the nominal position of the Alfvén wave, and B_a is the longitudinal component of magnetic field immediately behind it, which is obtained from (17) for $\epsilon y \gg 1$. In the strictly plane problem, this will cause charge to accumulate at the extremes (in the z -direction) of the problem, but contrary to Carrier and Greenspan,⁴ there is nothing artificial about this process. If the problem is considered as the limit of an axisymmetric one, then no charge accumulation is necessary.

d. Solution for $\epsilon \ll 1$ ($\sigma \ll 1$)

This solution is for the case most often encountered in practice. By performing the appropriate limiting process, the solutions for u and B are found to be

$$\frac{u}{U_o} = \frac{1}{2} \exp(\sqrt{\epsilon} y) \operatorname{erfc} \left(\frac{y}{2\sqrt{t}} + \sqrt{\epsilon t} \right) + \frac{1}{2} \exp(-\sqrt{\epsilon} y) \operatorname{erfc} \left(\frac{y}{2\sqrt{t}} - \sqrt{\epsilon t} \right) \quad (20)$$

$$\frac{B}{U_o} = -\frac{\sqrt{\epsilon}}{2} \left[\exp(\sqrt{\epsilon} y) \operatorname{erfc} \left(\frac{y}{2\sqrt{t}} - \sqrt{\epsilon t} \right) - \exp(-\sqrt{\epsilon} y) \operatorname{erfc} \left(\frac{y}{2\sqrt{t}} + \sqrt{\epsilon t} \right) - 2 \operatorname{erf} \sqrt{\epsilon t} \right]. \quad (21)$$

The solution for u is identical to that obtained by Rossow.¹⁹ It completely suppresses the Alfvén wave, and hence the solutions will be accurate relatively close to the plate, but will not be accurate far from the plate, where the Alfvén mechanism is dominant (however small) in any case.

The solution for $\epsilon \ll 1$ ($\nu \rightarrow 0$) can also be obtained; however it is of little practical interest and is omitted here.

2.3 THE ULTIMATE STATE

Now that this specific Rayleigh problem has been analyzed in rather elaborate detail, it is of interest to demonstrate how the essential features of the flow, both for this

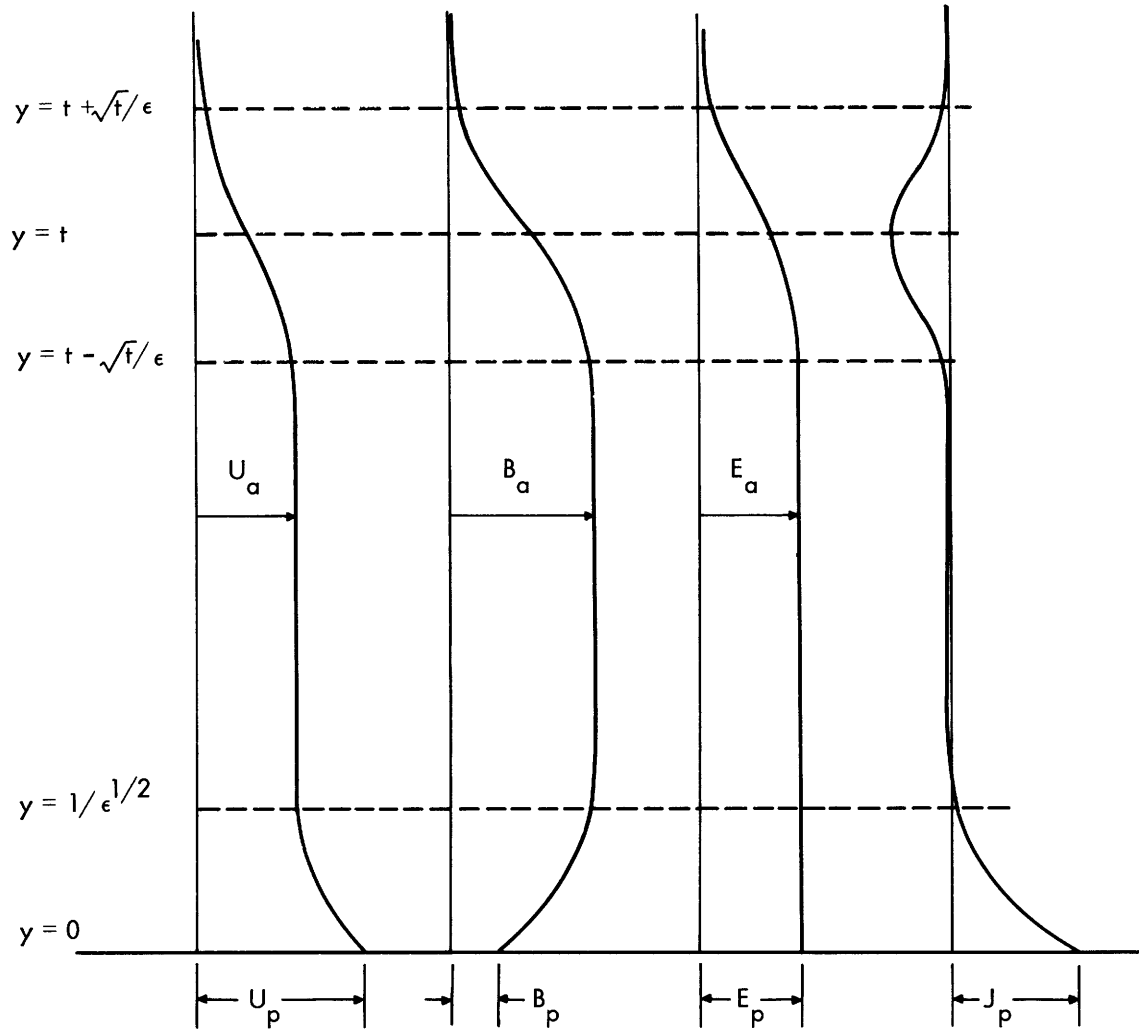


Fig. 6. Qualitative Rayleigh profiles for $t \gg 1$.

problem and other Rayleigh problems, may be determined without recourse to detailed analysis. This discussion will also serve to emphasize the physical aspects of the problem.

As has been shown, the significant features of the Rayleigh problem are the formulation of a Hartmann layer at the plate and the generation of an Alfvén wave that propagates away from the plate. At some time after the start of the motion the wave is clear of the layer and the flow behind the wave is quasi-steady. The qualitative character of this flow is shown in Fig. 6. We shall call this flow the ultimate state, and our interest in it will be confined to determining the time required for it to develop and the velocity and magnetic field changes across the Hartmann layer and the Alfvén wave. Henceforth, the problem considered will be of a more general type: It is assumed, as before, that the initial state is stationary and free of currents and that there is fluid on both sides of the plate; the plate, however, may be either nonconducting (as before) or it may be

a conducting plate which is insulated from the fluid, thereby permitting a current sheet as an initiating mechanism, or it may be an uninsulated conducting plate. The result of these considerations is that the initiating mechanism may either be a motion imparted to the plate, a longitudinal component of magnetic field applied at the surface of the plate, or both.

The time duration necessary for this flow to be established can be derived by observing that this time must be greater than the time required for the Hartmann layer to develop and such that the distance that the wave has traveled must be greater than both the width of the wave and the width of the Hartmann layer. By employing dimensional arguments or by perusing Eq. 20, the characteristic time for Hartmann layer development is given by $t_H \sim 1/\epsilon$, or in dimensional form $t_H^* \sim \rho^*/\sigma^* B_o^{*2}$. The width of the the Alfvén wave is given by \sqrt{Dt}^* , where D represents the larger of the two diffusivities ν or $1/\mu\sigma$; hence the time at which the wave is approximately as broad as the distance traveled is given by $t_D^* \sim D/a^2$, or in dimensionless form $t_D \sim D/\nu$. Finally, the thickness of the Hartmann layer, from Eq. 16, is $1/\sqrt{\epsilon}$; hence the time at which the wave has traveled an equal distance is given by $t_H \sim 1/\sqrt{\epsilon}$, or in dimensional form $t^* \sim \sqrt{\epsilon} \rho^*/\sigma^* B_o^{*2}$. These conditions reduce to the single requirement that $t^* \gg D\mu_o\rho/B_o^{*2}$ for the ultimate state to be achieved. In this sense the ultimate state is never achieved if either $\sigma \rightarrow 0$ or $B_o \rightarrow 0$. This is the principle difference between the ordinary Rayleigh problem and the various magnetohydrodynamic extensions.

The relations governing the relative strengths of the Hartmann layer and Alfvén wave are simply the statements that the change in magnetic field across the Hartmann layer is related to the velocity change by (using the notation of Fig. 6)

$$B_a^* - B_p^* = -\mu\sqrt{\sigma\rho\nu}(U_p^* - u_a^*) \quad (22)$$

and that the similar relation for the Alfvén wave is

$$B_a^* = -u_a^* \sqrt{\mu\rho}. \quad (23)$$

In dimensionless form these equations become

$$\left. \begin{aligned} B_a - B_p &= -\sqrt{\epsilon}(U_p - u_a) \\ u_a &= -B_a \end{aligned} \right\} \quad (24)$$

Equations 24 can be solved for u_a and B_a with the result

$$\left\{ \begin{aligned} U_a \\ -B_a \end{aligned} \right\} = -\frac{1}{1 + \sqrt{\epsilon}} B_p + \frac{\sqrt{\epsilon}}{1 + \sqrt{\epsilon}} U_p. \quad (25)$$

Using Ohm's Law, we further deduce that

$$E_a = -u_a = B_a. \quad (26)$$

The effects of the various initiating mechanisms are shown by Eqs. 25 and 26. If the plate is nonconducting, and given an initial velocity, which is the problem considered in detail in the previous section, then it is seen that

$$\begin{pmatrix} U_a \\ -B_a \end{pmatrix} = + \frac{\sqrt{\epsilon}}{1 + \sqrt{\epsilon}} U_p \quad (27)$$

which is in accord with our earlier result. If the plate is an insulated conductor and remains stationary, and an initial current is passed through the plate, then $U_p = 0$ and we obtain

$$\begin{pmatrix} U_a \\ -B_a \end{pmatrix} = - \frac{1}{1 + \sqrt{\epsilon}} B_p. \quad (28)$$

We point out in passing that if one desires to generate Alfvén waves, then the last excitation form is obviously the optimum method, since in general ϵ will be quite small.

If $B_p = -U_p$, no Hartmann layer develops. This is, in fact, the case if the plate is infinitely conducting and uninsulated (as considered by Chang and Yen⁵ and by Ludford¹⁴), since $E_a = -U_p$. Also, this is presumably the case some authors loosely refer to as "field-fixed-with-respect-to-plate" cases, due to the fact that $E^* = -U_p^* B_o^*$. For uninsulated conducting plates, an additional restriction must be placed on the time required for the ultimate state to be achieved: it must be shorter than the magnetic diffusion time across the plate. If $B_p = \sqrt{\epsilon} U_p$, then no Alfvén wave is present; this situation can arise only with use of an insulated conducting plate.

These considerations may be extended to various asymmetrical cases. For example, for fluid on one side only of an infinitely conducting plate, or an infinitely conducting pole piece, the result is the same as for the symmetrical case. For fluid on one side of an infinitely permeable magnet, the result is the same as for the nonconducting plate, since $B_p = 0$. There are obviously many more extensions and modifications of this type of problem, but it would be tedious and not very informative to explore them, since the essential features are no different from those previously discussed.

2.4 RELATION OF THE RAYLEIGH PROBLEM TO THE STEADY FLOW PAST A SEMI-INFINITE FLAT PLATE

As we have said, the Rayleigh problem may yield insight into the problem of steady flow past a semi-infinite plate. The purpose of this section is to construct this analogy and examine its validity both for the specific case to be considered in the rest of this report and also for other possible cases. The former analogy will also emphasize the physical aspects of the two-dimensional problem, while the latter will indicate the limits of applicability of the results obtained in subsequent sections.

a. The Nonconducting Plate Problem

The preceding analysis of the Rayleigh problem has shown that there are infinitely many variations, which depend upon the electromagnetic conditions imposed. These variations are also present when the steady flow past a semi-infinite flat plate is considered. The specific steady problem dealt with here is that of flow past a nonconducting flat plate, with an applied electric field that is such that the current far upstream of the plate is zero (see Fig. 2). The analogy with the Rayleigh problem is made by assuming that the behavior of a fluid particle at a given y coordinate as a function of time as measured from the time it passed the x coordinate of the leading edge is the same as the behavior of a fluid particle at the same y coordinate as a function of time measured from the start of the motion in the corresponding Rayleigh problem. Obviously, this analogy is not well made if in the steady problem a fluid particle attains a large y component of velocity, or if the y component of magnetic field differs appreciably from the upstream value. For the specific steady problem considered here it is evident that the corresponding Rayleigh problem is the one considered in detail in sections 2.1 and 2.2.

With this analogy it is a simple matter to construct the qualitative character of the steady flow, if the analogy is assumed to be valid. The result is shown in Fig. 7. Before such a flow pattern can be accepted, however, it is necessary to insure that the conditions under which the analogy was made have not been violated. The viscous layer around the plate will not distort the streamlines significantly; however, the current in this layer will, if the electrical conductivity is high, cause a significant increase in the y component of the magnetic field in the vicinity of the leading edge. Hence, if the conductivity is high, we may expect that the analogy is not well made. The Alfvén "line," which is somewhat analogous to the Mach line in compressible flow (the differences being that the Alfvén wave does not have an isotropic propagation and is a transverse wave), must be examined carefully. It may be verified that the existence of such a region is possible in incompressible flow. In addition, it can be shown that in order for the longitudinal component of velocity to decrease (in Fig. 7) and maintain the current in the direction shown, the fluid will be deflected toward the plate. If the conductivity is high, this deflection is large, and hence, again, the analogy is not well made and this simple concept of an Alfvén line needs modification. The necessary modifications are discussed in detail in Section V, but at present, the most that can be said about the qualitative nature of flows with high conductivity is that a viscous layer will certainly exist, but there may also be an appreciable region away from the plate in which the flow is significantly disturbed. Perhaps the most important single result of this work is the analysis of this effect, as it represents a significant departure from the character of the flow in the absence of a magnetic field.

When ϵ is small, which is a case of great practical interest, our analogy is quite well taken, since the effects of the current in the region away from the plate will not

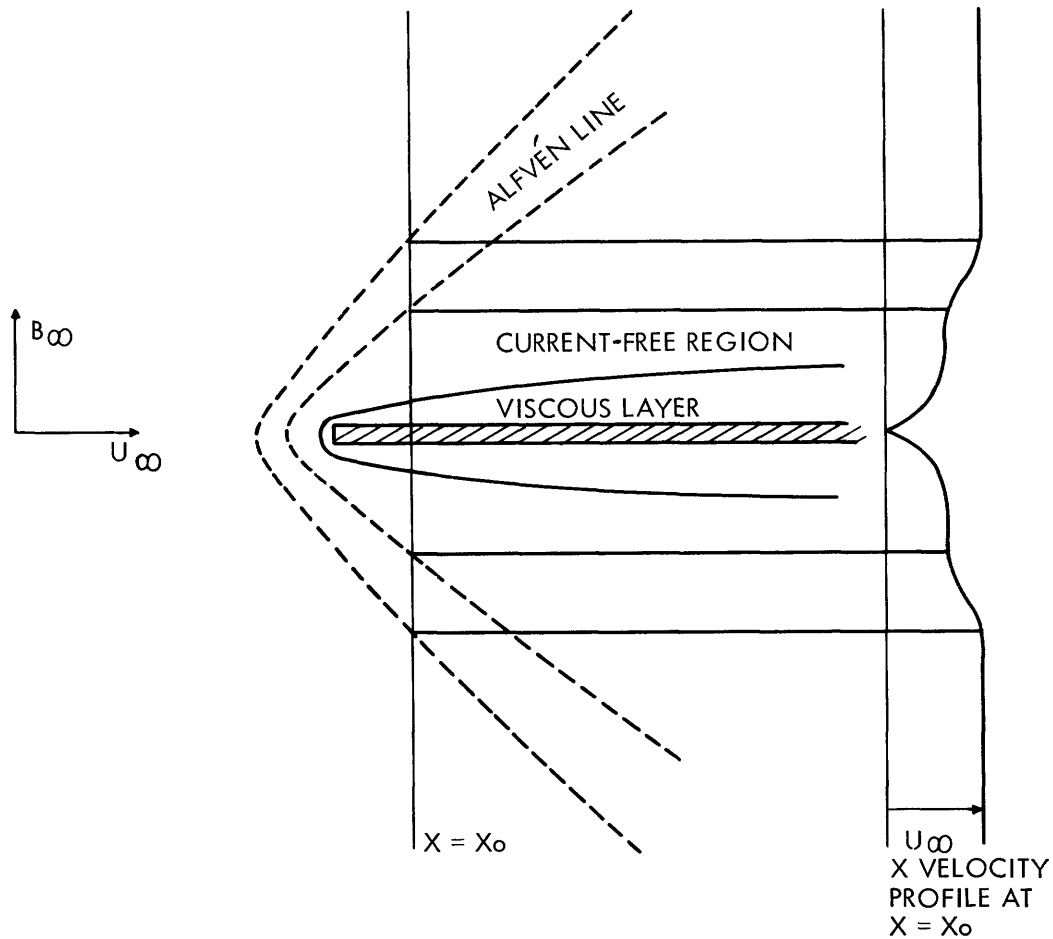


Fig. 7. Qualitative picture of flow past a semi-infinite flat plate as constructed from the corresponding Rayleigh problem.

affect the flow appreciably. Thus we expect a viscous layer that approaches the Hartmann layer asymptotically. This is expected on a physical basis, as the body forces caused by the current in the viscous layer are in the direction of motion, opposing the viscous forces, and it is therefore expected that the inertial forces will eventually vanish. Qualitatively useful results will be obtained for this case.

b. Other Possible Steady Flows

There are many other possible flows of interest. One of these is the steady flow past a nonconducting plate in which the applied electric field is not such that $\underline{E} + \underline{V}_\infty \times \underline{B}_\infty = 0$, and hence currents exist upstream of the plate. Situations of this type arise in generators and accelerators. The corresponding Rayleigh problem is the nonconducting plate problem in which currents exist in the initial state. For small ϵ , our analogy again holds, and it is seen that the fluid field is the same as in the previous case. This is due to the fact that although the $\underline{J}^* \times \underline{B}^*$ force in the viscous layer may either oppose or assist the viscous forces, the difference between this force and the

one existing in the $\underline{E} \times \underline{V}_\infty \times \underline{B}_\infty = 0$ case is exactly equal and opposite to the force caused by the longitudinal pressure gradient necessary to overcome the force caused by the free-stream currents. For cases in which ϵ is small, the velocity field to be presented for the $\underline{E} + \underline{V}_\infty \times \underline{B}_\infty = 0$ case will be accurate for these cases also. This problem cannot be formulated as the flow past a semi-infinite plate, because of the presence of currents in the free stream.

The other general class of steady flows of interest are those with $\underline{E} = 0$; these could arise in the flow about missiles traveling through the atmosphere. This is a different type of problem, however, in that the magnetic field is not applied externally. It has no corresponding Rayleigh problem, and, needless to say, the flow characteristics are quite different from the problems previously considered. This type of problem is not dealt with in this report.

III. THE LINEARIZED PROBLEM

3.1 FORMULATION OF THE GENERAL PROBLEM

a. Governing Equations

We consider the steady, two-dimensional flow past a semi-infinite flat plate with an applied magnetic field perpendicular to the plate (see Fig. 2). Far upstream, the flow is uniform and current-free, with velocity U_∞ and magnetic field B_∞ . The general equations governing this problem are:

$$\text{Continuity: } \nabla \cdot \underline{V}^* = 0 \quad (28)$$

$$\text{Momentum: } \rho(\underline{V} \cdot \nabla) \underline{V}^* = -\nabla p^* + \eta \nabla^2 \underline{V}^* + \underline{J}^* \times \underline{B}^* \quad (29)$$

$$\text{Ampère's Law: } \nabla \times \underline{B}^* = \mu_0 \underline{J}^* \quad (30)$$

$$\text{Faraday's Law: } \nabla \times \underline{E}^* = 0 \quad (31)$$

$$\text{Ohm's Law: } \underline{J}^* = \sigma(\underline{E}^* + \underline{V}^* \times \underline{B}^*) \quad (32)$$

$$\text{Conservation of Magnetic Flux: } \nabla \cdot \underline{B}^* = 0 \quad (33)$$

To obtain these equations in a workable form, we shall render them dimensionless; reduce them to the two-dimensional case, and introduce the stream function and magnetic vector potential.

These equations can be made dimensionless in a variety of ways; here, we shall introduce a reference length L , employ U_∞ and B_∞ as the characteristic velocity and field strength, respectively, and define the following parameters: (a) the Reynolds number, $R = U_\infty L / \nu$; (b) the magnetic Reynolds number, $R_m = \sigma \mu_0 U_\infty L$; and (c) the dimensionless Alfvén speed, $a^2 = B_\infty^2 / \mu_0 \rho U_\infty^2$.

From Eq. 31 and the fact that the flow is two-dimensional, it is seen that E_z^* is a constant, and hence from the imposed condition that there are no currents far upstream, $E_x^* = -U_\infty B_\infty$. Furthermore, in the absence of any source or initiating mechanism, it is seen that $E_x^* = E_y^* = J_x^* = B_z^* = V_z^* = 0$.

Equations 28 and 33 are sufficient for the introduction of the stream function and magnetic vector potential, respectively, defined as

$$\left. \begin{aligned} \nabla \times \underline{\psi} &= \underline{V} \\ \nabla \times \underline{A} &= \underline{B} \end{aligned} \right\} \quad (34)$$

In this two-dimensional case, $\underline{\psi}$ and \underline{A} have only z -components, denoted hereafter by ψ and A .

Following the procedure outlined above and some manipulation yield the governing equations in the following form (lower case letter subscripts denote partial

differentiation):

$$\frac{1}{R} \nabla^4 \psi + \psi_x \nabla^2 \psi_y - \psi_y \nabla^2 \psi_x = a^2 (A_x \nabla^2 A_y - A_y \nabla^2 A_x) \quad (35a)$$

$$\nabla^2 A = -Rm(\psi_x A_y - \psi_y A_x - 1). \quad (35b)$$

With solutions for ψ and A , the velocity and magnetic field components are obtained from (34) and the pressure distribution from (29). Observe that the parameters of the problem are R , Rm , and a^2 . The significance of these parameters is well known and need not be discussed here. There are two additional forms of these equations which will be of subsequent use. First, (35b) may be introduced into (35a), with the result

$$\frac{1}{R} \nabla^4 \psi + \psi_x \nabla^2 \psi_y - \psi_y \nabla^2 \psi_x = a^2 Rm [A_y (\psi_x A_y - \psi_y A_x)_x - A_x (\psi_x A_y - \psi_y A_x)_y]. \quad (36)$$

It will be seen that this form of (35a) is most convenient when Rm is small, so that the distortion of the applied magnetic field is also small. The combination $a^2 Rm$ has been called by some authors the interaction parameter, as it represents the ratio of magnetic forces to inertial forces, under the assumption that the magnetic field distortion is small. Note that the combination $a^2 R Rm$ is then the ratio of magnetic-to-viscous forces, and is the square of the Hartmann number.

Finally, in the present problem, there is no characteristic length evident from the geometry. Accordingly, we shall take as this length the characteristic viscous diffusion length (also referred to as the Reynolds number length): $L = \nu/U_\infty$. This is obtained from (35a) or (36) and (35b) by setting $R = 1$ and $Rm = \epsilon$. Hence the significant parameters are ϵ and a^2 .

b. Boundary Conditions

The appropriate boundary conditions for this problem are:

$$\left. \begin{array}{ll} \psi = \psi_y = 0 & \text{at } y = 0, x > 0 \\ A_y = 0 & \text{at } y = 0, x > 0 \\ \psi_x \rightarrow 0 & \text{as } x \rightarrow \pm\infty \\ A_x \rightarrow -1 & \\ A_y \rightarrow 0 & \text{as } x \rightarrow -\infty \\ \psi_y \rightarrow 1 & \\ A_x \text{ bounded} & \text{as } x \rightarrow +\infty \\ \psi_y, A_y \text{ bounded} & \text{as } y \rightarrow \pm\infty \end{array} \right\} \quad (37)$$

The first of these conditions is the usual fluid mechanic one; the second arises because of the symmetry of the problem; the third through the sixth establish the upstream conditions; the last two require reasonable behavior at infinity. It is necessary to point out here, for later use, that ψ_{yyy} is continuous across the plate; this can be verified by writing the x component of (29) at $y = 0+$ and $y = 0-$, and making use of known symmetry conditions.

Equations 35a or 36, 35b, and 37, with $R = 1$ and $Rm = \epsilon$ represent the complete mathematical formulation of the problem. It is seen that the equations are nonlinear, and hence offer no practical hope of any analytical solution.

3.2 FORMULATION OF THE LINEARIZED PROBLEM

It has been found, in the pure fluid mechanic case, that the governing equations may be linearized (the Oseen approximation) and that the solution to this linear problem yields qualitatively useful results. For example, the skin friction at the plate found from the linearized solution differs but by a constant multiplicative factor from that found by conventional boundary-layer treatments.

We shall linearize the present problem in the following manner. We write

$$\left. \begin{aligned} \psi &= y + \psi' \\ A &= A' - x \end{aligned} \right\} \quad (38)$$

and assume that the perturbation potentials ψ' and A' are small. This is of course identical to writing

$$\left. \begin{aligned} u &= 1 + u' \\ v &= v' \\ B_x &= B'_x \\ B_y &= 1 + B'_y \end{aligned} \right\} \quad (39)$$

where the primed quantities are again assumed small. On a physical basis, the assumption that u' is small is obviously not valid near the plate; similarly, the assumption that B'_y is small can only be justified for ϵ small. However, these deficiencies are certainly no greater than in the pure fluid mechanic case, so that informative results may be expected.

Making the substitutions (38) in (35a) and (35b) and neglecting terms of higher order (for example, $u'v'$), we obtain

$$\nabla^4 \psi' - \nabla^2 \psi'_x = +a^2 \nabla^2 A_y \quad (40)$$

$$\nabla^2 A' = +\epsilon(A'_x - \psi'_y) \quad (41)$$

and the boundary conditions become

$$\left. \begin{array}{ll}
\psi'_y = -1 & \text{at } y = 0, x > 0 \\
\psi' = 0 & \text{at } y = 0, x \geq 0 \\
A'_y = 0 & \text{at } y = 0, x \geq 0 \\
\psi'_x \rightarrow 0 & \text{as } x \rightarrow \pm\infty \\
A'_x = A'_y = \psi'_y \rightarrow 0 & \text{as } x \rightarrow -\infty \\
A'_x \text{ bounded} & \text{as } x \rightarrow +\infty \\
\psi_y, A'_y \text{ bounded} & \text{as } y \rightarrow \pm\infty
\end{array} \right\} \quad (42)$$

Equations 40, 41, and 42 are the complete mathematical formulation of this linearized problem. In the rest of this section, we shall drop the primes so that all quantities will be referred to as perturbations from upstream values.

Unfortunately, analysis of this problem is exceedingly complex (and equally unproductive, as applied by this author), so that it is beneficial to introduce another assumption. This is that the change of the normal component of magnetic field (B_y) in the y -direction is much less than the change of the longitudinal velocity component (u) in the y -direction ($A_{xy} \ll \psi_{yy}$). It can be readily shown that near the plate, where the right-hand side of Eq. 41 is largest in magnitude, this is a valid assumption. In the region away from the plate, this assumption may not be valid, but for small ϵ the contribution of both terms is small. Introducing this assumption into Eqs. 40 and 41 and rearranging, we obtain

$$\nabla^4 \psi - \nabla^2 \psi_x = \epsilon a^2 \psi_{yy} \quad (43)$$

$$\nabla^2 A = \epsilon (A_x - \psi_y). \quad (44)$$

It is now evident that (43) and (44) represent a relatively simple set, as the stream function is now uncoupled. In fact, Eq. 43 is the linearized form of the governing equations when the magnetic field is assumed to be undistorted.

3.3 SOLUTION OF THE LINEARIZED EQUATIONS

a. General Remarks

Although Eqs. 43 and 44 are relatively simple in form, the mathematical details of obtaining even an approximate solution are quite complex. Briefly, the procedure consists of: (a) applying Fourier transforms in x and y to the equations and boundary conditions, treating the skin friction at the plate [$\psi_{yy}(y=0+)$] as unknown; (b) obtaining the inverse transform in y ; (c) determining $\psi_{yy}(y=0+)$, in an approximate manner, from the boundary conditions by utilizing the Weiner-Hopf technique; and (d) obtaining the inverse transforms in x .

b. Applications of Fourier Transforms

We introduce the following transforms:

$$\bar{\psi}(p, y) = \bar{\psi} = \int_{-\infty}^{\infty} \psi e^{-ipx} dx \quad (45)$$

$$\hat{\psi}(x, r) = \hat{\psi} = \int_{-\infty}^{\infty} \psi e^{-iry} dy = \int_{-\infty}^{0-} \psi e^{-iry} dy + \int_{0+}^{\infty} \psi e^{-iry} dy. \quad (46)$$

Analogous transforms are introduced for A. The split in the y integration is necessary because ψ_{yy} is discontinuous at the plate. The inverse transforms corresponding to (45) and (46) are defined as

$$\psi(x, y) = \frac{1}{2\pi} \int_{-\infty}^{\infty} \bar{\psi} e^{ipx} dp \quad (47)$$

$$\psi(x, y) = \frac{1}{2\pi} \int_{-\infty}^{\infty} \hat{\psi} e^{iry} dr. \quad (48)$$

Introducing (45) and (46) into (43) and (44), we obtain the transformed equations:

$$(p^2 + r^2)^2 \hat{\psi} + (p^2 + r^2) ip \hat{\psi} + \epsilon a^2 r^2 \hat{\psi} = ir \bar{f} \quad (49)$$

$$-(p^2 + r^2) \hat{A} - \epsilon ip \hat{A} + \epsilon ir \hat{\psi} = 0. \quad (50)$$

Here, we have defined

$$\left. \begin{aligned} f(x, t) &= [\psi_{yy}(0+) - \psi_{yy}(0-)] & x \geq 0 \\ f(x, t) &= 0 & x < 0. \end{aligned} \right\} \quad (51)$$

Solving (49) and (50) for $\hat{\psi}$ and \hat{A} , respectively, we obtain

$$\hat{\psi} = \frac{ir \bar{f}}{(p^2 + r^2)(p^2 + r^2 + ip) + \epsilon a^2 r^2} \quad (52)$$

$$\hat{A} = - \frac{\epsilon r^2 \bar{f}}{(p^2 + r^2 + \epsilon ip)[(p^2 + r^2)(p^2 + r^2 + ip) + \epsilon a^2 r^2]}. \quad (53)$$

These equations may now be inverted with respect to r by making use of (48); evaluation of the resulting integrals reduces to determining residues. The procedure is quite straightforward, with the result

$$\frac{y}{|y|} \bar{\psi} = \frac{\bar{f}(p)}{2} \frac{e^{-|N_1||y|} - e^{-|N_2||y|}}{N_1^2 - N_2^2} \quad (54)$$

$$\bar{A} = \frac{\epsilon \bar{f}(p)}{2} \left[\frac{|N_2| \epsilon^{-|N_2|} |y|}{(N_3^2 - N_2^2)(N_1^2 - N_2^2)} + \frac{|N_1| \epsilon^{-|N_1|} |y|}{(N_1^2 - N_3^2)(N_1^2 - N_2^2)} - \frac{|N_3| \epsilon^{-|N_3|} |y|}{(N_1^2 - N_3^2)(N_3^2 - N_2^2)} \right] \quad (55)$$

Here,

$$N_{1,2}^2 = p^2 + \frac{ip}{2} + \frac{\epsilon a^2}{2} \pm \frac{1}{2} [(4\epsilon a^2 - 1)p^2 + 2\epsilon a^2 ip + \epsilon^2 a^4]^{1/2} \quad (56)$$

$$N_3^2 = p^2 + \epsilon ip. \quad (57)$$

Care must be exercised in selecting the branches of $|N_1|$, $|N_2|$, and $|N_3|$ so that the various exponentials decay (in order to maintain reasonable behavior far from the plate).

The boundary conditions at $y = 0$ may now be employed to determine \bar{f} . The first boundary condition of (42) is treated as follows:

$$\psi_y(y=0) = u_0 + u_1,$$

where

$$u_0 = \lim_{\delta \rightarrow 0} -e^{-\delta x} \quad x \geq 0 \quad (58a)$$

$$u_0 = 0 \quad x < 0 \quad (58b)$$

$$u_1 = 0 \quad x \geq 0 \quad (58c)$$

$$u_1 = u_1(x) \quad x < 0. \quad (58d)$$

Transforming this condition then yields

$$\bar{\psi}_y(y=0) = \frac{i}{p - i\delta} + \bar{u}_1. \quad (59)$$

From (54), we obtain

$$\bar{\psi}_y(y=0) = -\frac{\bar{f}}{2} \frac{1}{|N_1| + |N_2|} \quad (60)$$

Combining (58) and (59) yields

$$\frac{i}{p - i\delta} + \bar{u}_1 = -\frac{\bar{f}}{2} \frac{1}{|N_1| + |N_2|} = -\frac{\bar{f}}{2} \bar{K}(p). \quad (61)$$

Equation 61 is now in the conventional Wiener-Hopf form and it will be beneficial to outline the procedure before becoming immersed in details.

c. The Wiener-Hopf Procedure

The underlying concept of the Wiener-Hopf procedure is to rearrange (61) so that one side of the equation will contain only terms analytic in the upper half-plane of p , and the other side will contain only terms analytic in an overlapping lower half-plane. Then, from the theory of functions, the two sides are analytic continuations of each other, and must therefore be partial representations of the same function. Furthermore, from Liouville's theorem, this function must be a polynomial in p . From the known behavior of the functions or their transforms, this polynomial can be determined.

Proceeding along these lines, we first note that from the definitions (58c), (58d), and (51), \bar{u}_1 is analytic in the upper half-plane (denoted by \oplus), and \bar{f} is analytic in the lower half-plane (denoted by \ominus). Equation (61) can now be written

$$\left[\frac{i}{p-i\delta} \right]_{\ominus} + \bar{u}_1_{\oplus} = -\frac{\bar{f}_{\ominus}}{2} \bar{K}(p). \quad (62)$$

Now if we assume that $\bar{K}(p)$ can be decomposed so that $\bar{K}(p) = \bar{K}_{\oplus} \bar{K}_{\ominus}$, then (62) becomes

$$\left[\frac{i}{p-i\delta} \right]_{\ominus} \frac{1}{\bar{K}_{\oplus}} + \frac{\bar{u}_1_{\oplus}}{\bar{K}_{\oplus}} = -\frac{\bar{f}_{\ominus}}{2} \bar{K}_{\ominus}. \quad (63)$$

The first term in this equation can be written (an identity)

$$\frac{i}{(p-i\delta) \bar{K}_{\oplus}} = \frac{i}{p-i\delta} \left[\frac{1}{\bar{K}_{\oplus}} - \frac{1}{K_{\oplus}(i\delta)} \right] + \frac{i}{(p-i\delta)} \left[\frac{1}{K_{\oplus}(i\delta)} \right] \quad (64)$$

where the first term is analytic in the upper half-plane, and the second term is analytic in the lower half-plane. Hence, (63) and (64) yield

$$\frac{i}{(p-i\delta)} \left[\frac{1}{K_{\oplus}} - \frac{1}{K_{\oplus}(i\delta)} \right]_{\oplus} + \left[\frac{\bar{u}_1}{K_{\oplus}} \right]_{\oplus} = -\frac{\bar{f}_{\ominus}}{2} [K_{\ominus}]_{\ominus} - \left[\frac{i}{p-i\delta} \left(\frac{1}{K_{\oplus}(i\delta)} \right) \right]_{\ominus} \quad (65)$$

where the right-hand side is analytic in the lower half-plane and the left-hand side is analytic in an overlapping upper half-plane, the region of overlap being, in the limit, the real axis.

It is evident that the crux of the problem is in performing the decomposition $\bar{K} = \bar{K}_{\oplus} \bar{K}_{\ominus}$. In principle, there are two general methods for performing this decomposition (discussed in detail by Noble¹⁷). In the present case, however, the function \bar{K} is of such a complex nature that the results of either of these methods lead to functions K_{\oplus} and K_{\ominus} that involve definite integrals that can only be evaluated numerically. As the mathematical model of the physical problem is such that only qualitatively useful results are to be obtained, the labor involved in obtaining the exact decomposition is not merited. Indeed, we shall concentrate on approximating \bar{K} in such a way that the

decomposition can be easily performed, while retaining the qualitative features of the problem.

To this end, we first approximate N_1 and N_2 by assuming $\epsilon a^2 \ll 1$; then from (56) we have

$$N_1^2 \approx p^2 + ip + \epsilon a^2$$

$$N_2^2 \approx p^2$$

so that \bar{K} becomes

$$\bar{K}(p) = \frac{1}{|p| + |p^2 + ip + \epsilon a^2|^{1/2}} \quad (66)$$

The approximation technique now involves replacing $\bar{K}(p)$ by another function, $\bar{D}(p)$ say, which is easily factored and maintains the essential features of the flow. Carrier³ demonstrates that by requiring D to possess the same singularity and at least the same area and first moment as K , a very good approximation is obtained. (The area and all moments of K are defined by assigning successive values to n in $\int_{-\infty}^{\infty} x^n K(x) dx$.) In terms of the transforms D and K , these requirements take the form

$$\left. \begin{aligned} \bar{D}(p \rightarrow \infty) &= \bar{K}(p \rightarrow \infty) \\ \bar{D}(p=0) &= \bar{K}(p=0) \\ \bar{D}_p(p=0) &= \bar{K}_p(p=0) \end{aligned} \right\} \quad (67)$$

We choose \bar{D} to be of the following form:

$$\bar{D} = \frac{1}{(Ap+iB)^{1/2} (Cp-iD)^{1/2}} \quad (68)$$

where A , B , C , and D are positive real constants. This form has the obvious advantage of being readily decomposable. Substituting Eqs. 66 and 68 in Eqs. 67 yields the following conditions which must be satisfied:

$$(AC)^{1/2} = 2$$

$$(BD)^{1/2} = (\epsilon a^2)^{1/2}$$

$$i(BC-AD) = i + 2\sqrt{\epsilon a^2}$$

It is evident that the last condition cannot be satisfied exactly; here again we neglect the contribution of ϵa^2 . As it happens, with this assumption, all moments of K and D are equal. Hence, one approximate function is given by

$$D = \frac{1}{2\left(p + \frac{i}{4}\right)^{1/2} (p - i\epsilon a^2)^{1/2}} \quad (69)$$

and we may now set

$$\bar{K}_O = \frac{1}{2\left(p + \frac{i}{4}\right)^{1/2}} \quad (70)$$

$$\bar{K}_O = \frac{1}{(p - i\epsilon a^2)^{1/2}}$$

Introducing (70) into (65) yields

$$\begin{aligned} J(p) &= \frac{i}{p - i\delta} \left[2\left(p + \frac{i}{4}\right)^{1/2} - 2i^{1/2} \left(\delta + \frac{1}{4}\right)^{1/2} \right]_{\oplus} + 2\bar{u}_1 \left(p + \frac{i}{4}\right)^{1/2} \\ &= -\frac{\bar{f}}{2(p - i\epsilon a^2)^{1/2}} - \left[\frac{2i^{3/2}}{p - i\delta} \left(\delta + \frac{1}{4}\right)^{1/2} \right]_{\ominus} \end{aligned} \quad (71)$$

where $J(p)$ is an unspecified polynomial in p . The form of this polynomial can be determined by observing that $u_1(x)$ and $xf(x)$ must be bounded at $x = 0$. Hence their transforms must be such that $\bar{p}u_1$, and \bar{f} are bounded as $p \rightarrow \infty$. Thus, from (71) the polynomial $J(p)$ must be zero, and hence

$$\frac{\bar{f}}{2} = \frac{(p - i\epsilon a^2)^{1/2}}{i^{1/2}(p - i\delta)} \quad (72)$$

The inverse transform of \bar{f} can be obtained from any comprehensive table (for example, Campbell and Foster²):

$$f(x) = \frac{2}{\sqrt{\pi x}} e^{-\epsilon a^2 x} + 2\sqrt{\epsilon a^2} \operatorname{erf} \sqrt{\epsilon a^2 x} \quad (73)$$

d. Solution for $A_x(y=0, x>0)$

In principle, now that a solution for \bar{f} has been obtained, we are in a position to invert Eqs. 54 and 55 and obtain a solution for ψ and A . In practice, this is a very complex procedure, and we shall not attempt it here. Instead, we shall attempt to determine the normal component of magnetic field at the plate $[A_x(y=0, x>0) = -B_y(y=0, x>0)]$.

Recalling that the transform of the x derivative is related to the function by

$$\overline{A_x} = ip\bar{A}, \quad (74)$$

we obtain from (55)

$$\bar{A}_x(y=0) = \frac{\epsilon p}{2} \bar{f} \left[\frac{|N_2|}{(N_3^2 - N_2^2)(N_1^2 - N_2^2)} + \frac{|N_1|}{(N_1^2 - N_3^2)(N_1^2 - N_2^2)} - \frac{|N_3|}{(N_1^2 - N_3^2)(N_3^2 - N_2^2)} \right]. \quad (75)$$

Rearrangement of (75) yields

$$\bar{A}_x(y=0) = \frac{\epsilon p \bar{f}}{2} \left[\frac{(|N_1| + |N_2|)^{-1}}{N_1^2 + N_3^2} - \frac{(|N_2| + |N_3|)^{-1}}{N_1^2 - N_3^2} \right]. \quad (76)$$

Introducing our previous assumptions into (56) and (57) yields

$$(|N_1| + |N_2|)^{-1} \cong \left[2 \left(p + \frac{i}{4} \right)^{1/2} (p - i\epsilon a^2)^{1/2} \right]^{-1} \quad (77a)$$

$$N_1^2 - N_3^2 = ip + \epsilon a^2 \quad (77b)$$

$$(|N_2| + |N_3|)^{-1} \cong \lim_{k \rightarrow 0} (p - ik)^{1/2} [(p + ik)^{1/2} + (p + i\epsilon)^{1/2}]^{-1} \quad (77c)$$

The factor k has been introduced to avoid difficulties associated with a singularity on the real axis. For similar reasons, we replace p in (76) by $p - i\delta$, since we are interested in positive x . Equation 76 now becomes

$$\bar{A}_x(y=0) = \frac{i^{1/2} \epsilon}{(ip + \epsilon a^2)(4p + i)^{1/2}} - \frac{i^{1/2} \epsilon (p - i\epsilon a^2)^{1/2}}{(ip + \epsilon a^2)(p - ik)^{1/2} [(p + ik)^{1/2} + (p + i\epsilon)^{1/2}]} \quad (78)$$

This may now be inverted with the aid of the inversion formula (47). The first term reduces to the evaluation of the residue of the pole in the upper half p plane ($p = i\epsilon a^2$), with the result

$$\text{Term 1} = \epsilon e^{-\epsilon a^2 x}.$$

The second term requires a contour with nonzero contributions; this is rather tedious, and is performed in Appendix I. The result is

$$\text{Term 2} = -\frac{1}{\pi} \int_0^{\epsilon a^2} \frac{(r + \epsilon)^{1/2} - r^{1/2}}{(\epsilon a^2 - r)^{1/2} r^{1/2}} e^{-rx} dr$$

so that $A_x(y=0, x>0)$ is given by

$$A_x(y=0, x>0) = \epsilon e^{-\epsilon a^2 x} - \frac{1}{\pi} \int_0^{\epsilon a^2} \frac{(r + \epsilon)^{1/2} - r^{1/2}}{(\epsilon a^2 - r)^{1/2} r^{1/2}} e^{-rx} dr. \quad (79)$$

The integral in the second term must, of course, be evaluated numerically.

3.4 DISCUSSION OF LINEARIZED SOLUTION

a. General Remarks

Summarizing the results of section 3.3, we have obtained expressions for the skin friction and normal component of magnetic field at the plate. These solutions are given by

$$\psi_{yy}(y=0+) = \frac{1}{\sqrt{\pi x}} e^{-\epsilon a^2 x} + \sqrt{\epsilon a^2} \operatorname{erf} \sqrt{\epsilon a^2 x} \quad (80a)$$

$$B_y(y=0) = \frac{1}{\pi} \int_0^{\epsilon a^2} \frac{(r+\epsilon)^{1/2} - r^{1/2}}{(\epsilon a^2 - r)^{1/2} r^{1/2}} e^{-rx} dr - \epsilon e^{-\epsilon a^2 x} \quad (80b)$$

The assumptions made during the course of the solution restrict the validity of these results to those cases in which $\epsilon \ll 1$ and $\epsilon a^2 \ll 1$. These equations are plotted in Figs. 8 and 9.

As several approximations were employed in obtaining this solution, it is useful to obtain a check on the mathematical process if it is at all possible. Fortunately,

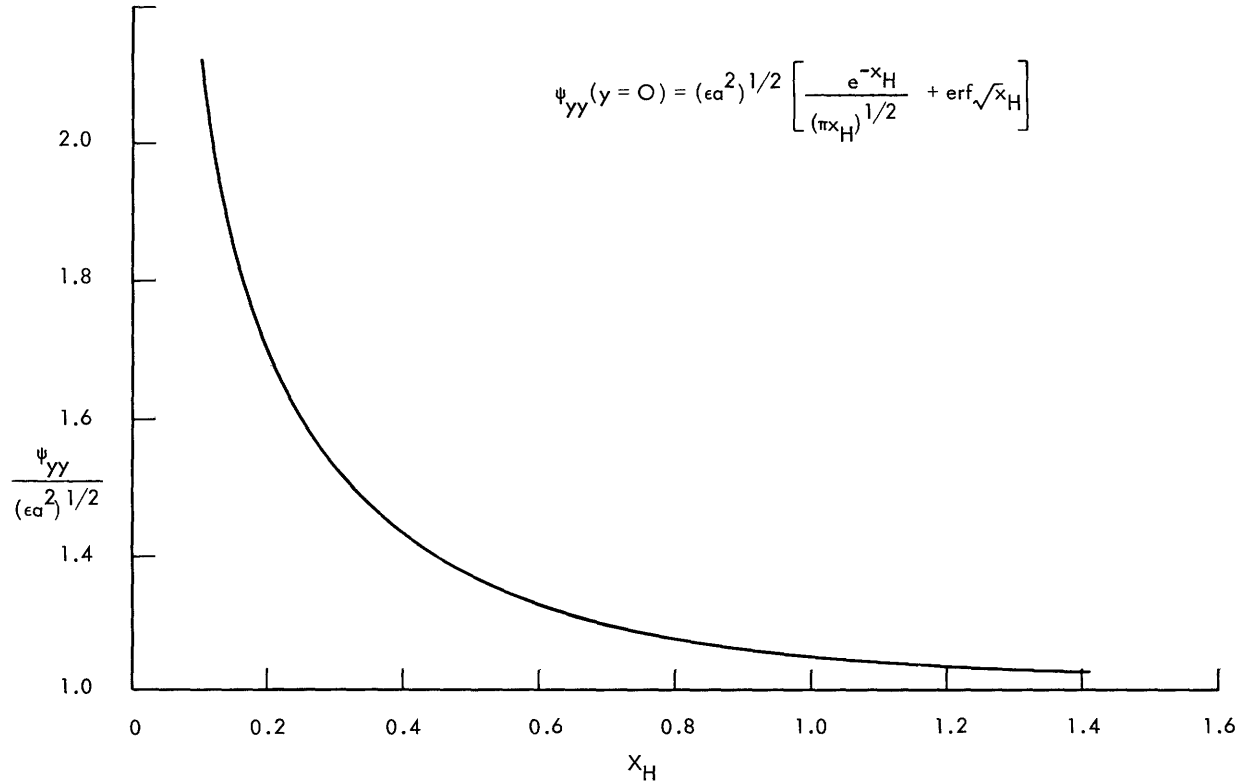


Fig. 8. Linearized solution for skin friction at plate.

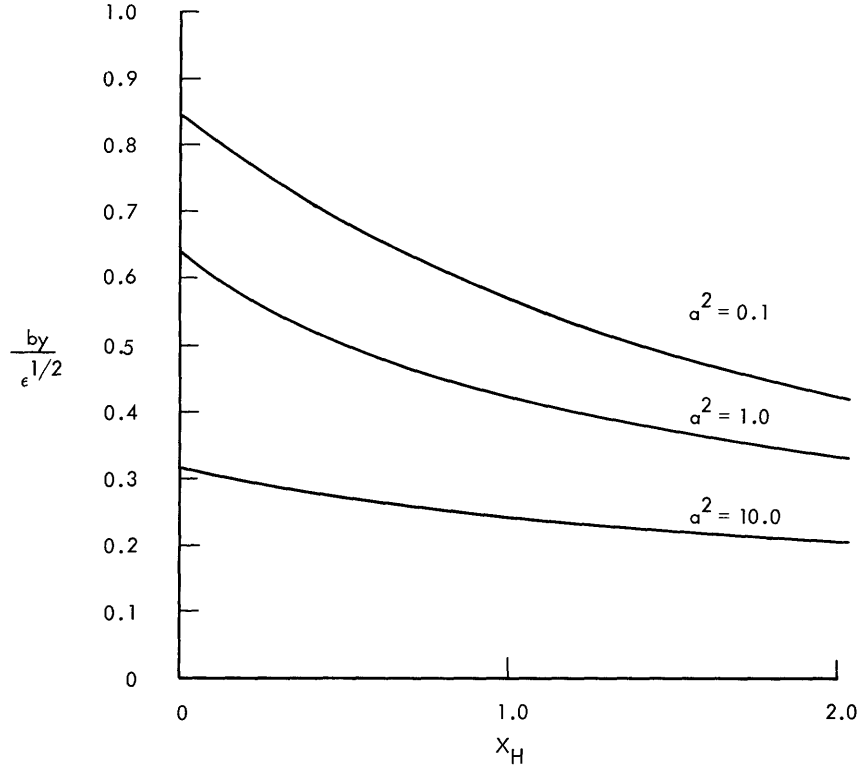


Fig. 9. Linearized solution for normal component of magnetic field at plate.

Eq. 43 can be attacked in a different manner, namely, by expanding ψ in a perturbation series in ϵa^2 , and the result for the skin friction so obtained can be compared with (80a). In Appendix II, the first two terms of this perturbation series are obtained, with the result

$$\psi_{yy}(y=0+) = \frac{1}{\sqrt{\pi x}} (1 - 2\epsilon a^2 + \epsilon a^2 x + \dots). \quad (81a)$$

In order to obtain a comparison, we must now expand (80a) for small values of $\epsilon a^2 x$:

$$\psi_{yy}(y=0+) = \frac{1}{\sqrt{\pi x}} (1 - \epsilon a^2 x + \dots) + \frac{2\sqrt{\epsilon a^2}}{\sqrt{\pi}} \int_0^{\epsilon a^2 x} (1 - y^2 + \dots) dy. \quad (81b)$$

Performing the integration and rearranging yields

$$\psi_{yy}(y=0+) = \frac{1}{\sqrt{\pi x}} (1 + \epsilon a^2 x). \quad (82)$$

A comparison of (81a) and (82) indicates that the results are identical for $x \gg 1$ and hence this is an additional restriction on (80a). (For the purposes of comparison $x \ll 1/\epsilon a^2$ if either of the expansions (81a) or (82) are to be valid.)

The physical basis of equation (80a) is easily seen. The first term is merely the

classical result of the pure fluid mechanics case multiplied by a decay factor. The second term is the skin friction attributed to a Hartmann boundary layer (that is, inertial forces become zero) multiplied by a growth factor. It is seen that the characteristic growth length, indicative of the distance from the leading edge at which the boundary layer is fully developed is given by $x_g = 1/\epsilon a^2$. If we introduce a characteristic length L , instead of ν/U_∞ , this yields $x_g^*/L = Re/H^2$, and the result is expected on dimensional grounds, since the ratio of the Reynolds number to the Hartmann number squared is merely the ratio of inertial forces to magnetic forces. It should be noted that this growth length is independent of viscosity.

From Fig. 9, it is seen that the maximum perturbation in the normal component of magnetic field at the plate occurs at the leading edge, and is of order $\epsilon^{1/2}$. This is physically reasonable, since more distortion is expected at higher conductivities (higher ϵ). Also, as a^2 is increased, the ultimate layer becomes thinner and is arrived at in a shorter distance; this indicates a smaller disturbance to the flow and hence one would expect the magnetic field distortion to decrease, which is indeed apparent in Fig. 9.

b. Comparison of the Linearized Problem with the Rayleigh Problem

We may expect a close analogy between the Rayleigh problem considered in Section II and the two-dimensional problem considered here when ϵ is small. It is of interest to examine this aspect more closely. If we differentiate Eq. 20 with respect to y and set $y = 0$, the skin friction of the Rayleigh problem is obtained:

$$-\frac{u_y}{U_0}(y=0) = \frac{1}{\sqrt{\pi t}} e^{-\epsilon t} + \sqrt{\epsilon} \operatorname{erf} \sqrt{\epsilon t}. \quad (83)$$

If t^* is replaced by x^*/U_∞ in Eq. 20, and the other dimensionless quantities are reformed so as to be consistent with those of this section, we obtain:

$$-\frac{1}{a} \frac{u_y}{U_0}(y=0) = \frac{1}{\sqrt{\pi a^2 x}} e^{-\epsilon a^2 x} + \sqrt{\epsilon} \operatorname{erf} \sqrt{\epsilon a^2 x} \quad (84)$$

which is identical to the result of the two-dimensional problem given in (73). The fact that these two expressions are identical confirms the fact that the analysis of the two-dimensional problem yields results that are qualitatively good and quantitatively poor.

c. Use of Weighted Averages for Linearization

It has been shown that, for small ϵ , the greatest deficiency in the linearization process was the replacement of u by $1 - u'$, with u' assumed small. From Eqs. 35 and 36, it is seen that the major effect of this linearization is in the inertial terms of Eq. 35, just as in the fluid mechanic case. If we write these terms using the vorticity, we have $u\xi_x + v\xi_y$, and hence the velocities govern the distribution of vorticity. It is obvious

that the average value $u = 1$ is a gross overestimate; in the fluid mechanic case, it has been found that selecting average values of $u = 0.335$, $v = 0$ distributes the vorticity in such a manner that the skin friction at the plate is identical to that obtained from the classical Blasius solution. It can be expected then that some improvement can be made in the present case by more judicious selection of this average value. For the present, we shall denote this value by K . Following through the preceding solution with this value, we find the skin friction and normal component of magnetic field at the plate to be given by

$$\psi_{yy}(y=0+) = \frac{1}{\sqrt{\pi x/K}} e^{-\epsilon a^2 x/K} + \sqrt{\epsilon a^2} \operatorname{erf} \sqrt{\epsilon a^2 x/K} \quad (85)$$

$$B_y(y=0) = \frac{1}{\pi \sqrt{K}} \int_0^{\epsilon a^2/K} \frac{(r+\epsilon)^{1/2} - r^{1/2}}{\left(\frac{\epsilon a^2}{K} - r\right)^{1/2} r^{1/2}} e^{-rx} dr - \frac{\epsilon}{K} e^{-\epsilon a^2 x/K}. \quad (86)$$

IV. NUMERICAL SOLUTION OF COMPLETE PROBLEM

4.1 FORMULATION OF NUMERICAL PROBLEM

a. General Remarks

From Sections II and III we have gained a great deal of insight into the problem of two-dimensional magnetohydrodynamic flow past a flat plate. For the case of ϵ small, we have obtained the qualitative behavior of this flow and the significant governing parameters. To obtain similar results for the case of ϵ not small (i.e., for significant magnetic-field distortion), and quantitatively useful results for all cases, it is necessary to resort to a more elaborate analysis. In the present case, this analysis takes the form of a numerical solution of the complete set of equations as formulated in Eqs. 35 or 35a and 36. This involves formulating the finite difference equations corresponding to the governing equations and boundary conditions, developing a solution technique for this set of simultaneous equations which is adaptable to a digital computer, and, finally, programming this procedure for digital computation. It is obvious that this is a complex process; there is no guarantee that the resulting finite difference equations can be solved in a feasible manner. It is therefore appropriate to mention that this phase of the problem must be approached with some spirit of adventure with regard to numerical techniques and that the technique employed here is the result of considerable trial and error. Furthermore, it should be emphasized that the purpose of this numerical analysis, in contrast to that of most numerical analyses, is to determine the character of the flow rather than to obtain a high degree of numerical accuracy.

b. Mathematical Model

Equations 35a and 36 comprise an elliptic set of equations, and the known conditions at the plate are not sufficient to treat the problem as an initial-value problem; hence the problem must be formulated as a boundary-value problem. The previously developed model of flow past a semi-infinite flat plate is obviously not readily adaptable to numerical techniques because of its infinite spacial extent. Some consideration must therefore be given to the construction of a mathematical model that adequately represents the desired flow and at the same time is readily adaptable to numerical techniques; in short, the model must have boundaries located at finite positions.

The model selected here can be visualized as the flow about a flat plate that is a member of a two-dimensional cascade of plates (Fig. 10). The boundaries parallel to the stream are then selected as the two lines of symmetry; one along the plate and one along the center line of a channel. The upstream boundary is selected at some arbitrary distance upstream from the leading edge, and the downstream boundary is selected some distance downstream from the leading edge. The boundary conditions at the center line and at the plate are determined from symmetry considerations and are given by

At $y = h$:

$$u_y = \psi_{yy} = 0$$

$$A_y = B_x = 0$$

$$\psi = \text{constant}$$

At $y = 0$ with $x_u \leq x < 0$:

$$u_y = \psi_{yy} = 0$$

$$A_y = +B_x = 0$$

$$\psi = 0$$

At $y = 0$ with $0 \leq x \leq l$:

$$u = \psi_y = 0$$

$$A_y = +B_x = 0$$

$$\psi = 0.$$

The conditions at the upstream and downstream boundaries are theoretically unknown in this problem. Physically, this means that whatever boundary conditions are employed here (unless by some fortuitous circumstance they are exact) will require placing fluid sources and sinks and electrical currents in the region outside the boundaries in order to satisfy the boundary conditions. However, by a careful choice of boundary conditions and positioning of boundaries, the contribution of these sources can be made small. In

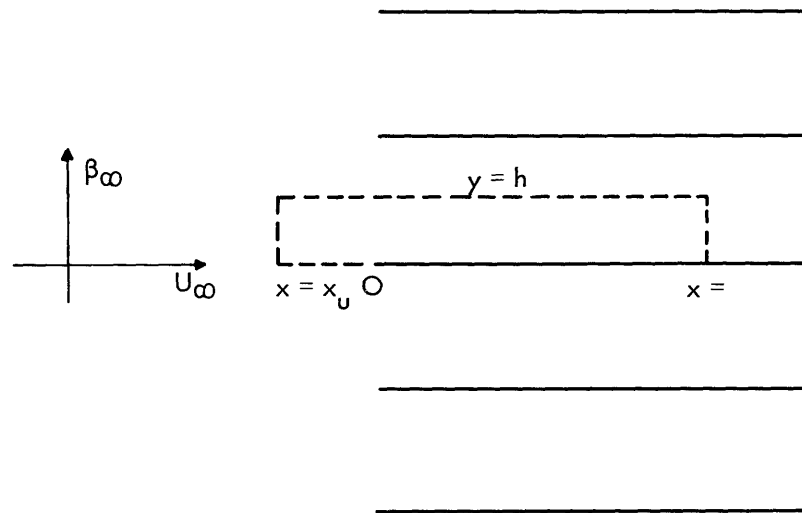


Fig. 10. Two-dimensional cascade of plates showing domain under consideration.

any case, this contribution can be evaluated by systematic repositioning of the boundaries. At the upstream boundary, we assume the flow to be uniform:

$$u = \psi_y = 1$$

$$v = -\psi_x = 0$$

$$B_y = -A_x = 1$$

$$B_x = A_y = 0; A = \text{constant.}$$

The downstream boundary condition is less well defined. For the present, we shall consider three types of boundary conditions on ψ and two types on A , with the understanding that some experimentation is necessary to determine the most suitable forms for each. The three types for ψ are:

ψ prescribed

$$\psi_x = 0$$

$$\psi_{xx} = 0.$$

The logical choice for ψ , if prescribed, is that obtained for Hartmann (fully developed, one-dimensional, laminar) flow in a channel of halfwidth h . The error incurred in this case is that due to placing the boundary at a distance insufficient for the complete development of Hartmann flow. The other two conditions on ψ are consistent with the Hartmann flow condition, but are weaker conditions (in the order listed); hence it is expected that the error incurred by placing the boundary at an insufficient downstream distance would be less than that for ψ prescribed.

The two types of conditions on A are:

$$A_x = -1$$

$$A_{xx} = 0.$$

The first condition represents the Hartmann flow condition that the normal magnetic-field component be unchanged from its upstream value. The second condition is consistent with the Hartmann condition and is somewhat weaker.

To complete the mathematical formulation it is convenient to introduce the vorticity into Eqs. 35a and 36 as an auxiliary variable. The governing equations then become

$$\nabla^2 \xi - R(\psi_x \xi_y - \psi_y \xi_x) = R \cdot Rm \cdot a^2 [-A_y(\psi_x A_y - \psi_y A_x)_x + A_x(\psi_x A_y - \psi_y A_x)_y] \quad (87)$$

$$\nabla^2 \psi = -\xi \quad (88)$$

$$\nabla^2 A = -Rm[\psi_x A_y - \psi_y A_x - 1], \quad (89)$$

where (89) may be introduced into (87) to obtain the form comparable to (35). (The introduction of a characteristic length here is somewhat artificial. It can be taken at any value, and the values of R and R_m adjusted accordingly. In the numerical computations, this length was adjusted for convenience in numerical magnitudes; all results, however, are presented in terms of the Reynolds number length, that is, $R = 1$, $R_m = \epsilon$ in the governing equations.) In the particular solution technique employed herein, these equations have the advantage that (87) is linear in ξ , (88) is linear in ψ , and (89) is linear in A . The boundary conditions in terms of these variables become:

At $y = h$:

$$\psi = \text{constant} \quad (90a)$$

$$\xi = 0 \quad (90b)$$

$$A_y = 0 \quad (90c)$$

At $y = 0$ with $x_u \leq x \leq 0$:

$$\psi = 0 \quad (91a)$$

$$\xi = 0 \quad (91b)$$

$$A_y = 0 \quad (91c)$$

At $y = 0$ with $0 \leq x \leq \ell$:

$$\psi_y = 0 \quad (92a)$$

$$\xi = -\psi_{yy} \quad (92b)$$

$$A_y = 0 \quad (92c)$$

At $x = x_u$:

$$\psi = y \quad (93a)$$

$$\xi = 0 \quad (93b)$$

$$A = \text{constant} \quad (93c)$$

At $x = \ell$:

$$(a) \begin{cases} \psi \text{ prescribed} & (94a) \\ \psi_x = 0 & (94b) \\ \psi_{xx} = 0 & (94c) \end{cases}$$

$$(b) \begin{cases} \xi \text{ prescribed} & (95a) \\ \xi_x = 0 & (95b) \\ \xi_{xx} = 0 & (95c) \end{cases}$$

$$(c) \begin{cases} A_x = -1 \\ A_{xx} = 0 \end{cases} \quad \begin{matrix} (96a) \\ (96b) \end{matrix}$$

This completes the mathematical formulation for the problem considered in the remainder of this section. Note that the variables are all governed by second-order equations, and therefore we should expect that prescribing each function or a value of a normal derivative along the boundaries will yield a mathematically well posed problem.

c. The Finite Difference Approximation

The standard finite difference procedure (for a comprehensive survey of finite difference methods see Crandall⁷) employed here is merely to replace our region of interest by some pattern of discrete points within this region, as shown in Fig. 11, and seek approximate values of the dependent variables at these points. The equations governing these approximate values are obtained from the governing equations and boundary conditions stated above by replacing the various derivatives with suitable finite difference approximations.

These finite difference approximations to the derivatives at a given point are obtained by expressing adjacent values of the dependent variable as Taylor's series expanded

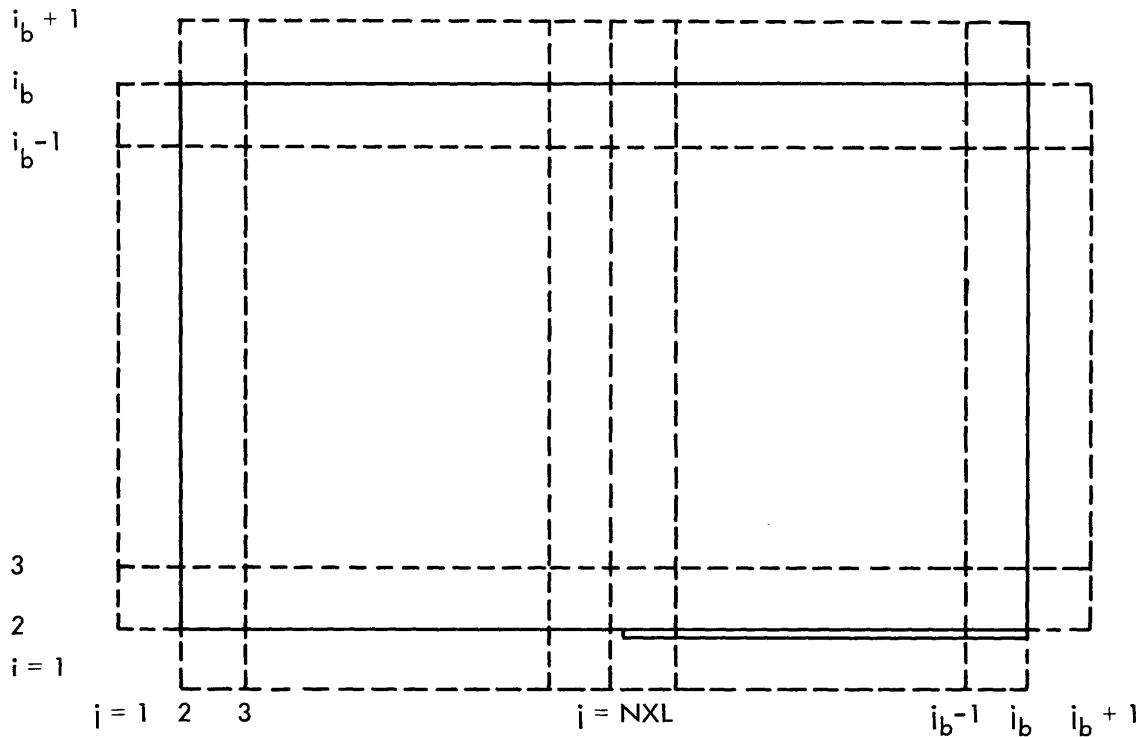
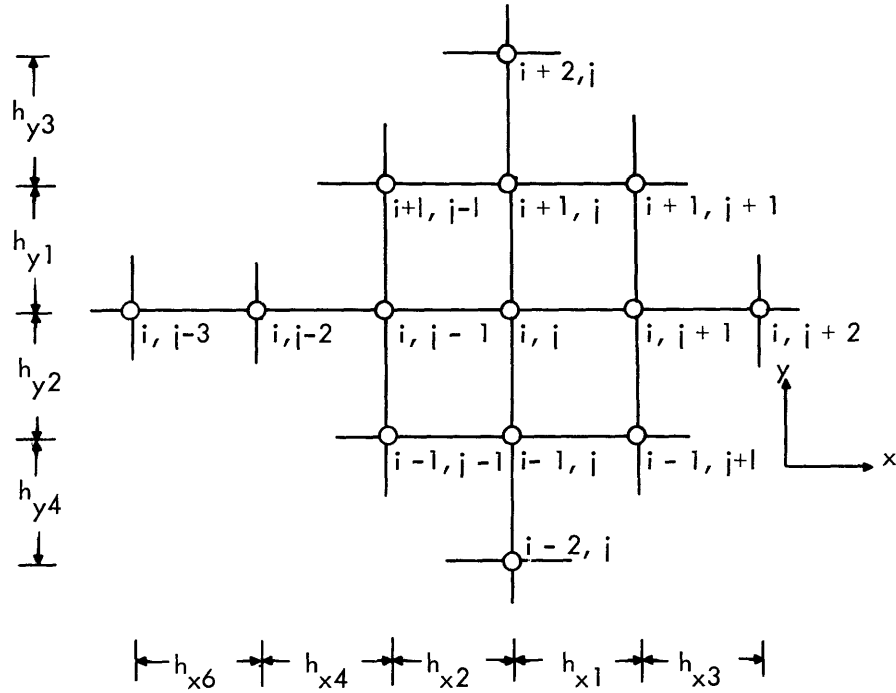


Fig. 11. Finite-difference net for the numerical problem.



$$c_1 = h_{x2}/h_{x1}$$

$$c_2 = h_{x3}/h_{x1}$$

$$c_3 = h_{x4}/h_{x1}$$

$$c_5 = h_{x6}/h_{x1}$$

$$d_1 = h_{y2}/h_{y1}$$

$$d_2 = h_{y3}/h_{y1}$$

$$d_3 = h_{y4}/h_{y1}$$

Fig. 12. General finite-difference net.

about the point of interest and solving the resultant equations for the desired derivative. It is evident that an ill-patterned array of points will lead to great algebraic complexity. For this reason, the most common procedure is to select a square net of discrete points; however, in the present case it is anticipated that in the region near the plate the stream function and vorticity will vary quite rapidly. This requires a very small net spacing to obtain reasonable accuracy, and if a square net were employed, would result in an enormous number of discrete net points. To avoid this difficulty, the net employed here is variably spaced, but is rectangular in order to retain some degree of simplicity in

the equations. It now remains to derive the appropriate finite difference equations for the various derivatives of interest.

To demonstrate the procedure, we consider the general net shown in Fig. 12, and seek appropriate approximations to the derivatives of a dependent variable, ψ say, at the point (i, j) . Writing the values ψ at the four nearest points as Taylor's series expansions yields:

$$\psi_{i+1,j} = \psi_{i,j} + h_{y1} \left(\frac{\partial \psi}{\partial y} \right)_{i,j} + \frac{h_{y1}^2}{2} \left(\frac{\partial^2 \psi}{\partial y^2} \right)_{i,j} + \frac{h_{y1}^3}{6} \left(\frac{\partial^3 \psi}{\partial y^3} \right)_{i,j} + \dots \quad (97a)$$

$$\psi_{i-1,j} = \psi_{i,j} - h_{y2} \left(\frac{\partial \psi}{\partial y} \right)_{i,j} + \frac{h_{y2}^2}{2} \left(\frac{\partial^2 \psi}{\partial y^2} \right)_{i,j} - \frac{h_{y2}^3}{6} \left(\frac{\partial^3 \psi}{\partial y^3} \right)_{i,j} + \dots \quad (97b)$$

$$\psi_{i,j+1} = \psi_{i,j} + h_{x1} \left(\frac{\partial \psi}{\partial x} \right)_{i,j} + \frac{h_{x1}^2}{2} \left(\frac{\partial^2 \psi}{\partial x^2} \right)_{i,j} + \frac{h_{x1}^3}{6} \left(\frac{\partial^3 \psi}{\partial x^3} \right)_{i,j} + \dots \quad (97c)$$

$$\psi_{i,j-1} = \psi_{i,j} - h_{x2} \left(\frac{\partial \psi}{\partial x} \right)_{i,j} + \frac{h_{x2}^2}{2} \left(\frac{\partial^2 \psi}{\partial x^2} \right)_{i,j} - \frac{h_{x2}^3}{6} \left(\frac{\partial^3 \psi}{\partial x^3} \right)_{i,j} + \dots \quad (97d)$$

Equations 97a and 97b can be solved for the first two derivatives in y , and (97c) and (97d) can be solved for the first two derivatives in x . The results are:

$$\left(\frac{\partial \psi}{\partial y} \right)_{i,j} = \frac{1}{h_{y1}} \left[-\frac{1}{d_1(1+d_1)} \psi_{i-1,j} + \frac{1-d_1^2}{d_1(1+d_1)} \psi_{i,j} + \frac{d_1}{1+d_1} \psi_{i+1,j} \right] - h_{y1} \frac{d_1}{6} \left(\frac{\partial^3 \psi}{\partial y^3} \right)_{i,j} + \dots \quad (98a)$$

$$\left(\frac{\partial^2 \psi}{\partial y^2} \right)_{i,j} = \frac{1}{h_{y1}^2} \left[\frac{2}{d_1(1+d_1)} \psi_{i-1,j} - \frac{2}{d_1} \psi_{i,j} + \frac{2}{1+d_1} \psi_{i+1,j} \right] - h_{y1} \frac{1-d_1^2}{3(1+d_1)} \left(\frac{\partial^3 \psi}{\partial y^3} \right)_{i,j} + \dots \quad (98b)$$

with analogous results for the x derivatives. It is seen that the truncation error is of order h^2 for the first derivative, and of order h (unless successive points are equally spaced) for the second derivative. The cross derivative $\partial^2 \psi / \partial x \partial y$ can be found in a similar way, if desired, by incorporating Taylor's series for ψ values at the diagonal points in Fig. 12. However, the approximation employed here for this derivative will be that obtained by differentiating (98a) with respect to x . As will be seen, this offers the advantage of reducing the storage requirements for digital computation.

Higher order derivatives can be obtained in a completely analogous way, by merely extending the net in Fig. 12 to include points at $(i-2, j)$, $(i+2, j)$, $(i, j-2)$, $(i, j+2)$.

Table I. Finite-difference approximations.

Accuracy: Even Derivatives; $O(h)$
Odd Derivatives; $O(h^2)$

| Der. | Coeff. | Value | Der. | Coeff. | Value |
|--|-------------|---|--|-------------|------------------------|
| $\frac{\partial \psi}{\partial x}$ | $F_{1x4,j}$ | $\frac{c_1}{1+c_1}$ | $\frac{\partial^2 \psi}{\partial x^2}$ | $F_{2x4,j}$ | $\frac{2}{1+c_1}$ |
| | $F_{1x3,j}$ | $\frac{1-c_1^2}{c_1(1+c_1)}$ | | $F_{2x3,j}$ | $-\frac{2}{c_1}$ |
| | $F_{1x2,j}$ | $-\frac{1}{c_1(1+c_1)}$ | | $F_{2x2,j}$ | $\frac{2}{c_1(1+c_1)}$ |
| Der. | Coeff. | Value | | | |
| $\frac{\partial^3 \psi}{\partial x^3}$ | $F_{3x5,j}$ | $\frac{6}{Dc_2} [(1+c_1)(1+c_3^3) - (1+c_1^3)(1+c_3)]$ | | | |
| | $F_{3x4,j}$ | $-\frac{6}{D} [(c_1+c_2)c_3^3 + (c_1-c_3)c_2^3 - (c_2+c_3)c_1^2]$ | | | |
| | $F_{3x3,j}$ | $- [F_{3x5,j} + F_{3x4,j} + F_{3x2,j} + F_{3x1,j}]$ | | | |
| | $F_{3x2,j}$ | $\frac{6}{Dc_1} [(1+c_3)(c_2^3 - 1) - (c_2-1)(1+c_3^3)]$ | | | |
| | $F_{3x1,j}$ | $-\frac{6}{Dc_3} [(1+c_1)(c_2^3 - 1) - (1+c_1^3)(c_2-1)]$ | | | |
| $\frac{\partial^4 \psi}{\partial x^4}$ | $F_{4x5,j}$ | $\frac{24}{Dc_2} [(1-c_1^2)(1+c_3) - (1+c_1)(1-c_3^2)]$ | | | |
| | $F_{4x4,j}$ | $\frac{24}{D} [(c_1-c_3)c_2^2 + (c_2+c_3)c_1^2 - (c_1+c_2)c_3^2]$ | | | |
| | $F_{4x3,j}$ | $- [F_{4x5,j} + F_{4x4,j} + F_{4x2,j} + F_{4x1,j}]$ | | | |
| | $F_{4x2,j}$ | $\frac{24}{Dc_1} [(c_2-1)(1-c_3^2) - (c_2^2-1)(1+c_3)]$ | | | |
| | $F_{4x1,j}$ | $-\frac{24}{Dc_3} [(1-c_1^2)(c_2-1) - (1+c_1)(c_2^2-1)]$ | | | |

Table I (continued)

| Der. | Coeff. | Skew Forms |
|---|-------------|--|
| $\frac{\partial^3 \psi}{\partial x^3}$ | $F_{3x4,j}$ | $+\frac{6}{D_1} [c_1^3(c_3-c_5)+c_3^3(c_5-c_1)+c_5^3(c_1-c_3)]$ |
| | $F_{3x3,j}$ | $- [F_{3x4,j}+F_{3x2,j}+F_{3x1,j}+F_{3x0,j}]$ |
| | $F_{3x2,j}$ | $-\frac{6}{D_1 c_1} [(1+c_3)(1+c_5^3)-(1+c_3^3)(1+c_5)]$ |
| | $F_{3x1,j}$ | $\frac{6}{D_1 c_3} [(1+c_1)(1+c_5^3)-(1+c_1^3)(1+c_5)]$ |
| | $F_{3x0,j}$ | $\frac{6}{D_1 c_5} [(1+c_1)(1+c_3^3)-(1+c_1^3)(1+c_3)]$ |
| $\frac{\partial^4 \psi}{\partial x^4}$ | $F_{4x4,j}$ | $-\frac{24}{D_1} [c_3(c_5^2-c_1^2)+c_5(c_1^2-c_3^2)+c_1(c_3^2-c_5^2)]$ |
| | $F_{4x3,j}$ | $- [F_{4x4,j}+F_{4x2,j}+F_{4x1,j}+F_{4x0,j}]$ |
| | $F_{4x2,j}$ | $\frac{24}{D_1 c_1} [(1+c_3)(1-c_5^2)-(1+c_5)(1-c_3^2)]$ |
| | $F_{4x1,j}$ | $-\frac{24}{D_1 c_3} [(1+c_1)(1-c_5^2)-(1+c_5)(1-c_1^2)]$ |
| | $F_{4x0,j}$ | $\frac{24}{D_1 c_5} [(1+c_1)(1-c_3^2)-(1+c_3)(1-c_1^2)]$ |
| $D = (1+c_1)(c_2^2-1)(1+c_3^3)+(1-c_1^2)(c_2^3-1)(1+c_3)+(1+c_1^3)(c_2-1)$ $(1-c_3^2)-(1+c_3)(c_2^2-1)(1+c_1^3)-(1-c_3^2)(c_2^3-1)(1+c_1)-(1+c_3^2)$ $(c_2-1)(1-c_1^2)$ | | |
| $D_1 = [(1+c_1)(1-c_3^2)(1+c_5^3)+(1+c_3)(1-c_5^2)(1+c_1^3)+(1+c_5)(1-c_1^2)$ $(1+c_3^3)-(1+c_1^3)(1-c_3^2)(1+c_5)-(1+c_3^3)(1-c_5^2)(1+c_1)-(1+c_5^3)$ $(1-c_1^2)(1+c_3)]$ | | |

In general, we shall adopt the notation that any derivative can be represented by the expressions:

$$\frac{\partial^n \psi}{\partial x^n} = \frac{1}{h_{x1}^n} \sum_{\ell=2}^4 F_{n\ell, j} \psi_{i, j+\ell-3} \quad 0 < n \leq 2 \quad (99)$$

$$\frac{\partial^n \psi}{\partial x^n} = \frac{1}{h_{x1}^n} \sum_{\ell=1}^5 F_{n\ell, j} \psi_{k, j+\ell-3} \quad 2 < n \leq 4 \quad (100)$$

or, with cross derivatives,

$$\frac{\partial^n \psi}{\partial x^m \partial y^{n-m}} = \frac{1}{h_{x1}^m h_{y1}^{n-m}} \sum_{\ell=2}^4 \sum_{k=2}^4 (F_{m\ell, j} F_{(n-m)k, i} \psi_{i+k-3, j+\ell-3}) \quad 0 < n \leq 4 \quad (101)$$

The complete results for x-derivatives up to and including the fourth order are listed in Table I.

d. Finite Difference Equations

It is now a relatively straightforward matter to construct the finite difference equations corresponding to the governing differential equations and boundary conditions formulated in section 4.1b. For every interior point of the finite difference net (Fig. 12) we have the following difference equations corresponding to (87), (88), and (89), respectively:

$$\begin{bmatrix} F_{2y4, i} + R \left(\frac{h_{y1}}{h_{x1}} \right) \left(\sum_{\ell} F_{1\ell, j} \psi_{i, j+\ell-3} \right) \cdot F_{1y4, i} \\ \left(\frac{h_{y1}^2}{h_{x1}^2} \right) F_{2x4, j} - R \left(\frac{h_{y1}}{h_{x1}} \right) \left(\sum_k F_{1yk, i} \psi_{i+k-3, j} \right) F_{1x4, j} \\ F_{2y3, i} + \left(\frac{h_{y1}^2}{h_{x1}^2} \right) F_{2x3, j} - R \left(\frac{h_{y1}}{h_{x1}} \right) \left[\sum_k F_{1yk, i} \psi_{i+k-3, j} \right. \\ \left. \times F_{1x3, j} - \left(\sum_{\ell} F_{1\ell, j} \psi_{i, j+\ell-3} \right) F_{1y3, i} \right] \\ \left(\frac{h_{y1}^2}{h_{x1}^2} \right) F_{2x2, j} - R \left(\frac{h_{y1}}{h_{x1}} \right) \left(\sum_k F_{1yk, i} \psi_{i+k-3, j} \right) \cdot F_{1x2, j} \\ F_{2y2, i} + R \left(\frac{h_{y1}}{h_{x1}} \right) \left(\sum_{\ell} F_{1\ell, j} \psi_{i, j+\ell-3} \right) F_{1y2, i} \end{bmatrix}^T \begin{bmatrix} \xi_{i+1, j} \\ \xi_{i, j+1} \\ \xi_{i, j} \\ \xi_{i, j-1} \\ \xi_{i-1, j} \end{bmatrix} = [FF \xi_{i, j}] \quad (102)$$

$$\begin{bmatrix} F_{2y4,i} \\ \left(\frac{h_{y1}^2}{h_{x1}^2}\right) F_{2x4,j} \\ F_{2y3,i} + \left(\frac{h_{y1}^2}{h_{x1}^2}\right) F_{2x3,j} \\ \left(\frac{h_{y1}^2}{h_{x1}^2}\right) F_{2x2,j} \\ F_{2y2,i} \end{bmatrix}^T \begin{bmatrix} \psi_{i+1,j} \\ \psi_{i,j+1} \\ \psi_{i,j} \\ \psi_{i,j-1} \\ \psi_{i-1,j} \end{bmatrix} = \begin{bmatrix} -\xi_{i,j} h_{y1}^2 \end{bmatrix} \quad (103)$$

$$\begin{bmatrix} F_{2y4,i} + \text{Rm} \left(\frac{h_{y1}}{h_{x1}} \right) \left(\sum_{\ell} F_{1x\ell,j} \psi_{i,j+\ell-3} \right) F_{1y4,i} \\ \left(\frac{h_{y1}^2}{h_{x1}^2} \right) F_{2x4,j} - \text{Rm} \left(\frac{h_{y1}}{h_{x1}} \right) \left(\sum_k F_{1yk,i} \psi_{i+k-3,j} \right) F_{1x4,j} \\ \left(\frac{h_{y1}^2}{h_{x1}^2} \right) F_{2x3,j} + F_{2y3,i} + \text{Rm} \left(\frac{h_{y1}}{h_{x1}} \right) \left[\left(\sum_{\ell} F_{1x\ell,j} \psi_{i,j+\ell-3} \right) \right. \\ \left. \times F_{1x3,i} - \left(\sum_k F_{1yk,i} \psi_{i+k-3,j} \right) F_{1x3,j} \right] \\ \left(\frac{h_{y1}^2}{h_{x1}^2} \right) F_{2x2,j} - \text{Rm} \left(\frac{h_{y1}}{h_{x1}} \right) \left(\sum_k F_{1yk,i} \psi_{i+k-3,j} \right) F_{1x2,j} \\ F_{2y2,i} + \text{Rm} \left(\frac{h_{y1}}{h_{x1}} \right) \left(\sum_{\ell} F_{1x\ell,j} \psi_{i,j+\ell-3} \right) F_{1y2,i} \end{bmatrix}^T \begin{bmatrix} A_{i+1,j} \\ A_{i,j+1} \\ A_{i,j} \\ A_{i,j-1} \\ A_{i-1,j} \end{bmatrix} = \begin{bmatrix} \text{Rm} \cdot h_{y1}^2 \end{bmatrix} \quad (104)$$

Here, we define

$$FF\xi_{i,j} = \frac{(R)(\text{Rm})(a^2)}{h_{x1}^2} \left\{ 2 \left(\sum_{\ell} F_{1x\ell,j} A_{i,j+\ell-3} \right) \left(\sum_k \sum_{\ell} F_{1x\ell,j} F_{1y\ell,i} \psi_{i+k-3,j+\ell-3} \right) \right\}$$

$$\begin{aligned}
& \times \left(\sum_k F_{1yk, i} A_{i+k-3, j} \right) + \left(\sum_\ell F_{1x\ell, j} A_{i, j+\ell-3} \right) \left[\left(\sum_\ell F_{1x\ell, j} \psi_{i, j+\ell-3} \right) \right. \\
& \times \left(\sum_k F_{2yk, i} A_{i+k-3, j} \right) - \left(\sum_k F_{2yk, i} \psi_{i+k-3, j} \right) \left(\sum_\ell F_{1x\ell, j} A_{i, j+\ell-3} \right) \\
& - \left(\sum_k F_{1yk, i} \psi_{i+k-3, j} \right) \left(\sum_k \sum_\ell F_{1yk, i} F_{1x\ell, j} A_{i+k-3, j+\ell-3} \right) \Big] \\
& - \left(\sum_k F_{1yk, i} A_{i+k-3, j} \right) \left[\left(\sum_\ell F_{2x\ell, j} \psi_{i, j+\ell-3} \right) \left(\sum_k F_{1yk, i} A_{i+k-3, j} \right) \right. \\
& + \left(\sum_\ell F_{1x\ell, j} \psi_{i, j+\ell-3} \right) \left(\sum_k \sum_\ell F_{1x\ell, j} F_{1yk, i} A_{i+k-3, j+\ell-3} \right) \\
& \left. \left. - \left(\sum_k F_{1yk, i} \psi_{i+k-3, j} \right) \left(\sum_\ell F_{2x\ell, j} A_{i, j+\ell-3} \right) \right] \right\} \quad (105)
\end{aligned}$$

for the form corresponding to (87) and (35a), and

$$\begin{aligned}
FF\xi_{i, j} = & -\frac{(R)(a^2)}{h_{x1}h_{y1}} \left\{ \left(\sum_\ell F_{1x\ell, j} A_{1, j+\ell-3} \right) \left[\left(\frac{h_{y1}^2}{h_{x1}^2} \right) \left(\sum_k \sum_\ell F_{2x\ell, j} F_{1yk, i} A_{i+k-3, j+\ell-3} \right) \right. \right. \\
& + \sum_{k=1}^5 F_{3yk, \ell} A_{i+k-3, j} \Big] - \left(\sum_k F_{1yk, i} A_{i+k-3, j} \right) \left[\left(\frac{h_{y1}^2}{h_{x1}^2} \right) \left(\sum_{\ell=1}^5 F_{3x\ell, j} A_{i, j+\ell-3} \right) \right. \\
& \left. \left. + \sum_k \sum_\ell F_{1x\ell, j} F_{2yk, i} A_{i+k-3, j+\ell-3} \right] \right\} \quad (106)
\end{aligned}$$

for the form corresponding to (35). The summations k and ℓ are understood to occur over 2, 4 unless otherwise indicated.

Some consideration must be given to the net points at which the equations above may be written; this depends upon the boundary conditions employed. We shall employ the standard procedure consistent with second-order equations that if a function is prescribed at a boundary, then the finite difference equation is not written at that point. If, however, a normal derivative is prescribed, then the finite difference equation is written at the point, thereby introducing a fictitious point outside the boundary. The value of the function at this fictitious point may be found from the boundary condition. Following this procedure, we see from Eqs. 90-96 that the points at which Eqs. 102-104 are written are as follows:

$$\text{Equation 102: } 3 \leq i \leq i_b - 1, \quad 3 \leq j \leq j_b - 1 \quad \text{if (95a) is used}$$

$$3 \leq i \leq i_b - 1, \quad 3 \leq j \leq j_b - 1 \quad \text{if (95b, c) are used}$$

Equation 103: $3 \leq i \leq i_b - 1, 3 \leq j \leq j_b - 1$ if (94a) is used

$3 \leq i \leq i_b - 1, 3 \leq j \leq j_b$ if (94b, c) are used

Equation 104: $2 \leq i \leq i_b, 3 \leq j \leq j_b$.

If the form (106) is employed for $FF\xi_{i,j}$ in (102), then the summations representing third derivatives of A must be replaced by their appropriate skew forms (Table I) at the boundary points so that only one fictitious point is introduced. In addition, note that Eq. 104 written along the boundaries $i = 2, i = i_b, j = j_b$ requires values of ψ at the external points $i = 3, i = i_b + 1, j = j_b + 1$; these values are obtained by solving Eq. 103 written at the respective boundary points.

The finite difference forms of boundary conditions (90)-(96) are listed in Table II, with their corresponding points of application. Anticipating somewhat the technique of solution to be employed, we shall combine these equations with the governing difference equations in such a manner that, if the other two independent variables are known, equations of the form (102), (103), and (104) may be solved simultaneously for ξ, ψ , and A, respectively, where the values of the dependent variable at fictitious points have been eliminated from the relevant set of equations. The values at these fictitious points are then obtained by utilizing the values obtained from the simultaneous solution and the boundary conditions.

The general form of these equations is then

$$\begin{bmatrix} C1Q_{i,j} \\ C2Q_{i,j} \\ C3Q_{i,j} \\ C4Q_{i,j} \\ C5Q_{i,j} \end{bmatrix}^T \begin{bmatrix} Q_{i+1,j} \\ Q_{i,j+1} \\ Q_{i,j} \\ Q_{i,j-1} \\ Q_{i-1,j} \end{bmatrix} = [FFQ_{i,j}] \quad (107)$$

where Q may be ξ, ψ , or A. These coefficients, for each variable, are defined in Table III for each of the downstream boundary conditions listed in Table II. Also included in Table III are the regions of the net where equations of the form (107) apply, and the equations yielding values of the variables at the fictitious net points. Hence Table III is a summary of the complete finite difference problem formulation, restricted, however, to the use of Eq. 105 for $FF\xi_{i,j}$.

e. Modifications for Numerical Accuracy

Since $A \sim x$ and $\psi \sim y$ at a number of net points (those where the disturbance is small), the expressions of the type $\sum_{\ell} F_{nx\ell,j} \psi_{i,j+\ell-3}$ and $\sum_k F_{nyk,i} A_{i+k-3,j}$ may involve small

Table II. Finite-difference form of boundary conditions.

| Math Condition (Equation No.) | Finite Difference Equation | Points of Application |
|----------------------------------|--|----------------------------|
| 90a | $\psi_{1j} = y_1$ | $1=1_b, 3 \leq j \leq j_b$ |
| 90b | $\xi_{1j} = 0$ | $1=1_b, 3 \leq j \leq j_b$ |
| 90c | $\sum_{k=2}^4 F_{1yk,i} A_{1+k-3,j} = 0$ | $1=1_b, 3 \leq j \leq j_b$ |
| 91a | $\psi_{1j} = 0$ | $1=2, 3 \leq j < NXL$ |
| 91b | $\xi_{1j} = 0$ | $1=2, 3 \leq j < NXL$ |
| 91c | $\sum_{k=2}^4 F_{1yk,i} A_{1+k-3,j} = 0$ | $1=2, 3 \leq j < NXL$ |
| 92a | $\sum_{k=2}^4 F_{1yk,i} \psi_{1+k-3,j} = 0$ | $1=2, NXL \leq j \leq j_b$ |
| 92b | $\xi_{1j} = - \sum_{k=2}^4 F_{2yk,i} \psi_{1+k-3,j}$ | $1=2, NXL \leq j \leq j_b$ |
| 92c | $\sum_{k=2}^4 F_{1yk,i} A_{1+k-3,j} = 0$ | $1=2, NXL \leq j \leq j_b$ |
| 93a | $\psi_{1j} = y_1$ | $2 \leq i \leq 1_b, j=2$ |
| 93b | $\xi_{1j} = 0$ | $2 \leq i \leq 1_b, j=2$ |
| 93c | $A_{1j} = 0$ | $2 \leq i \leq 1_b, j=2$ |
| 94a | $\psi_{1j} = \left(\psi_P \right)_{1j}$ | $2 < i < 1_b, j=j_b$ |
| 94b | $\sum_{l=2}^4 F_{1xl,j} \psi_{1,j+l-3} = 0$ | $2 < i < 1_b, j=j_b$ |

Table II (continued)

| Math Condition (Equation No.) | Finite Difference Equation | Points of Application |
|----------------------------------|--|------------------------------|
| 94c | $\sum_{l=2}^4 F_{2xl,j} \psi_{1,j+l-3} = 0$ | $2 \leq i \leq i_b, j = j_b$ |
| 95a | $\xi_{1j} = \left(\xi_P \right)_{1j}$ | $2 \leq i \leq i_b, j = j_b$ |
| 95b | $\sum_{l=2}^4 F_{1xl,j} \xi_{1,j+l-3} = 0$ | $2 \leq i \leq i_b, j = j_b$ |
| 95c | $\sum_{l=2}^4 F_{2xl,j} \xi_{1,j+l-3} = 0$ | $2 \leq i \leq i_b, j = j_b$ |
| 96a | $\sum_{l=2}^4 F_{2xl,j} A_{1,j+l-3} = -h_{x1}^2$ | $2 \leq i \leq i_b, j = j_b$ |
| 96b | $\sum_{l=2}^4 F_{2xl,j} A_{1,j+l-3} = 0$ | $2 \leq i \leq i_b, j = j_b$ |

differences of large numbers. Numerical calculations have indicated that this poses a problem in the computation of $FF\xi$. To alleviate this difficulty, expressions of this type are replaced by

$$\sum_l F_{nxl,j} (\psi_{i,j+l-3} - \psi_{i,j}) = F_{nx2,j} \psi_{i,j-1} + F_{nx4,j} \psi_{i,j+1}$$

and

$$\sum_k F_{nyk,i} (A_{i+k-3,j} - A_{i,j}) = F_{ny2,i} A_{i-1,j} + F_{ny4,i} A_{i+1,j},$$

respectively. These expressions have the same value as the original ones, since

$$\sum_l F_{nxl,j} = \sum_k F_{nyk,i} = 0.$$

f. Leading-Edge Singularity

Before proceeding to a discussion of the technique employed for solving the finite difference equations, some consideration must be given to the nature of the solution at the leading edge of the plate. It appears fairly certain that in the solution of the differential problem in the purely fluid mechanics case, the vorticity will be singular at the leading edge (see Lin and Carrier²⁵), and hence it is expected that it will be singular in the magnetohydrodynamic case. Obviously, the finite difference problem will not yield a satisfactory approximation to the vorticity function in the region of leading edge.

Table III. Complete finite-difference formulation.

| VORTICITY FUNCTION | | | | | |
|-------------------------------|--|--|---|--------------------------------------|---|
| Downstream Boundary Condition | Region of Application | COEFFICIENT DEFINITION | | AUXILIARY POINTS | |
| | | Region | Definition | Region | Given By: |
| I: (95a) | $3 \leq i \leq b-1$ $3 \leq j \leq b-1$ | $3 \leq i \leq b-1$ $3 \leq j \leq b-1$ | As Defined by (102), (105) ¹¹ | ----- | None Required |
| II: (95b) | $3 \leq i \leq b-1$ $3 \leq j \leq b$ | (a) $3 \leq i \leq b-1$ $3 \leq j \leq b-1$ (b) $3 \leq i \leq b-1$ $j = j_b$ | As Defined by (102), (105), (106) $C2^{\xi}_{1,j} = 0$ $C3^{\xi}_{1,j} = C3^{\xi}_{1,j}(102) - C2^{\xi}_{1,j}(102) \frac{F_{1x3,j}}{F_{1x4,j}}$ $C4^{\xi}_{1,j} = C4^{\xi}_{1,j}(102) - C2^{\xi}_{1,j}(102) \frac{F_{1x2,j}}{F_{1x4,j}}$ | $3 \leq i \leq b-1$ $j = j_b + 1$ | $\xi_{1,j} = \frac{-[(F_{1x2,j-1})(\xi_{1,j-2}) + (F_{1x3,j-1})(\xi_{1,j-1}))]}{F_{1x4,j-1}}$ |
| III: (95c) | $3 \leq i \leq b-1$ $3 \leq j \leq b$ | (a) $3 \leq i \leq b-1$ $3 \leq j \leq b-1$ (b) $3 \leq i \leq b-1$ $j = j_b$ | As Defined by (102), (105), (106) $C2^{\xi}_{1,j} = 0$ $C3^{\xi}_{1,j} = C3^{\xi}_{1,j}(102) - C2^{\xi}_{1,j}(102) \frac{F_{2x3,j}}{F_{2x4,j}}$ $C4^{\xi}_{1,j} = C4^{\xi}_{1,j}(102) - C2^{\xi}_{1,j}(102) \frac{F_{2x2,j}}{F_{2x4,j}}$ | $3 \leq i \leq b-1$ $j = j_b + 1$ | $\xi_{1,j} = \frac{-[(F_{2x2,j-1})(\xi_{1,j-2}) + (F_{2x3,j-1})(\xi_{1,j-1}))]}{F_{2x4,j-1}}$ |

11. Unless otherwise specified, all coefficients are defined by equations (102), (103), or (104). To avoid confusion the notation $C1^{\xi}_{1,j}(102)$ also indicates a coefficient defined by these equations.

Table III (continued)

| STREAM FUNCTION, | | | | |
|-------------------------------|--|--|---------------------|--|
| Downstream Boundary Condition | COEFFICIENT DEFINITION | | AUXILIARY POINTS | |
| | Region of Application | Region | Definition | Region |
| I: (94a) | $3 \leq i \leq b-1$ $3 \leq j \leq b$ | $3 \leq i \leq b-1$ $3 \leq j \leq b$ | As Defined by (103) | (a) $3 \leq i \leq b$ $i=1, b+1$ |
| | | | | $\psi_{1,j} = \frac{-[(P_{2x2,i-1})(\psi_{1-2,i}) + (P_{2y3,i-1})(\psi_{1-1,i})]}{P_{2x4,i-1}}$ |
| | | | | (b) $3 \leq j \leq NXL$ $i=1$ |
| | | | | $\psi_{1,j} = \frac{-[(P_{2x4,i+1})(\psi_{1+2,j}) + (P_{2y3,i+1})(\psi_{1+1,j})]}{P_{2y2,i+1}}$ |
| II: (94b) | $3 \leq i \leq b-1$ $3 \leq j \leq b$ | $3 \leq i \leq b-1$ $3 \leq j \leq b$ | As Defined by (103) | (c) $NXL \leq j \leq b$ $i=1$ |
| | | | | $\psi_{1,j} = \frac{-[(P_{1y4,i+1})(\psi_{1+2,j}) + (P_{1y3,i+1})(\psi_{1+1,j})]}{P_{1y2,i+1}}$ |
| | | | | (d) $2 \leq i \leq b$ $j=j_b+1$ |
| | | | | $\psi_{1,j} = \frac{1}{PPV_{1,j-1}} \begin{bmatrix} C1V_{1,j-1} & V_{1+1,j-1} \\ C3V_{1,j-1} & \psi_{1,j-1} \\ C4V_{1,j-1} & \psi_{1,j-2} \\ C5V_{1,j-1} & \psi_{1+1,j-1} \end{bmatrix}$ |
| III: (94c) | $3 \leq i \leq b-1$ $3 \leq j \leq b$ | $3 \leq i \leq b-1$ $3 \leq j \leq b$ | As Defined by (103) | (a) $3 \leq j \leq b$ $i=1, b+1$ |
| | | | | Same as (a) above |
| | | | | (b) $3 \leq j \leq NXL$ $i=1$ |
| | | | | Same as (b) above |
| | $3 \leq i \leq b-1$ $3 \leq j \leq b$ | $3 \leq i \leq b-1$ $3 \leq j \leq b$ | As Defined by (103) | (c) $NXL \leq j \leq b$ $i=1$ |
| | | | | Same as (c) above |
| | | | | (d) $2 \leq i \leq b$ $j=j_b+1$ |
| | | | | $\psi_{1,j} = \frac{-[(F_{1x2,i-1})(\psi_{1,i-2}) + (F_{1x3,i-1})(\psi_{1,i-1})]}{F_{1x4,i-1}}$ |
| | $3 \leq i \leq b-1$ $3 \leq j \leq b$ | $3 \leq i \leq b-1$ $3 \leq j \leq b$ | As Defined by (103) | (a) $3 \leq j \leq b$ $i=1, b+1$ |
| | | | | Same as (a) above |
| | | | | (b) $3 \leq j \leq NXL$ $i=1$ |
| | | | | Same as (b) above |
| | $3 \leq i \leq b-1$ $3 \leq j \leq b$ | $3 \leq i \leq b-1$ $3 \leq j \leq b$ | As Defined by (103) | (c) $NXL \leq j \leq b$ $i=1$ |
| | | | | Same as (c) above |
| | | | | (d) $2 \leq i \leq b$ $j=j_b+1$ |
| | | | | $\psi_{1,j} = \frac{-[(F_{2x2,i-1})(\psi_{1,i-2}) + (F_{2x3,i-1})(\psi_{1,i-1})]}{F_{2x4,i-1}}$ |

Table III (continued)

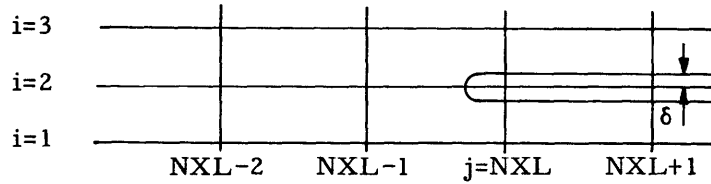
| MAGNETIC POTENTIAL FUNCTION, A | | | | | |
|--------------------------------|--|--|---|--------------------------------------|---|
| Downstream Boundary Condition | Region of Application | COEFFICIENT DEFINITION | | AUXILIARY POINTS | |
| | | Region | Definition | Region | Given By: |
| I: (96a) | $2 \leq i \leq i_b$ $3 \leq j \leq j_b$ | (a) $3 \leq i \leq i_b - 1$ $3 \leq j \leq j_b - 1$ | As Defined by (104) | (a) $3 \leq i \leq i_b$ $i = i_b$ | $A_{i+1,j} = \frac{-[F_{1y2,i} A_{i-1,j} + F_{1y3,i} A_{i,j}]}{F_{1y4,i}}$ |
| | | (b) $i = i_b$ $3 \leq j \leq j_b - 1$ | $C1A_{1,j} = 0$ $C3A_{1,j} = C3A_{1,j}(104) - C1A_{1,j}(104) \frac{F_{1y3,i}}{F_{1y4,i}}$ | (b) $3 \leq i \leq i_b$ $i = 2$ | $A_{i-1,j} = \frac{-[F_{1y3,i} A_{i,j} + F_{1y4,i} A_{i+1,j}]}{F_{1y2,i}}$ |
| | | (c) $i = 2$ $3 \leq j \leq j_b - 1$ | $C5A_{1,j} = C5A_{1,j}(104) - C1A_{1,j}(104) \frac{F_{1y2,i}}{F_{1y4,i}}$ | (c) $2 \leq i \leq i_b$ $j = j_b$ | $A_{i,j+1} = \frac{-[h_{x1} + F_{1x2,i} A_{i,j-1} + F_{1x3,i} A_{i,j}]}{F_{1x4,j}}$ |
| | $3 \leq i \leq i_b - 1$ | (c) $i = 2$ | $C1A_{1,j} = C1A_{1,j}(104) - C5A_{1,j}(104) \frac{F_{1y4,i}}{F_{1y2,i}}$ $C3A_{1,j} = C3A_{1,j}(104) - C5A_{1,j}(104) \frac{F_{1y3,i}}{F_{1y2,i}}$ $C5A_{1,j} = 0$ | | |
| | | (d) $3 \leq i \leq i_b - 1$ $j = j_b$ | $C2A_{1,j} = 0$ $C3A_{1,j} = C3A_{1,j}(104) - C2A_{1,j}(104) \frac{F_{1x3,i}}{F_{1x4,j}}$ $C4A_{1,j} = C4A_{1,j}(104) - C2A_{1,j}(104) \frac{F_{1x2,i}}{F_{1x4,j}}$ $FPA_{1,j} = FPA_{1,j}(104) + C2A_{1,j}(104) \frac{h_{x1}}{F_{1x4,j}}$ | | |
| | | (e) $i = i_b$ $j = j_b$ | $C1A_{1,j} = 0$ $C2A_{1,j} = 0$ $C3A_{1,j} = C3A_{1,j}(104) - C2A_{1,j}(104) \frac{F_{1x2,i}}{F_{1x4,j}}$ $C4A_{1,j} = C4A_{1,j}(104) - C2A_{1,j}(104) \frac{F_{1x3,i}}{F_{1x4,j}}$ $C5A_{1,j} = C5A_{1,j}(104) - C1A_{1,j}(104) \frac{F_{1y2,i}}{F_{1y4,i}}$ | | |

Table III (continued)

| MAGNETIC POTENTIAL FUNCTION, A (Cont'd) | | | | | AUXILIARY POINTS | |
|---|--|--|---|--|--|--|
| Downstream Boundary Condition | Region of Application | COEFFICIENT DEFINITION | | Region | Given By: | |
| | | Region | Definition | | | |
| I: (96a) | $2 \leq i \leq i_b$ $3 \leq j \leq j_b$ | (f) $i=2$ $j=j_b$ | $C1A_{1,j} = C1A_{1,j}(104) - C5A_{1,j}(104) \frac{F_{1y4,1}}{F_{1y2,1}}$ $C2A_{1,j} = 0$ | | | |
| | | | $C3A_{1,j} = C3A_{1,j}(104) - C2A_{1,j}(104) \frac{F_{1x3,1}}{F_{1x4,1}}$ $- C5A_{1,j}(104) \frac{F_{1y3,1}}{F_{1y2,1}}$ | | | |
| | | | $C4A_{1,j} = C4A_{1,j}(104) - C2A_{1,j}(104) \frac{F_{1x2,1}}{F_{1x4,1}}$ | | | |
| | | | $C5A_{1,j} = 0$ | | | |
| | | | As Defined by (104) | (a) $3 \leq i \leq i_b$ $3 \leq j \leq j_b$ | $A_{i+1,j} = \frac{-[F_{1y2,1}A_{1,j-1} + F_{1y3,1}A_{1,j}]}{F_{1y4,1}}$ | |
| II: (96b) | $2 \leq i \leq i_b$ $3 \leq j \leq j_b$ | (a) $3 \leq i \leq i_b - 1$ $3 \leq j \leq j_b - 1$ | | | Same as (b) on preceding page | |
| | | (b) $i=i_b$ $3 \leq j \leq j_b - 1$ | | | | |
| | | (c) $i=2$ $3 \leq j \leq j_b - 1$ | | | | |
| | | (d) $3 \leq i \leq i_b - 1$ $j=j_b$ | $C2A_{1,j} = 0$ $C3A_{1,j} = C3A_{1,j}(104) - C2A_{1,j}(104) \frac{F_{2x3,1}}{F_{2x4,1}}$ | | | |
| | | | $C4A_{1,j} = C4A_{1,j}(104) - C2A_{1,j}(104) \frac{F_{2x2,1}}{F_{2x4,1}}$ | | | |
| | | (e) $i=i_b$ $j=j_b$ (f) $i=2$ $j=j_b$ | Replace F_{1x1} by F_{2x1} in (c) on preceding page ($i = 2, 3, 4$) Replace F_{1x1} by F_{2x1} in (f) above | | | $A_{1,j+1} = \frac{-[F_{2x2,1}A_{1,j-1} + F_{2x3,1}A_{1,j}]}{F_{2x4,1}}$ |

The major question is then whether the error in the finite difference approximation can be confined to a small area surrounding the leading edge.

Physically, there is reason to believe that this error can be confined to the vicinity of the leading edge. Consider a finite difference net in the region of a plate with finite thickness and a rounded leading edge as sketched below.



The solution to the corresponding differential problem will possess no singularities, and it is expected that a satisfactory finite difference approximation can be achieved. If, however, the net spacing, h , is such that $h \gg \delta$, but is still small compared with the boundary layer thickness a short distance downstream of the leading edge, it is expected that the solution to the finite difference problem will be in error around the leading edge, but will be accurate away from the leading edge. In this case, the finite difference problem is essentially independent of the thickness of the plate, and hence is identical to the problem considered here. Numerical evidence is presented in section 4.3 which supports this conclusion. It is noted in passing that the position of the leading edge in the finite difference problem is defined only with respect to the including x interval.

4.2 SOLUTION TECHNIQUE

a. General Method

Performing a direct solution of the equations for ψ , ξ , and A involves the simultaneous solution of a set of approximately $3(i_b - 3)(j_b - 3)$ nonlinear algebraic equations. For a net of reasonable size, this is not a feasible procedure. Therefore the general method employed here is one of iteration, where the equations for ψ , ξ , and A are solved separately, under the assumption that the other two dependent variables are known, and hence involves only linear algebraic equations. The specific procedure is as follows:

- (i) Estimate the unknown values of ξ and A at the net points.
- (ii) Solve the stream function (ψ) equations, using current values of ξ and A .
- (iii) Calculate the vorticity at the plate from the current ψ values.
- (iv) Solve the vorticity (ξ) equations, using current ψ and A values and the values of ξ at the plate calculated in (iii).
- (v) Repeat steps (ii)-(iv) until satisfactory agreement is obtained between two successive sets of values of ξ .
- (vi) Solve the magnetic potential (A) equations, using current values of ψ and ξ .
- (vii) Repeat steps (ii)-(vi) until satisfactory agreement between two successive sets of values of A are obtained.

There are a few details of this procedure which merit additional mention. First, in all cases reported here, the initial estimates of A were those corresponding to a uniform transverse magnetic field; hence the completion of step (v) yields a solution for no magnetic-field distortion (which will henceforth be referred to as "Hartmann flow"). Second, the criteria for obtaining satisfactory agreement between two successive sets of values is based on a maximum allowable percentage change, for example, if

$$\left| \frac{Q^{(n+1)} - Q^{(n)}}{Q^{(n)}} \right| \leq \text{TOL}Q$$

at every point in the net, then agreement is satisfactory. In the case of the vorticity, however, this is modified to

$$\left| \frac{Q^{(n+1)} - Q^{(n)}}{Q^{(n)} + K} \right| \leq \text{TOL}Q,$$

where K is a number much smaller than the peak value of vorticity. This is designed to avoid requiring excessive accuracy at points for which the magnitude of the vorticity is so small as to be negligible.

Finally, as the magnitude of the stream function is very small near the plate, the values here are very sensitive to the current value of ξ . Due to this fact, it is necessary to introduce a weighting factor into the calculation of step (iii) to achieve convergence. The vorticity at the plate is then recalculated according to the relation

$$\xi_{2j}^{(n+1)} = \xi_{2j}^{(n)} + w(\xi_{2j}^{(n+1)} - \xi_{2j}^{(n)}),$$

where w is a weighting factor whose value is between 0 and 1. In addition, the convergence tolerance on these values is double that allowed on ξ -values at interior points. Numerical computations have shown that w must generally be less than 0.20 to achieve convergence.

It has also been convenient to introduce a weighting factor into step (iv) by computing the coefficients of the ξ equations from a weighted average of the last two successive sets of ψ values; this is useful in the initial stages of the calculation.

b. Block Iteration

We turn now to the solution of the individual sets of equations for ξ , ψ , and A . Although each set of equations is linear in the unknown variable, a direct simultaneous solution of the approximately $(i_p - 3)(j_p - 3)$ equations is a formidable task for a reasonably sized net. For this reason, each set of equations is solved by the following iterative process, which is essentially a block relaxation technique. Beginning at the i row nearest the plate (or for A , the i row at the plate), we solve the set of equations formed

by the finite difference equations of every relevant point in the row simultaneously for the values of the variable at the points in the row, holding constant the values at points not in the row. These values then replace the original values and we repeat the process for every row in the net, moving from the plate outward, to complete one iteration. This iteration process is then repeated until satisfactory agreement between two successive sets of values of the dependent variable is obtained.

c. IBM 709 Program

The finite difference problem formulated in this section was programmed for solution, in the manner described above, on the IBM 709 digital computer. The resulting program is, of course, rather lengthy, and the details are not very informative. It will therefore suffice to describe what problems this program is capable of handling.

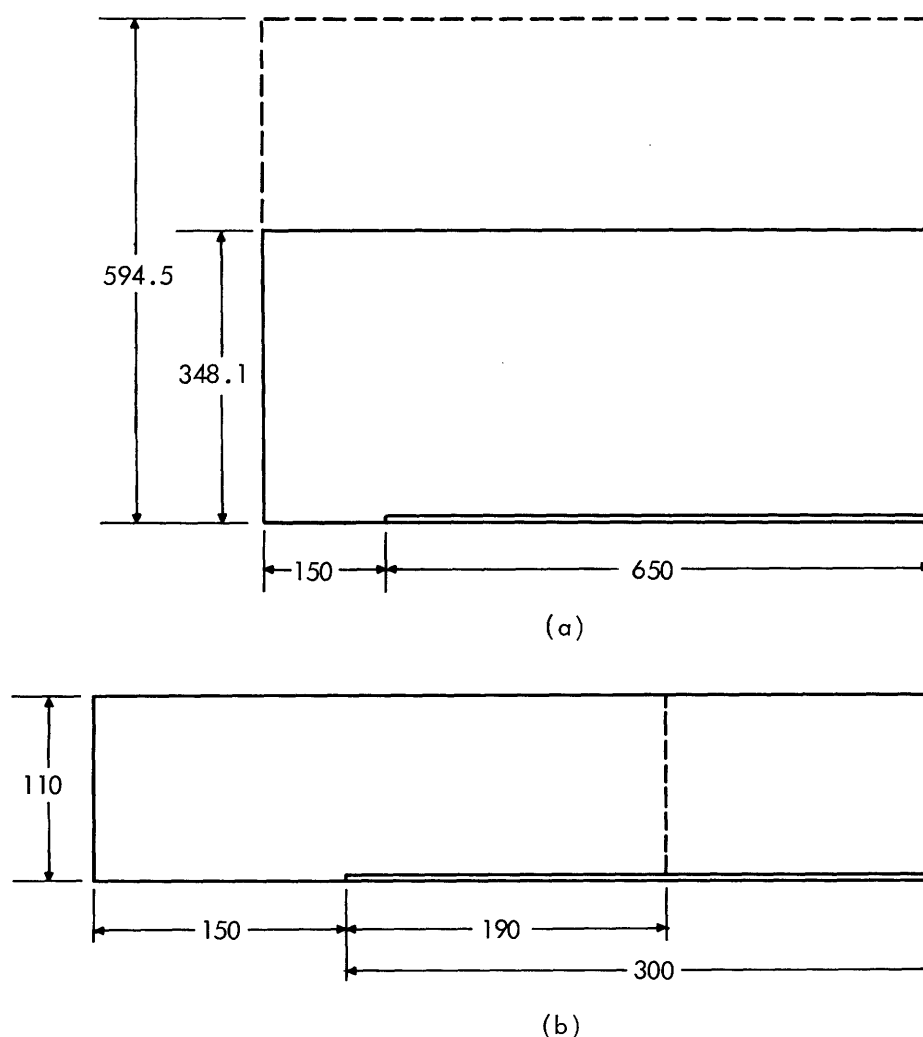


Fig. 13. Boundary placement arrangements for $\epsilon a^2 = 10^{-3}$ (top) and $\epsilon a^2 = 10^{-2}$ (bottom). Distances shown are based on Reynolds number.

It will treat all downstream boundary conditions listed in Table II, and can employ either of the forms (105) or (106) for $FF\xi$. The tolerances used as criteria for convergence may be specified, as well as the weighting factors for the vorticity at the plate and the coefficients of the vorticity equations. The maximum size of the finite difference net is 29 x-points and 43 y-points; this is due to the core-storage limitations of the computer. The individual x and y coordinates may be specified arbitrarily, as well as the x-position of the plate within the net. The program will also treat various subnets located at any position within the primary net; this is useful in obtaining more accurate solutions in regions where the dependent variables are varying rapidly with distance.

4.3 RESULTS

a. Boundary Placement

All cases investigated here had as their origin one of two basic Hartmann (no magnetic-field distortion) flows. These flows are characterized solely by the value of the parameter ϵa^2 , and the two values employed were 10^{-2} and 10^{-3} . These values result in Hartmann layer thicknesses ($\delta_H = 1/\sqrt{\epsilon a^2}$) of 10 and 31.6, respectively, and characteristic growth lengths $x_g = 1/\epsilon a^2$ of 100 and 1000, respectively.

A basic boundary placement arrangement corresponding to each of these basic flows was employed, as shown in Fig. 13. In addition, to determine the effects of boundary position on the results obtained, one boundary position was altered in each of these basic arrangements, as shown in Fig. 13. These arrangements will be referred to as numbers 1, 2, 3, and 4, corresponding to the basic arrangements for $\epsilon a^2 = 10^{-3}$ and 10^{-2} , the basic arrangement for $\epsilon a^2 = 10^{-3}$ with the transverse boundary placed further from the plate, and the basic arrangement for $\epsilon a^2 = 10^{-2}$ with the downstream boundary placed closer to the leading edge, respectively.

The significant features of these arrangements are characterized by two length ratios: the ratio of the Hartmann thickness, δ_H , to the half-channel width, h , and the ratio of the distance from the leading edge to the downstream boundary, ℓ , to the characteristic growth length of the Hartmann layer, x_g . The first ratio indicates the magnitude of channeling effects, while the second ratio indicates the relative importance of the downstream boundary position. The values of these ratios for the four boundary arrangements are listed in tabular form as follows:

| Arrangement | δ_H/h | ℓ/x_g |
|-------------|--------------|------------|
| 1 | ~0.1 | 0.65 |
| 2 | ~0.1 | 3.0 |
| 3 | ~0.05 | 0.65 |
| 4 | ~0.1 | 1.90 |

b. Cases Investigated

Each case for which results are presented will be referred to by the notation Case N-M, where N will refer to the boundary placement arrangement and M will refer, in general, to increasing values of ϵ . Numerical results were obtained, and some form of results are presented for the twelve cases listed in tabular form as follows:

| Case | ϵa^2 | ϵ | Remarks |
|--------|----------------|------------|--|
| 1-0,00 | 10^{-3} | 0 | Leading-edge effect |
| 1-1 | 10^{-3} | 0 | Hartmann type of flow |
| 1-2 | 10^{-3} | 10^{-3} | None |
| 1-3 | 10^{-3} | 10^{-2} | None |
| 1-4 | 10^{-3} | 10^{-1} | None |
| 2-1 | 10^{-2} | 0 | Hartmann type of flow |
| 2-2 | 10^{-2} | 10^{-1} | None |
| 3-1 | 10^{-3} | 0 | Transverse boundary effect, Hartmann type of flow |
| 3-2 | 10^{-3} | 10^{-1} | Transverse boundary effect |
| 4-1 | 10^{-2} | 0 | Downstream boundary effect, Hartmann type of flow |
| 4-2 | 10^{-2} | 10^{-1} | Downstream boundary effect |

The last ten of these cases represent results of physical interest, while the first two cases, which will be discussed in detail below, are designed to investigate the behavior of the numerical error introduced because of the singularity in vorticity at the leading edge of the plate.

Before introducing the results for the cases investigated, a few general remarks are in order. First, the downstream boundary conditions employed in all cases are Eqs. 94a, 95a, and 96b. The prescribed values of ψ and ξ are those of fully developed Hartmann flow. Although we felt, at first, that conditions on the derivatives would be preferable at the downstream boundary, we found that convergence of the solution technique was very difficult to obtain when these conditions were employed.

Second, the convergence tolerances employed in all cases were 0.005 for ξ , and 0.003 for ψ . It was found by decreasing these tolerances that the only significant quantities that changed by a percentage equivalent to that indicated by the tolerances were the vorticity values at the plate near the downstream boundary, and the stream function at the points next to the plate near the downstream boundary. In other regions, changes in significant results obtained were confined to the fourth and fifth significant figure.

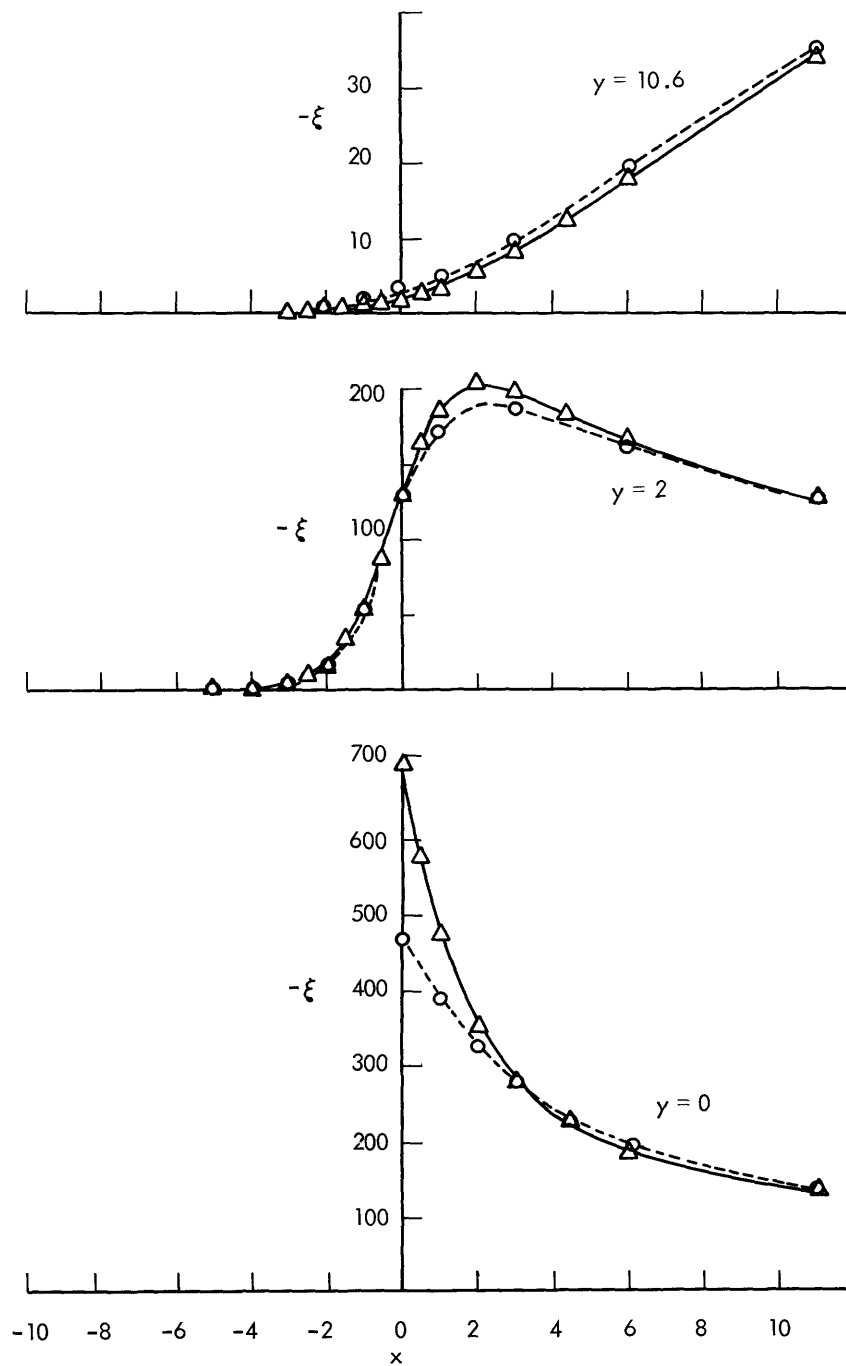


Fig. 14. Effect of net spacing on vorticity near leading edge of plate.
Solid line is refined net; broken line is coarse net.

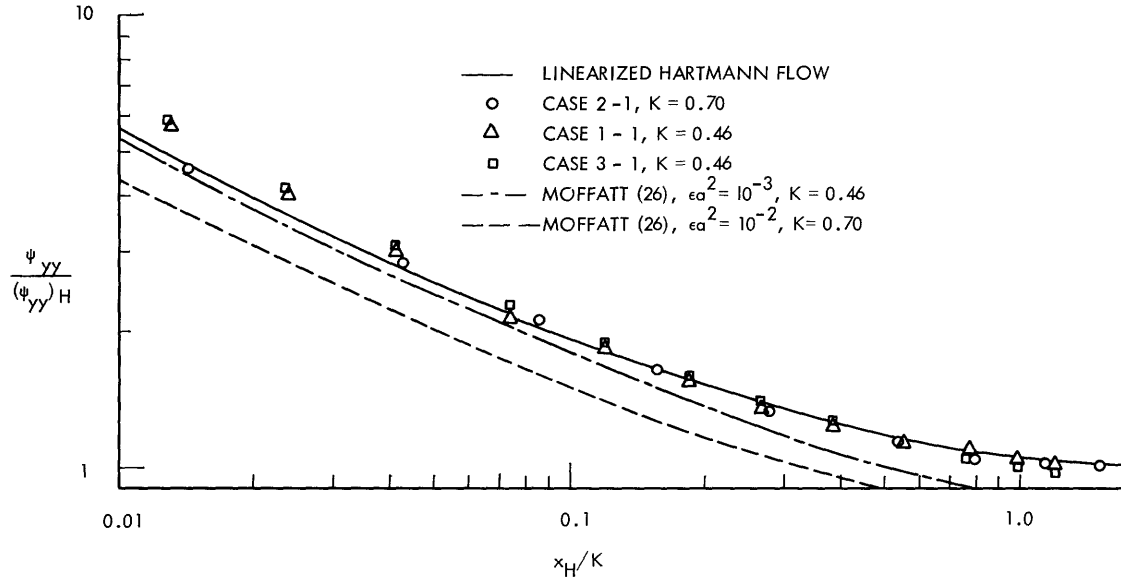


Fig. 15. Comparison of skin friction as obtained from numerical solution with that of linearized solution.

The convergence tolerances employed for A were 3×10^{-5} (Cases 1-4, 2-2, 3-2, and 4-2), 10^{-6} (Case 1-3) and 4×10^{-7} (Case 1-2).

Third, the net spacing employed was selected of the general form $\Delta x_n = a e^{-bn}$, where a and b were determined by a trial-and-error process. Exceptions to this form occur in the x -spacing very near the leading edge of the plate and at large distances from the leading edge, where equal spacing is employed in both regions. An identical net was employed for cases 1-1 through 1-4, a different identical net for cases 2-1 and 2-2, while the nets for cases 3-1, 3-2 and 4-1, 4-2 were obtained by adding y -points or deleting x -points from their respective basic nets.

Finally, it was necessary to choose the net spacings with some care, as the solution tended to oscillate because of truncation error. Hence, if any single spacing were very large, a very large oscillation was introduced into the solution. The results presented here retain this oscillatory character, but not to an appreciable extent; for example, the maximum oscillation in the vorticity is of the order of 1 per cent of the fully developed Hartmann-flow value. This oscillation has the most pronounced effect near the downstream boundary, as can be seen by comparing the velocity profiles presented in Figs. 24, 25, 26, and 27, for example.

The results for the various cases are presented in selected graphical form as follows. Figure 14 is a comparison of vorticity values near the leading edge of the plate for cases 1-0 and 1-00. Figure 15 compares the skin friction in the case of no magnetic field distortion (cases 1-1, 2-1, and 3-1) with that obtained from the linearized solution of Section III. Table IV shows the effect of increasing the parameter ϵ on the skin friction (cases 1-1 through 1-4 and cases 2-1 and 2-2). Figures 16-27 are velocity and

Table IV. Effect on skin friction of increasing parameter ϵ .

| Skin Friction, $(-\xi)_{y=0}$ | | | | | | |
|-------------------------------|---------|---------|---------|---------|--------|--------|
| x \ case | 1-1 | 1-2 | 1-3 | 1-4 | 3-1 | 3-2 |
| 0 | 0.451 | 0.451 | 0.449 | 0.445 | 0.445 | 0.437 |
| 1 | 0.373 | 0.374 | 0.372 | 0.369 | 0.368 | 0.362 |
| 3 | 0.265 | 0.265 | 0.264 | 0.261 | 0.261 | 0.257 |
| 6 | 0.184 | 0.185 | 0.184 | 0.182 | 0.182 | 0.179 |
| 11 | 0.132 | 0.132 | 0.132 | 0.131 | 0.130 | 0.128 |
| 19 | 0.0992 | 0.0991 | 0.0988 | 0.0983 | 0.973 | 0.961 |
| 34 | 0.0749 | 0.0748 | 0.0746 | 0.0744 | 0.732 | 0.726 |
| 55.1 | 0.0603 | 0.0600 | 0.0599 | 0.0600 | 0.585 | 0.583 |
| 83.9 | 0.0509 | 0.0507 | 0.0506 | 0.0509 | 0.491 | 0.492 |
| 123.5 | 0.0448 | 0.0447 | 0.0445 | 0.0449 | 0.430 | 0.433 |
| 178 | 0.0408 | 0.0408 | 0.0405 | 0.0409 | 0.389 | 0.392 |
| 253 | 0.0384 | 0.0386 | 0.0380 | 0.0382 | 0.366 | 0.367 |
| 357 | 0.0373 | 0.0373 | 0.0366 | 0.0363 | 0.348 | 0.344 |
| 454 | 0.0358 | 0.0361 | 0.0355 | 0.0360 | 0.339 | 0.348 |
| 552 | 0.0345 | 0.0344 | 0.0344 | 0.0364 | 0.321 | 0.357 |
| 650 | 0.0348* | 0.0348* | 0.0348* | 0.0348* | 0.332* | 0.332* |
| x \ case | 2-1 | 2-2 | 4-1 | 4-2 | | |
| 0 | 0.773 | 0.748 | 0.773 | 0.748 | | |
| 1 | 0.466 | 0.451 | 0.466 | 0.451 | | |
| 3 | 0.296 | 0.288 | 0.296 | 0.288 | | |
| 6 | 0.218 | 0.213 | 0.218 | 0.213 | | |
| 11 | 0.170 | 0.168 | 0.170 | 0.168 | | |
| 19 | 0.140 | 0.140 | 0.140 | 0.140 | | |
| 34 | 0.121 | 0.122 | 0.121 | 0.122 | | |
| 55.1 | 0.113 | 0.113 | 0.113 | 0.113 | | |
| 80 | 0.110 | 0.109 | 0.109 | 0.109 | | |
| 105 | 0.109 | 0.107 | 0.109 | 0.108 | | |
| 131 | 0.109 | 0.107 | 0.109 | 0.108 | | |
| 159 | 0.109 | 0.107 | 0.110 | 0.110 | | |
| 190 | 0.109 | 0.107 | 0.110* | 0.110* | | |
| 224 | 0.109 | 0.107 | | | | |
| 261 | 0.109 | 0.108 | | | | |
| 300 | 0.110* | 0.110* | | | | |

* Denotes prescribed boundary value

current distribution profiles at various x-positions for cases 1-1, 1-3, and 1-4. Similarly, Figs. 28-39 and Figs. 40-51 are these profiles for cases 2-1, 2-2, 4-1, 4-2 and cases 3-1, 3-2, respectively. As will be discussed in Section V, the locations of significant features of the current distribution are plotted in Figs. 52, 53, and 54 for cases 1-3, 1-4, and 2-2, respectively. The locations of selected streamlines are plotted for cases 2-1 and 2-2 in Fig. 55. The normal component of the magnetic field at the plate for cases 1-2, 1-3, 1-4, 3-2, and cases 2-2, 4-2, is plotted in Figs. 56 and 57, respectively. Finally, typical velocity profiles near the plate for cases 2-1 and 2-2 are shown in Fig. 58.

c. Effect of Singularity in Vorticity at Leading Edge

The vorticity is singular at the leading edge of the plate, and hence the finite difference approximation is in error here. To evaluate this error two cases were calculated with the sole difference that in the second case (1-00) the net spacing in the vicinity of the leading edge was approximately one half of that of the first case (1-0). Specifically, the second net was obtained from the first by adding net points approximately in the center of the first three x-spaces at either side of the leading edge, and to the first four y-spaces from the leading edge.

The results for the vorticity in the vicinity of the leading edge are shown in Fig. 14. As can be seen, the value of the vorticity at the leading edge is changed appreciably by the smaller net spacing (increased by more than 40 per cent). However, the most significant feature is that the region in which the vorticity is changed appreciably is confined to a small region near the leading edge. Thus it can be concluded that the results obtained for the entire flow field are not significantly affected by the truncation error encountered at the leading edge.

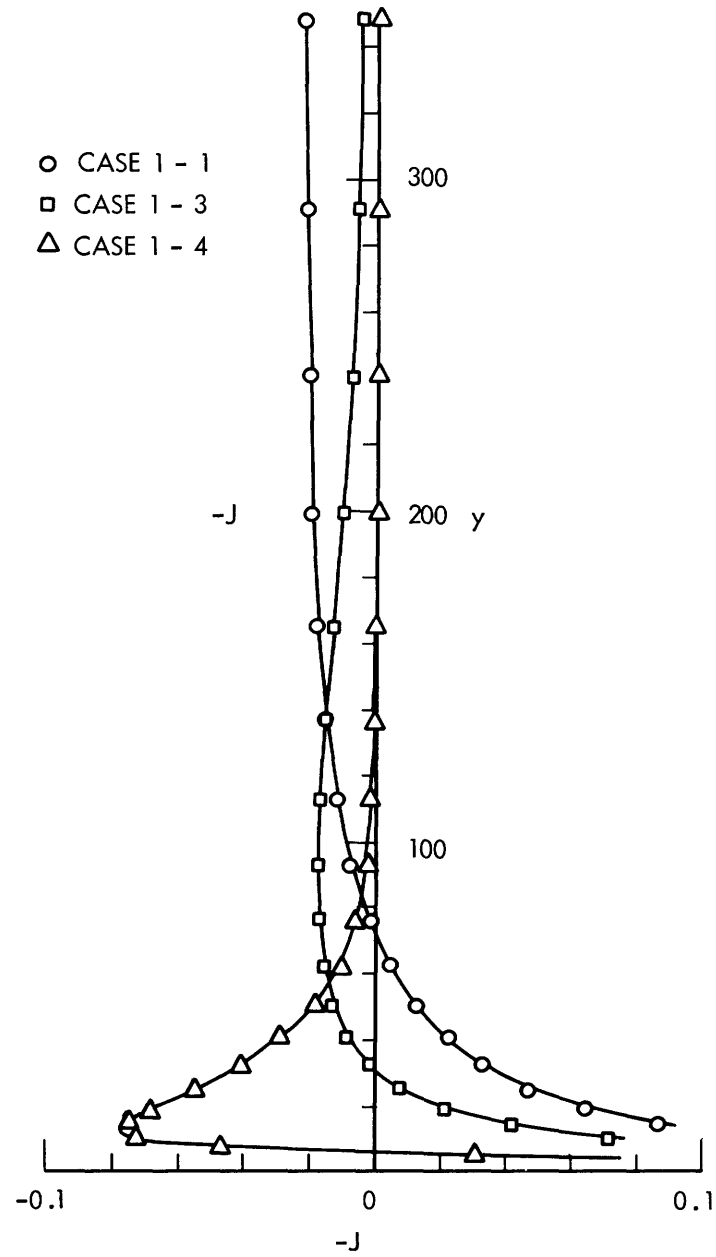


Fig. 16. Current-density profiles, Cases 1-1, 1-3, and 1-4, $x=0$.

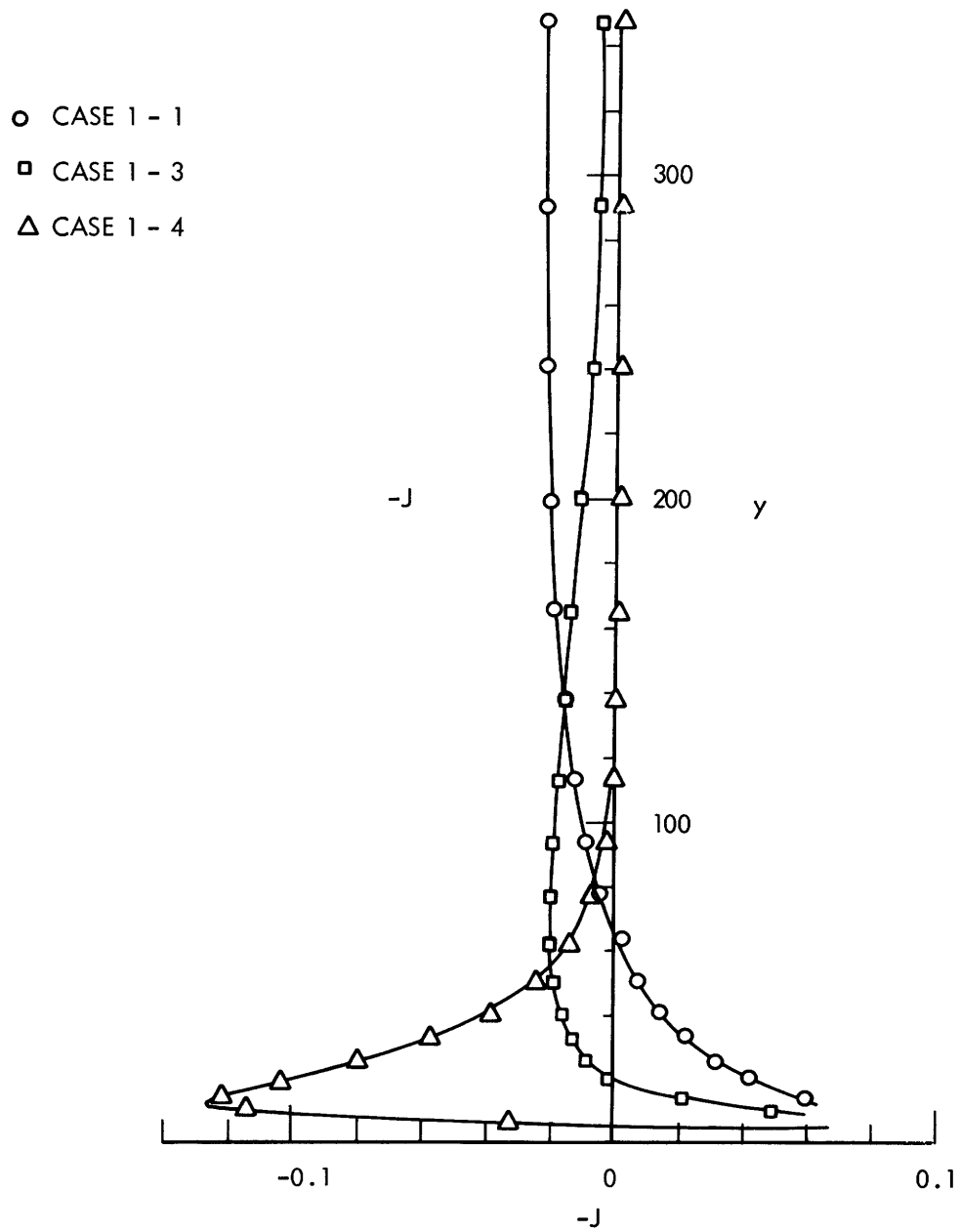


Fig. 17. Current-density profiles, Cases 1-1, 1-3, and 1-4, $x=6$.

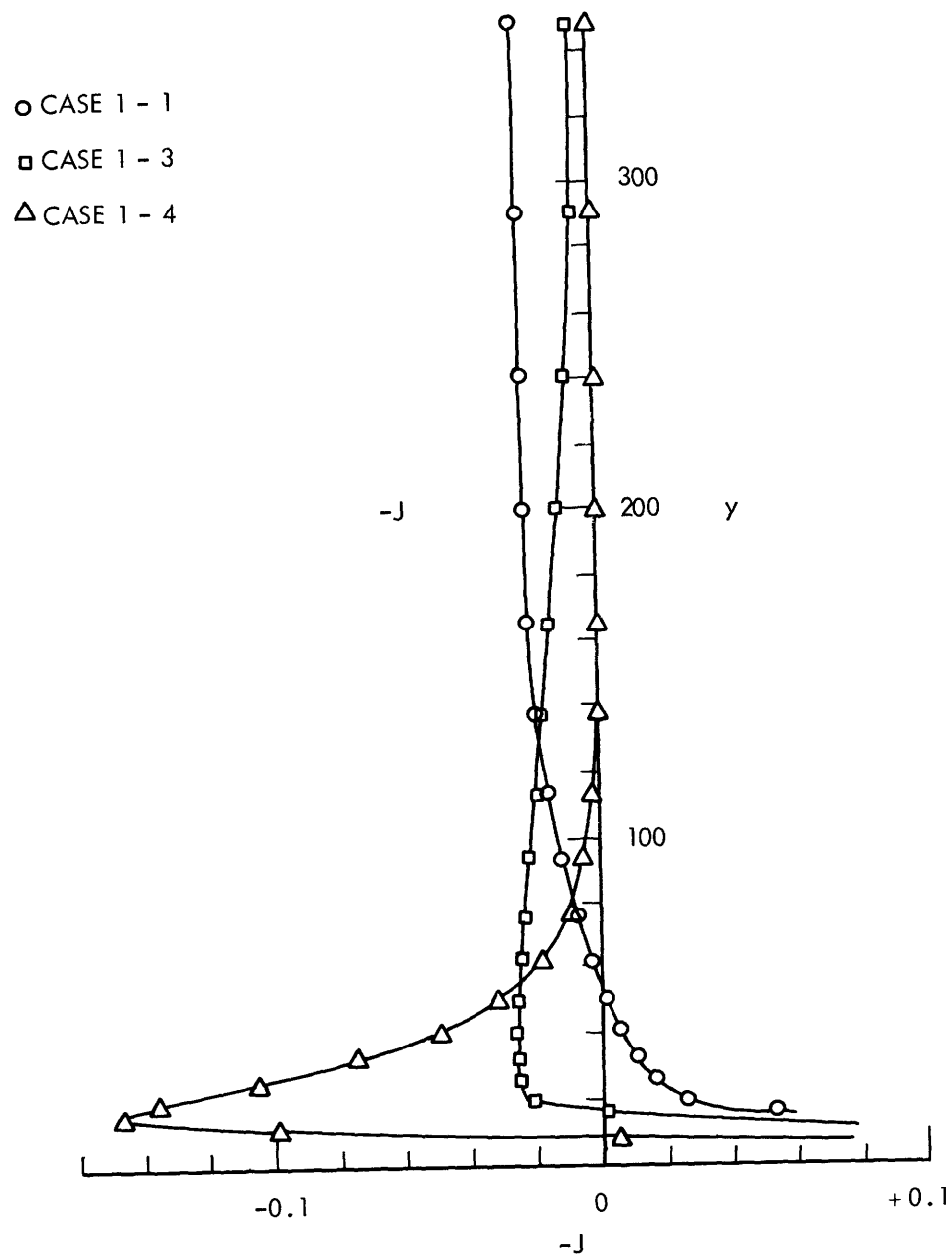


Fig. 18. Current-density profiles, Cases 1-1, 1-3, and 1-4, $x=11$.

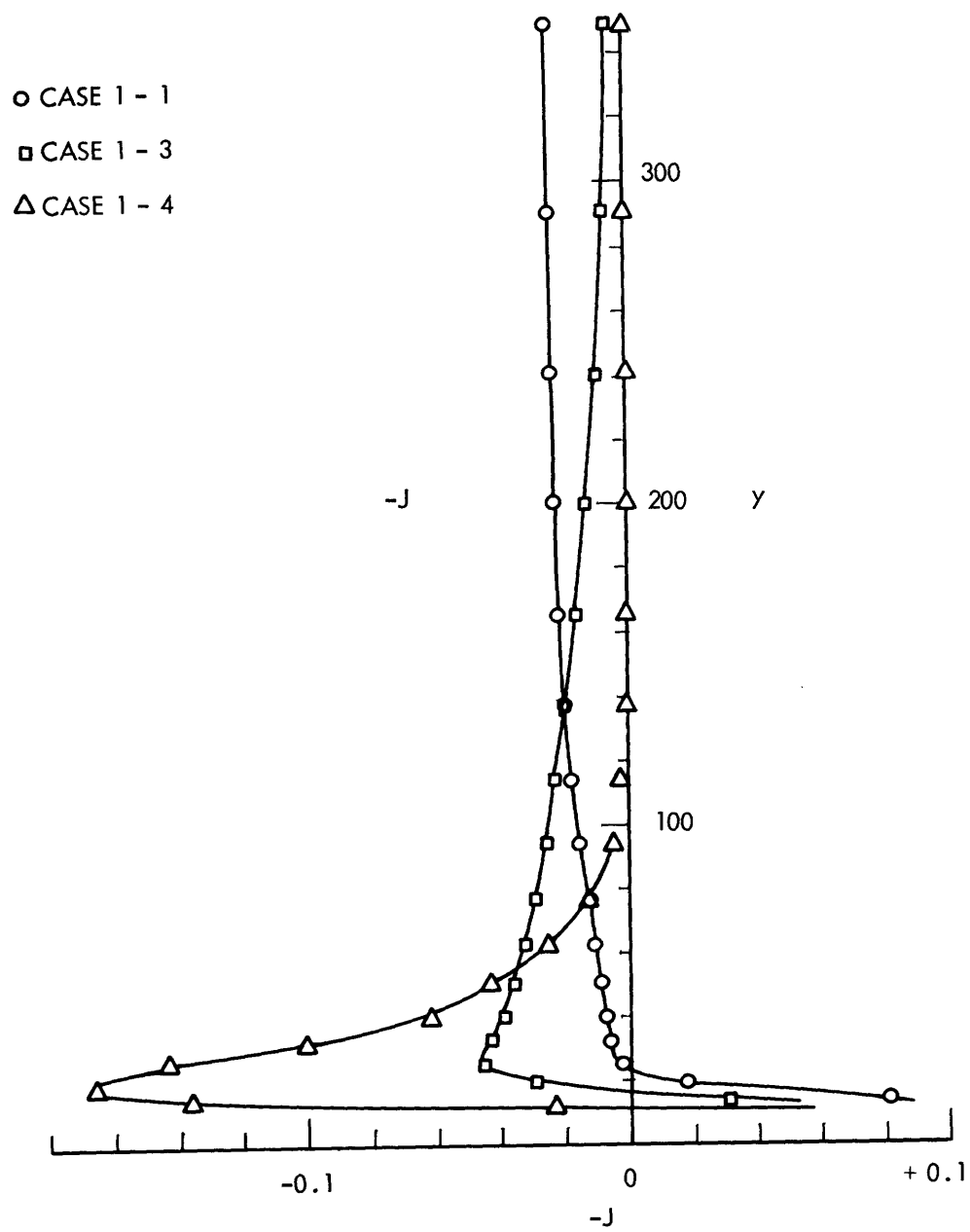


Fig. 19. Current-density profiles, Cases 1-1, 1-3, and 1-4, $x=19$.

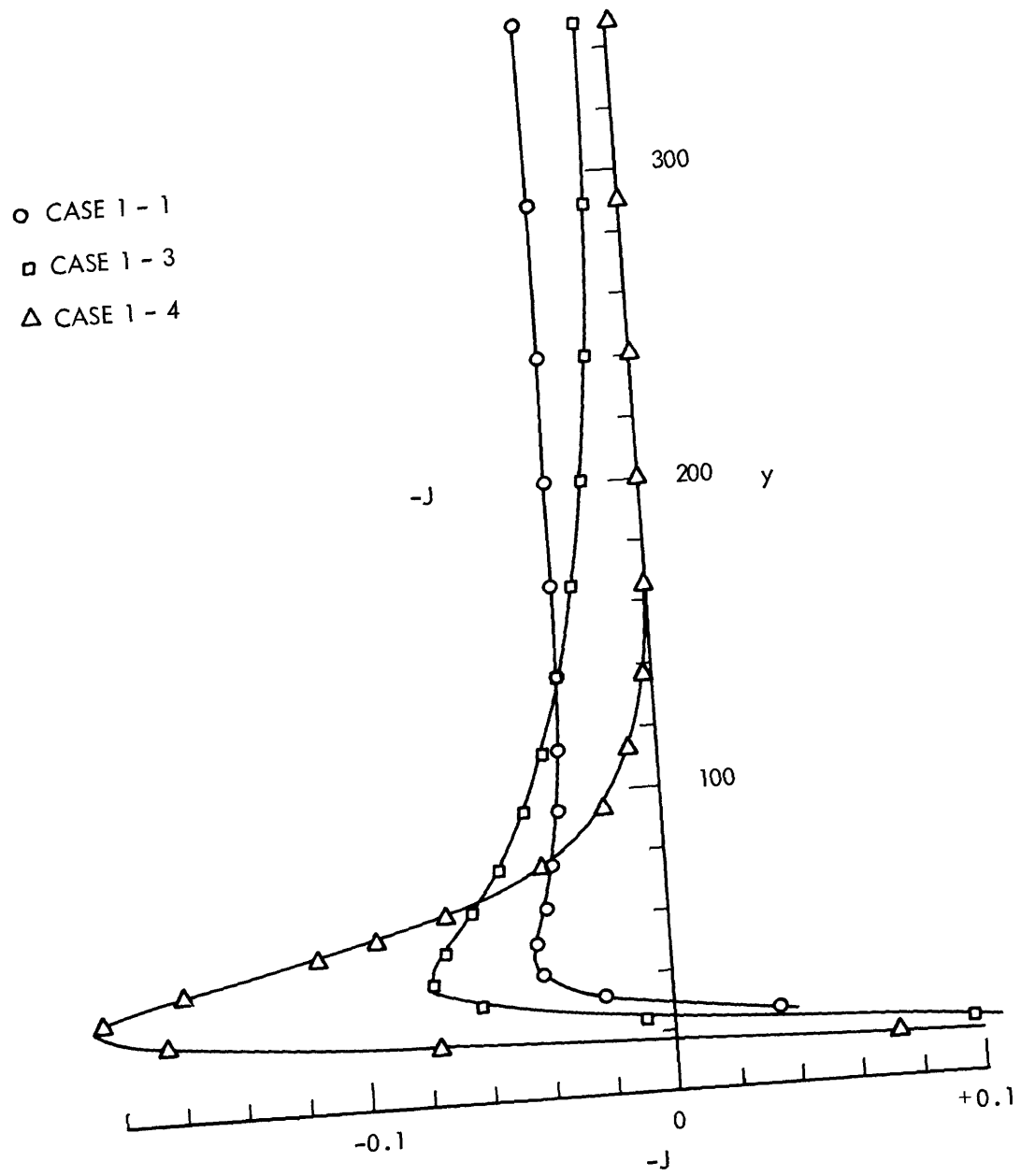


Fig. 20. Current-density profiles, Cases 1-1, 1-3, and 1-4, $x=55.1$.

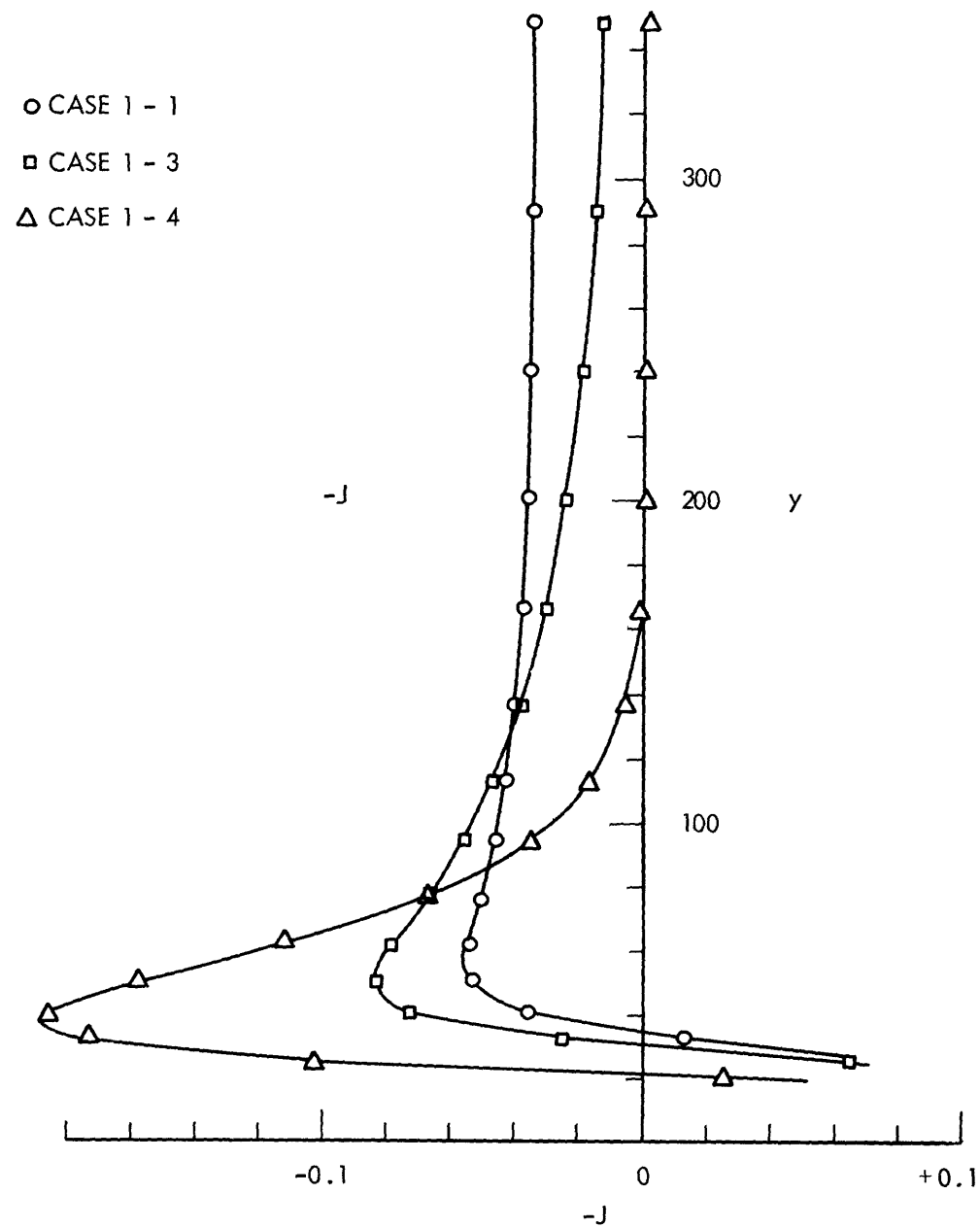


Fig. 21. Current-density profiles, Cases 1-1, 1-3, and 1-4, $x=83.9$.

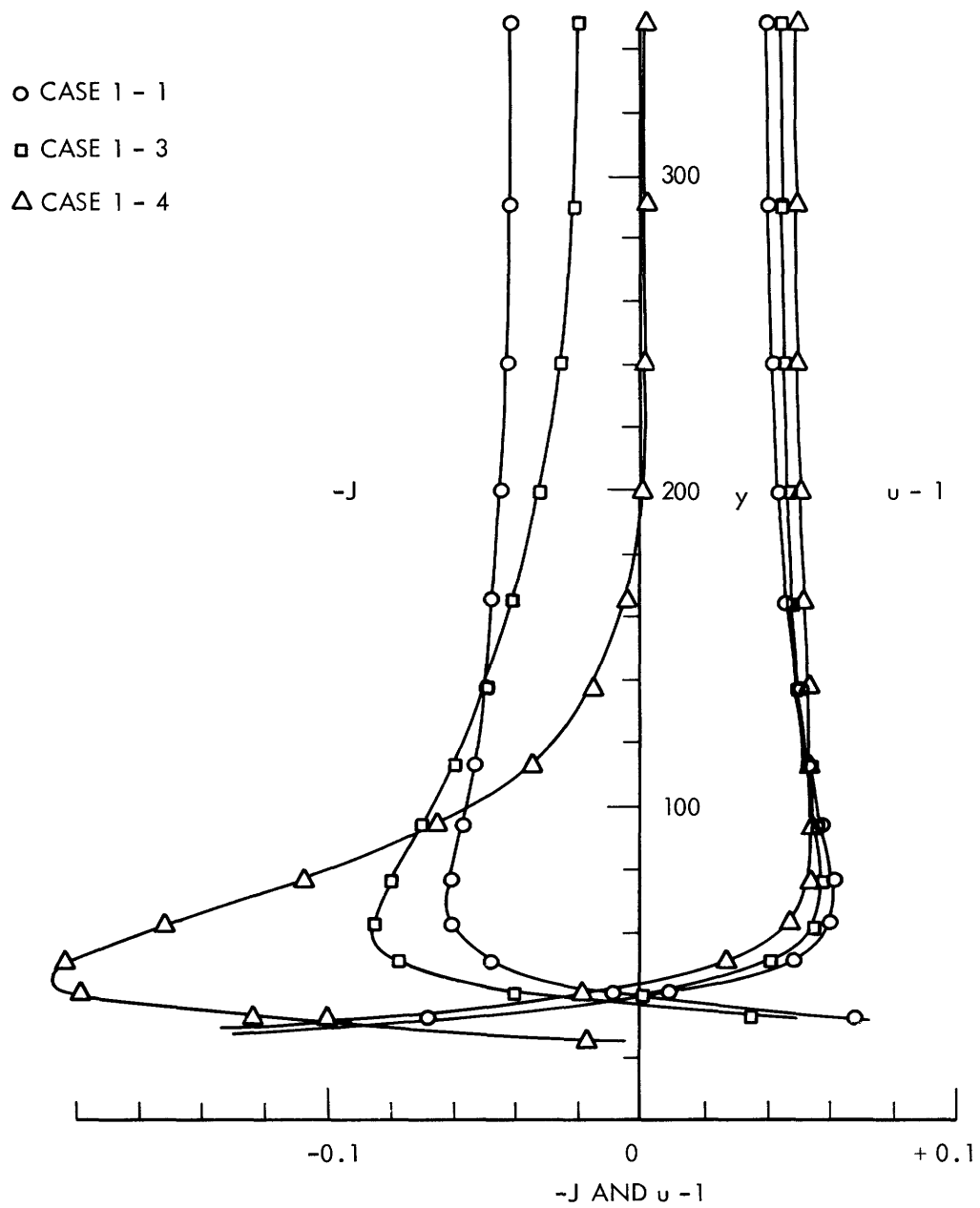


Fig. 22. Current-density and velocity profiles, Cases 1-1, 1-3, and 1-4, $x=123.5$.

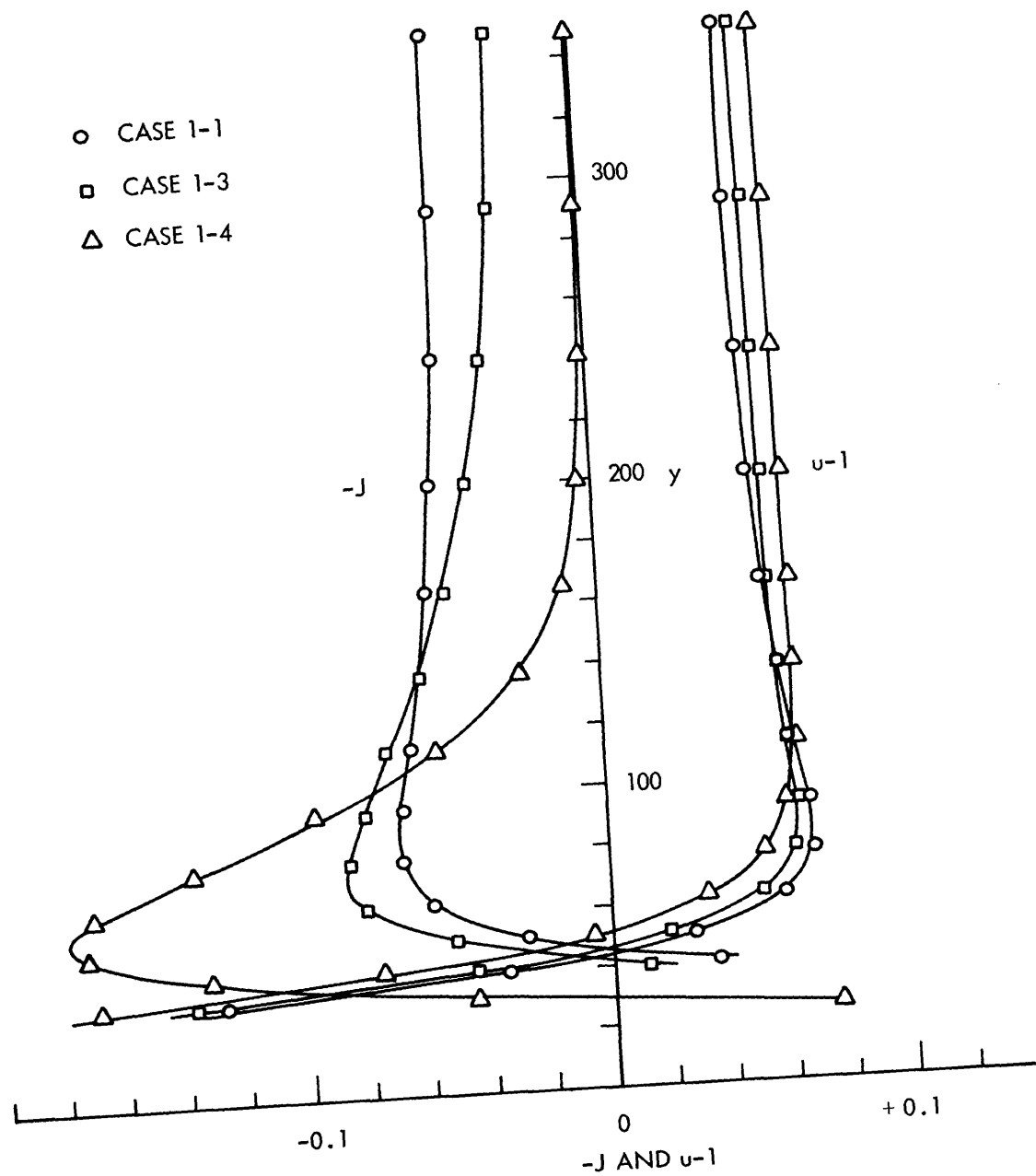


Fig. 23. Current-density and velocity profiles, Cases 1-1, 1-3, and 1-4, $x=178$.

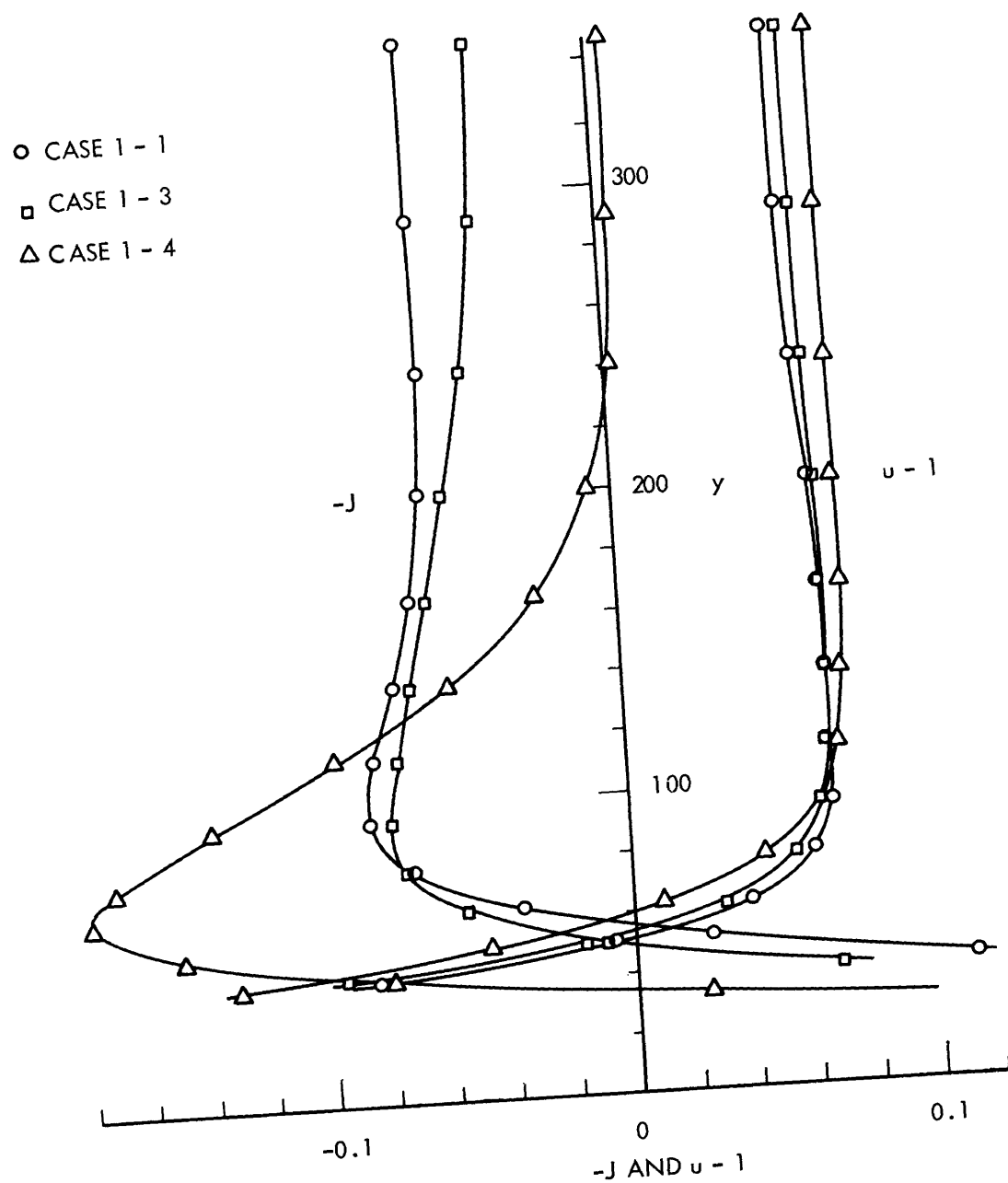


Fig. 24. Current-density and velocity profiles, Cases 1-1, 1-3, and 1-4, $x=253$.

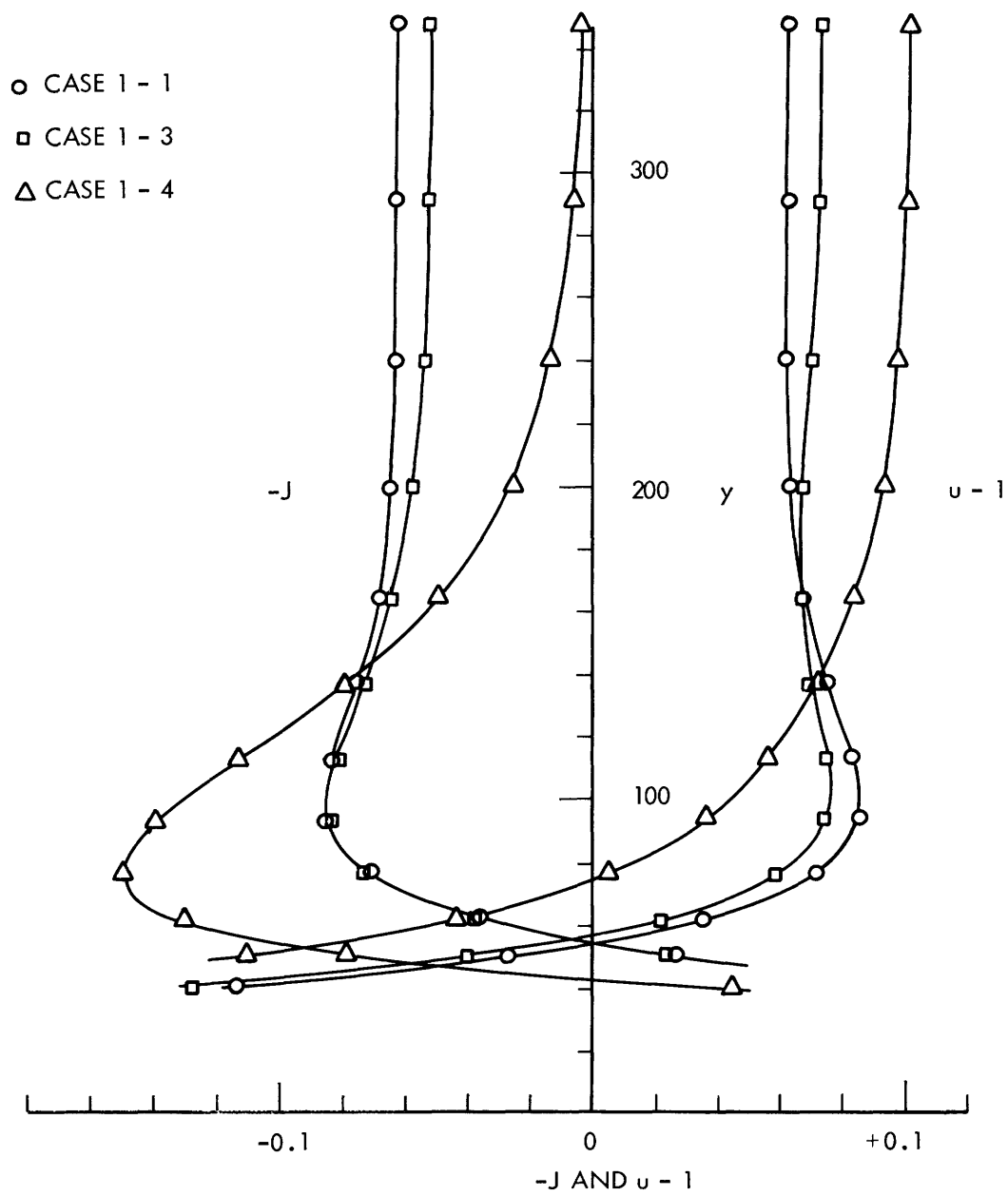


Fig. 25. Current-density and velocity profiles, Cases 1-1, 1-3, and 1-4, $x=357$.

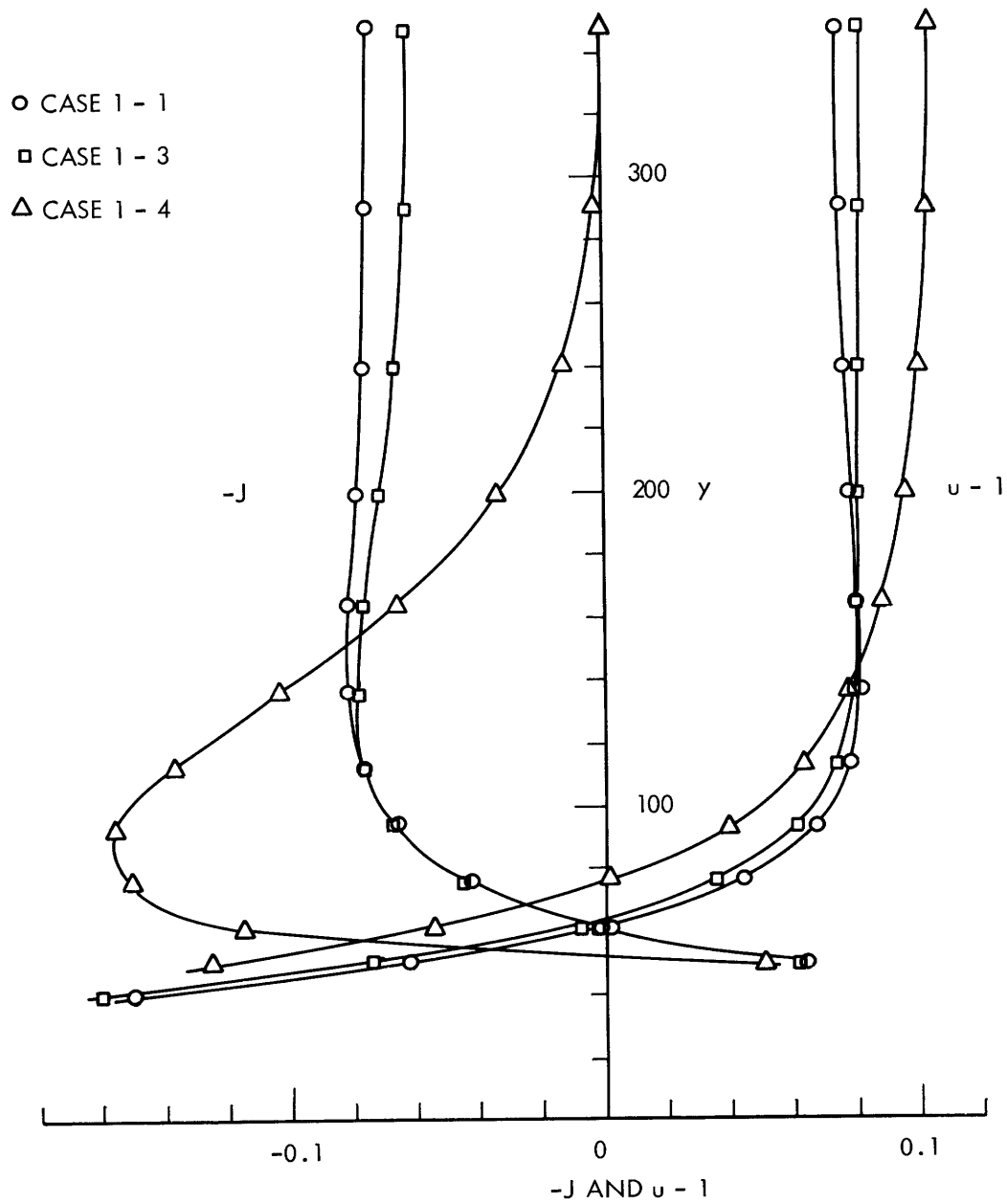


Fig. 26. Current-density and velocity profiles, Cases 1-1, 1-3, and 1-4, $x=454$.

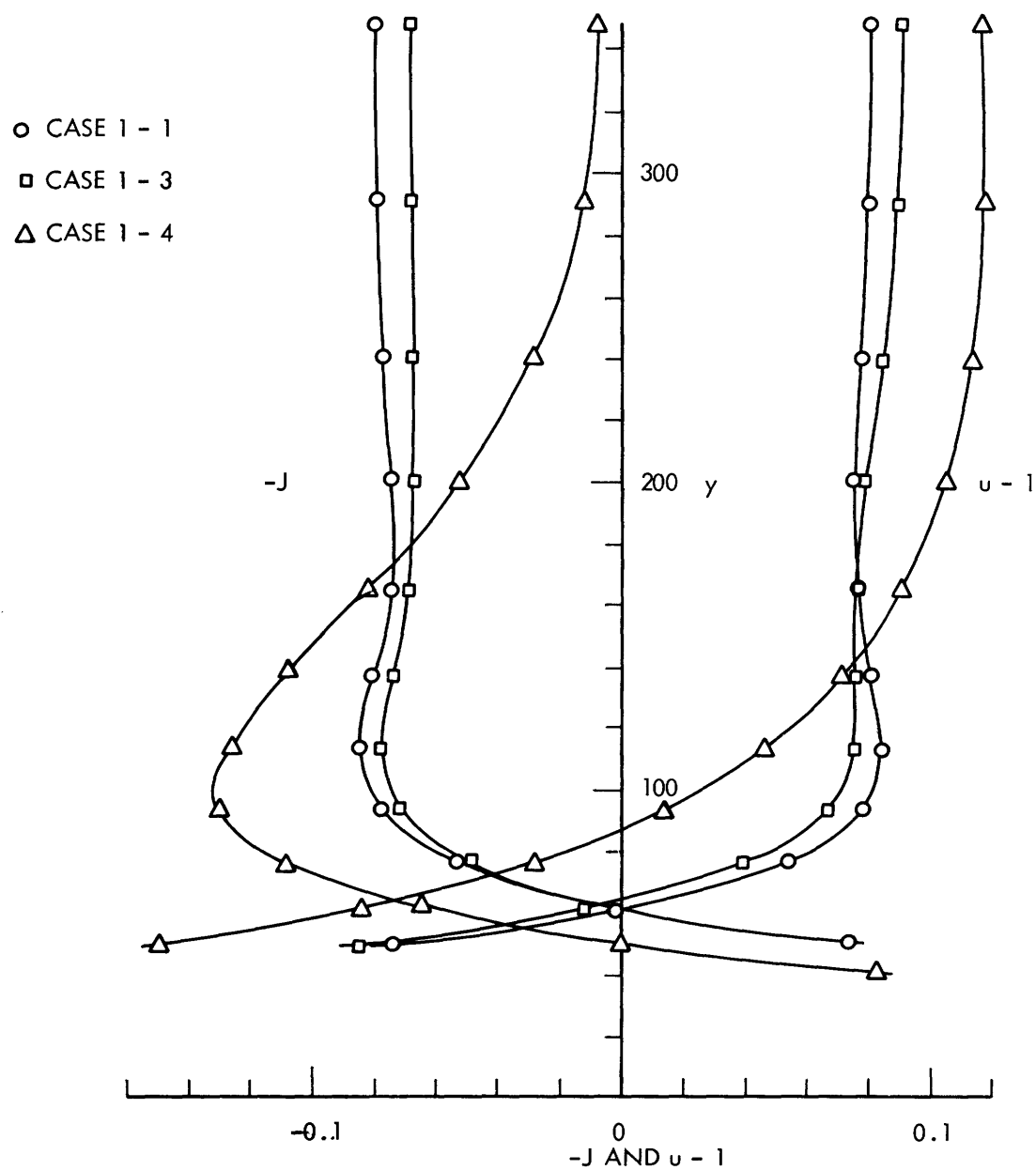


Fig. 27. Current-density and velocity profiles, Cases 1-1, 1-3, and 1-4, $x=552$.

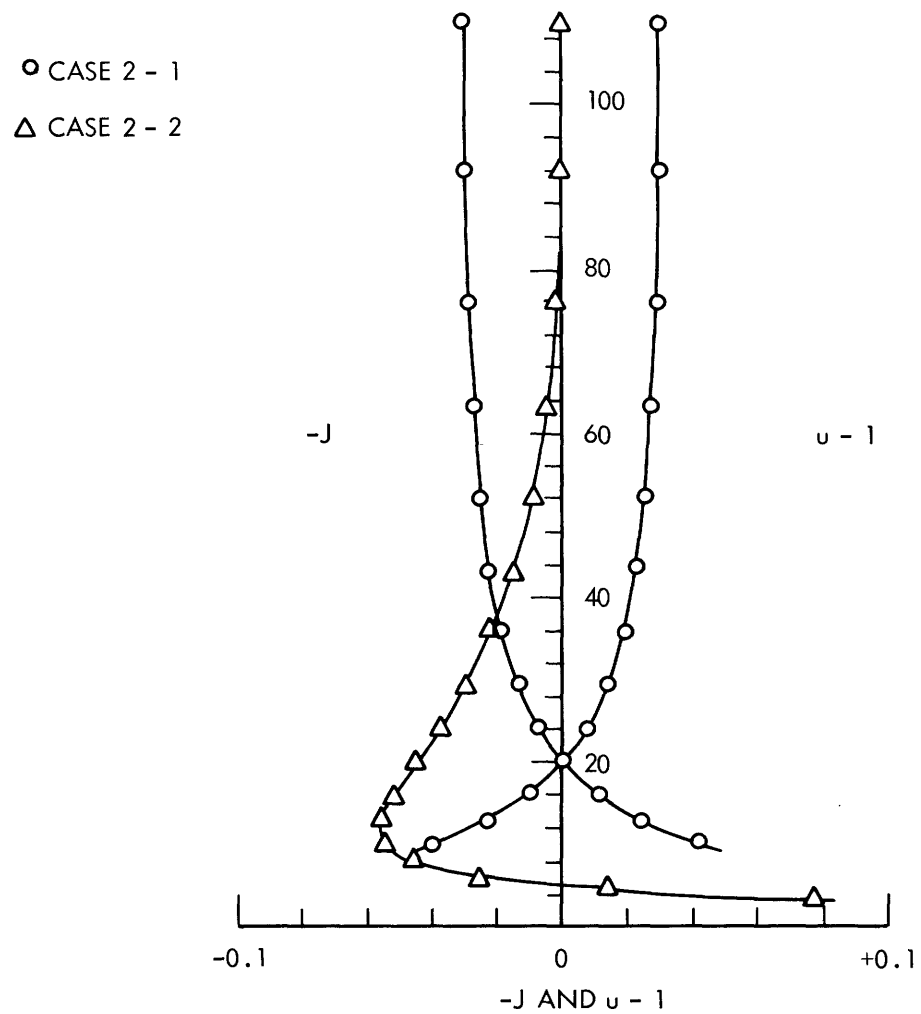


Fig. 28. Current-density and velocity profiles, Cases 2-1 and 2-2, $x=0$. (Velocity profile for Case 2-2 is not shown.)

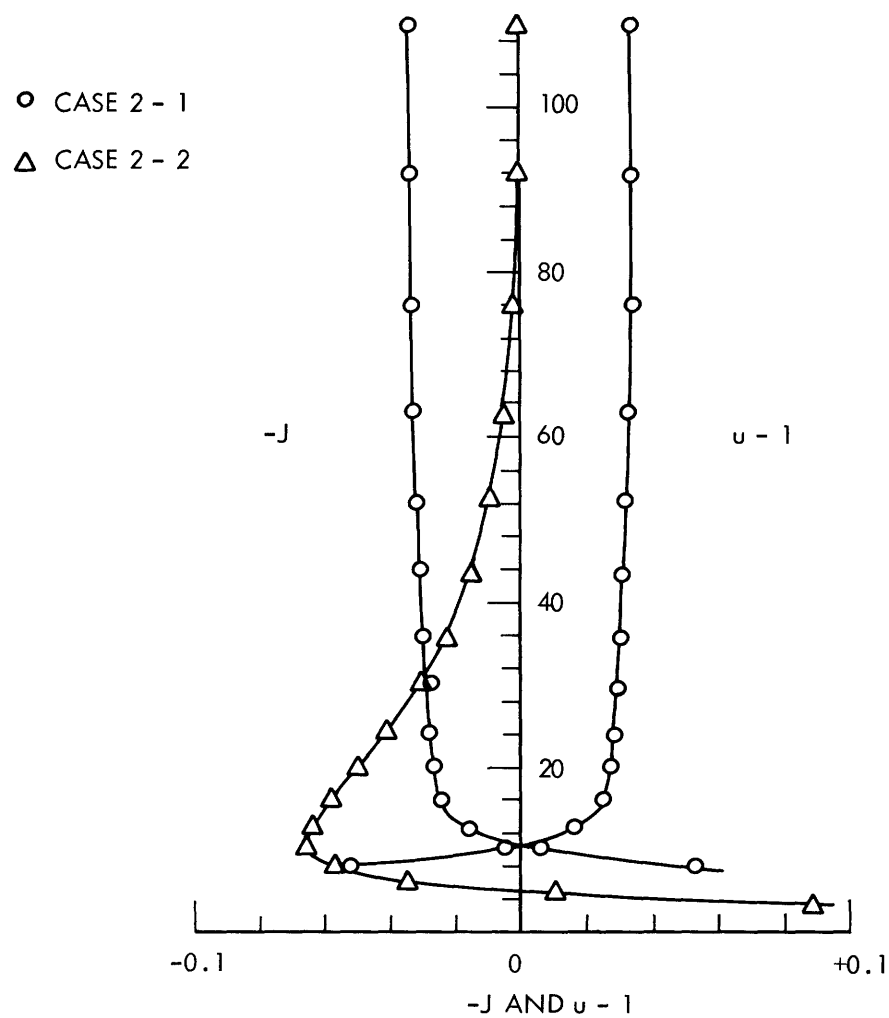


Fig. 29. Current-density and velocity profiles, Cases 2-1 and 2-2, $x=6$. (Velocity profile for Case 2-2 is not shown.)

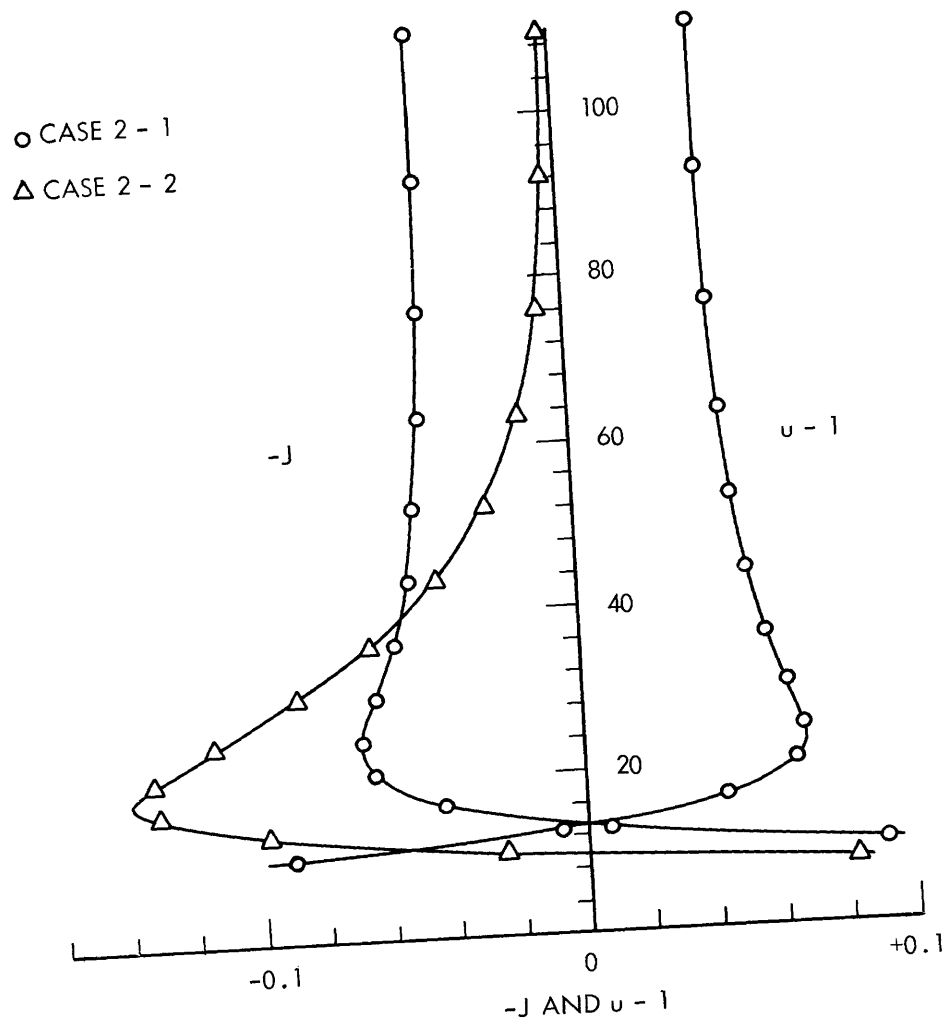


Fig. 30. Current-density and velocity profiles, Cases 2-1 and 2-2, $x=19$. (Velocity profile for Case 2-2 is not shown.)

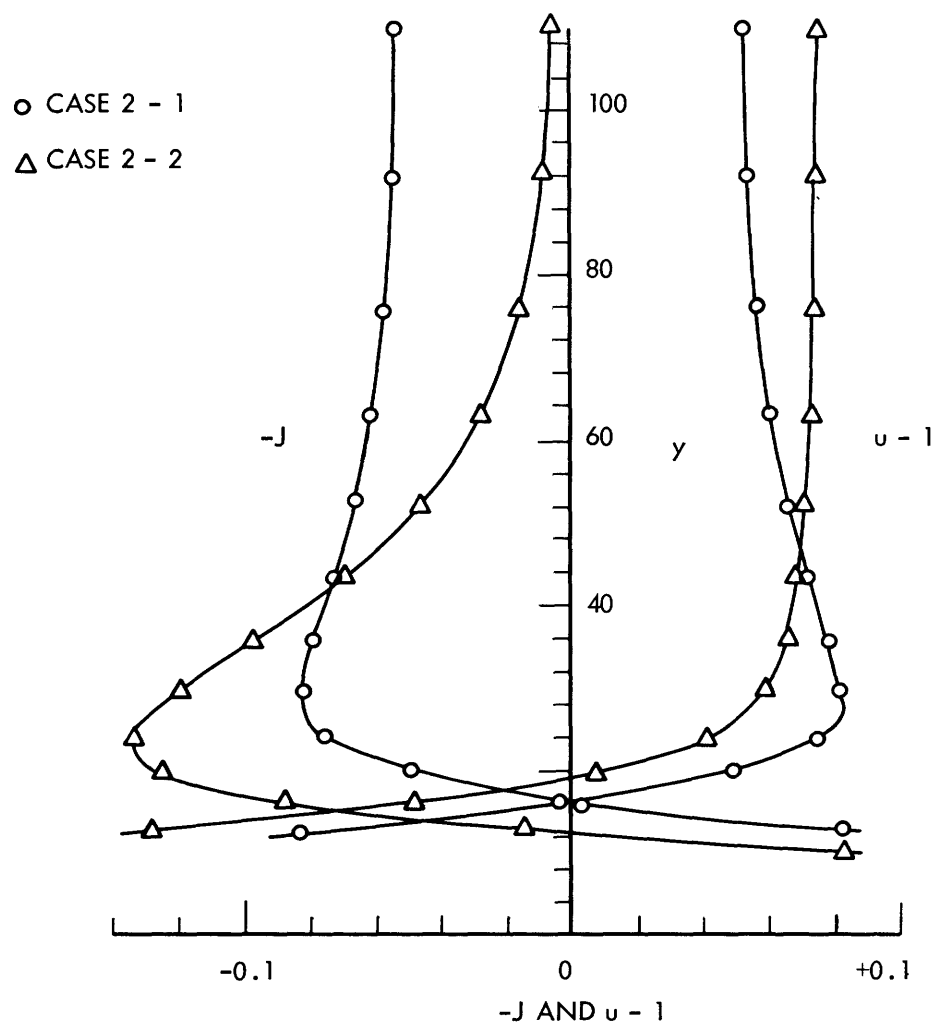


Fig. 31. Current-density and velocity profiles, Cases 2-1 and 2-2, $x=34$.

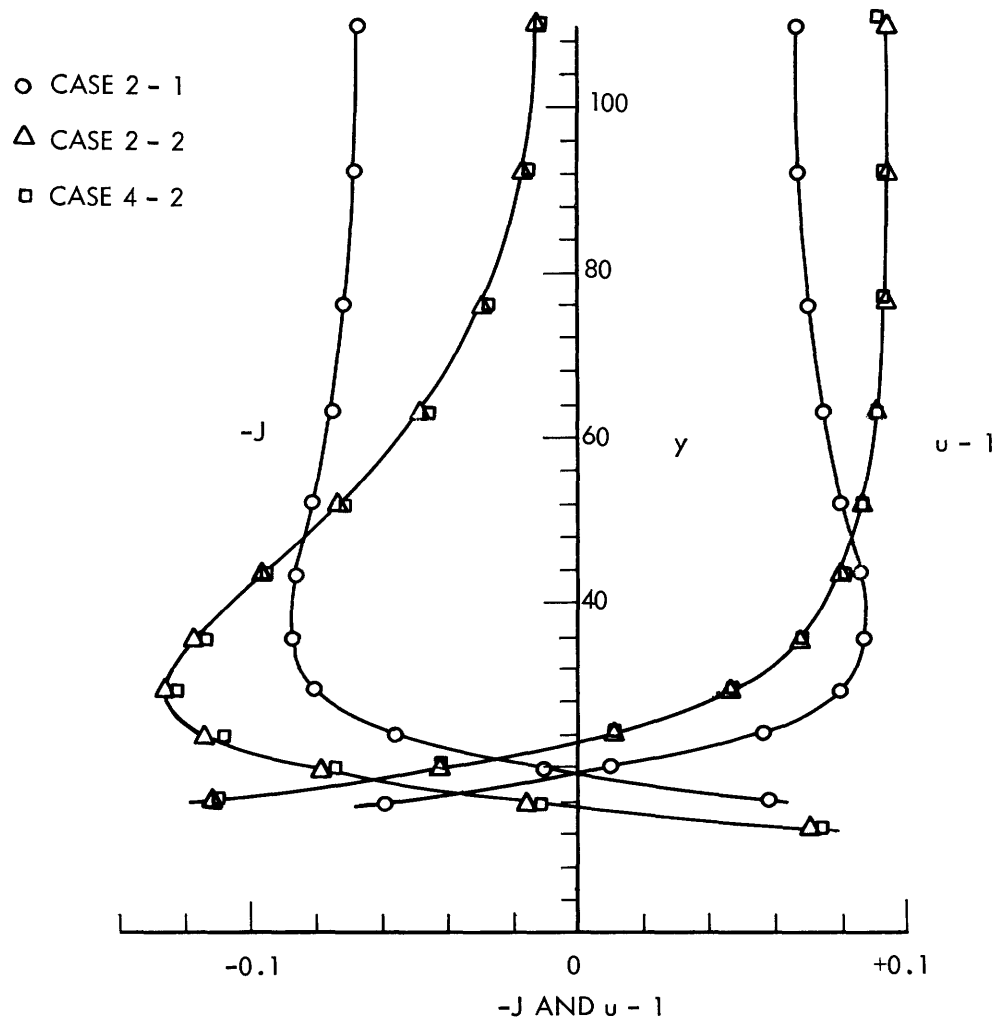


Fig. 32. Current-density and velocity profiles, Cases 2-1 and 2-2, $x=55.1$.

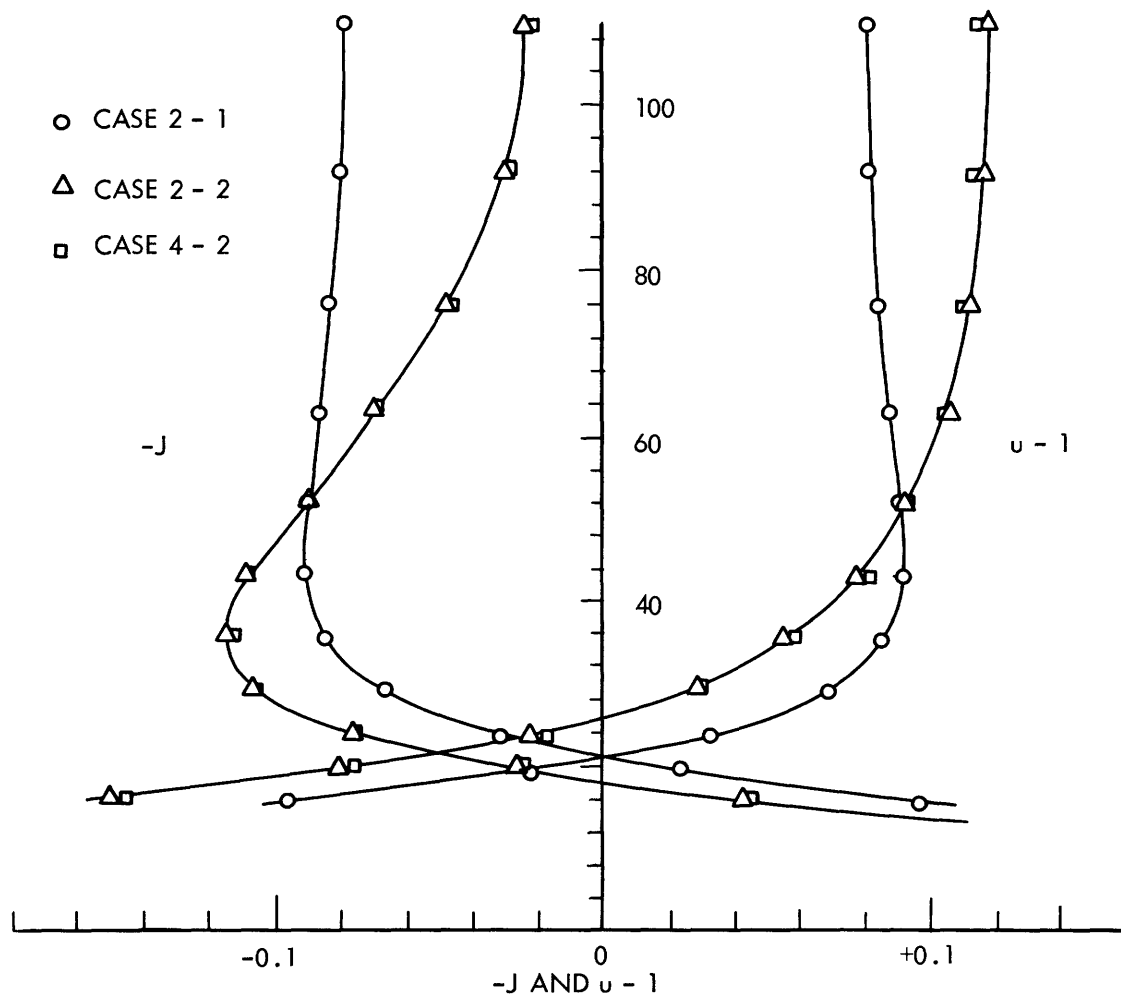


Fig. 33. Current-density and velocity profiles, Cases 2-1, 2-2, and 4-2, $x=80$.

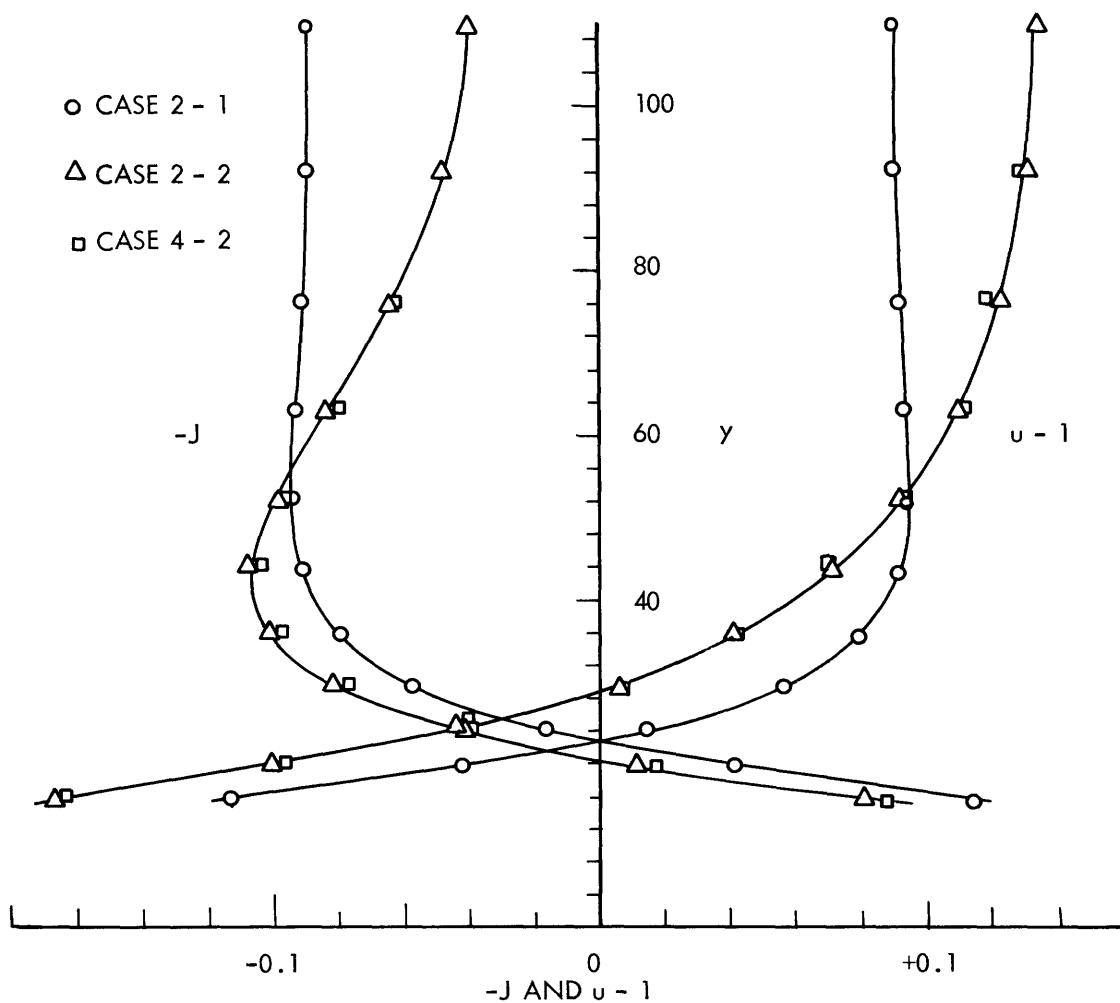


Fig. 34. Current-density and velocity profiles, Cases 2-1, 2-2, and 4-2, $x=105$.

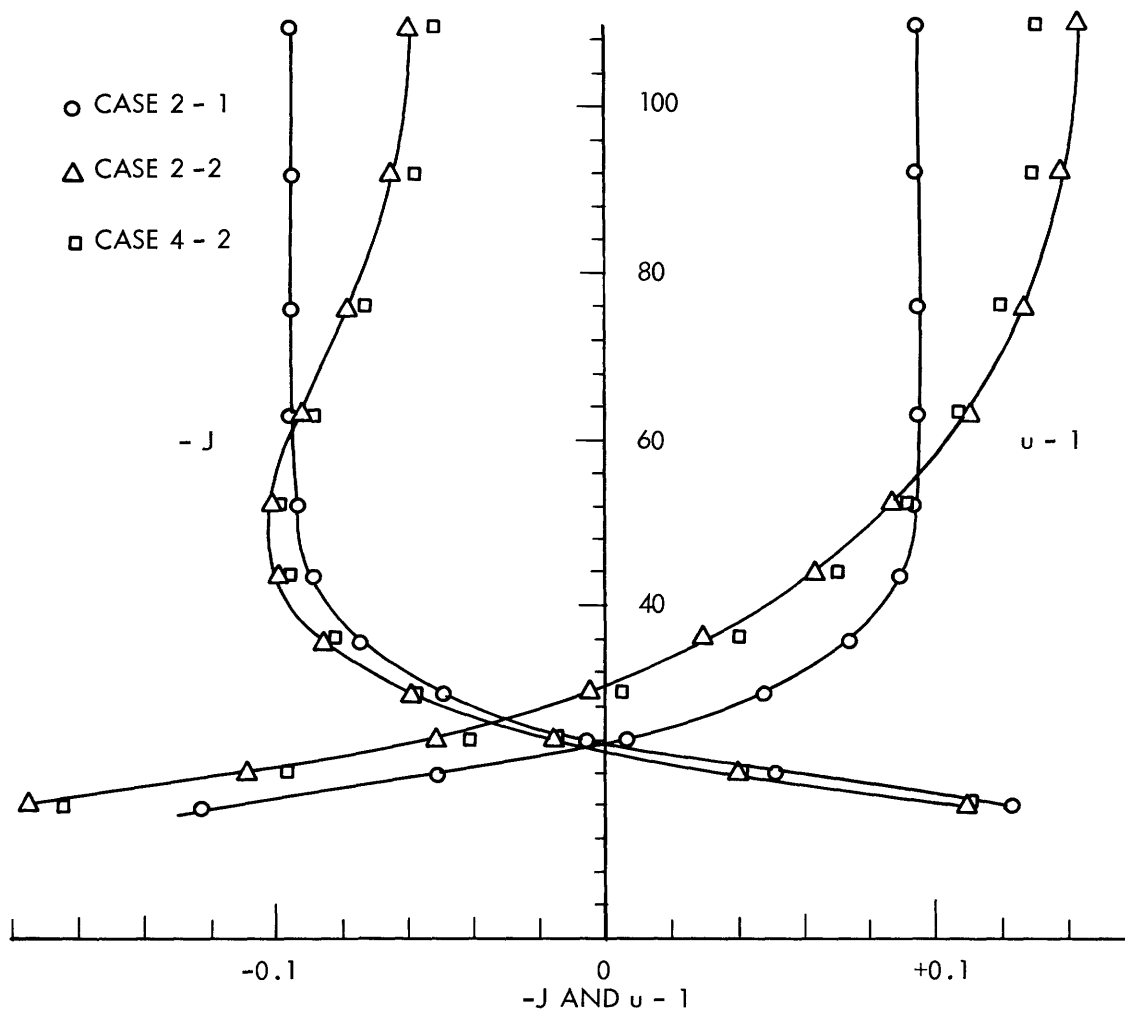


Fig. 35. Current-density and velocity profiles, Cases 2-1, 2-2, and 4-2, $x=131$.

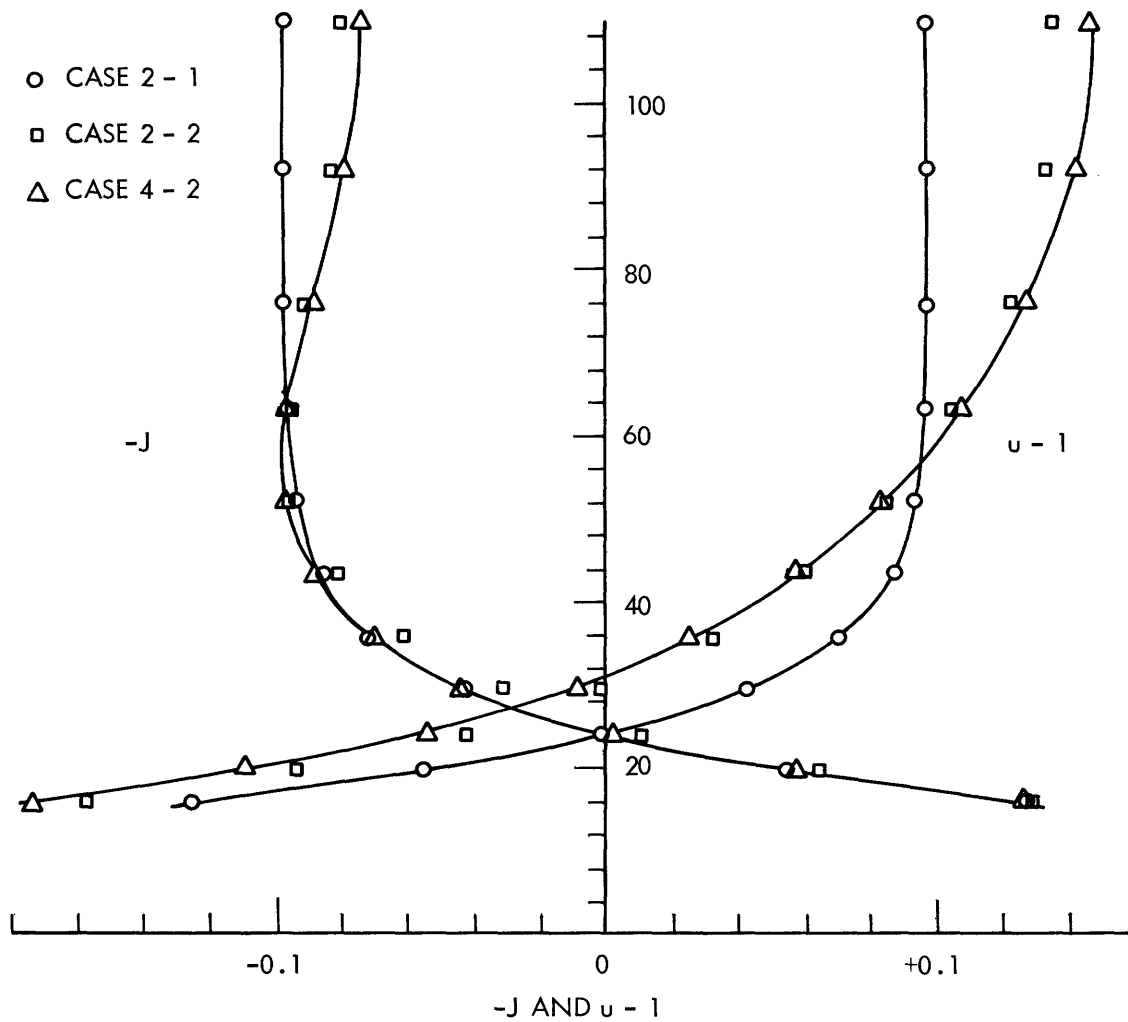


Fig. 36. Current-density and velocity profiles, Cases 2-1, 2-2, and 4-2, $x=159$. (Note that current density for Case 4-2 has become more negative than Case 2-1 (Hartmann flow). This spurious effect is attributed to proximity of downstream boundary and can also be seen in Figs. 37-39 for Case 2-2.)

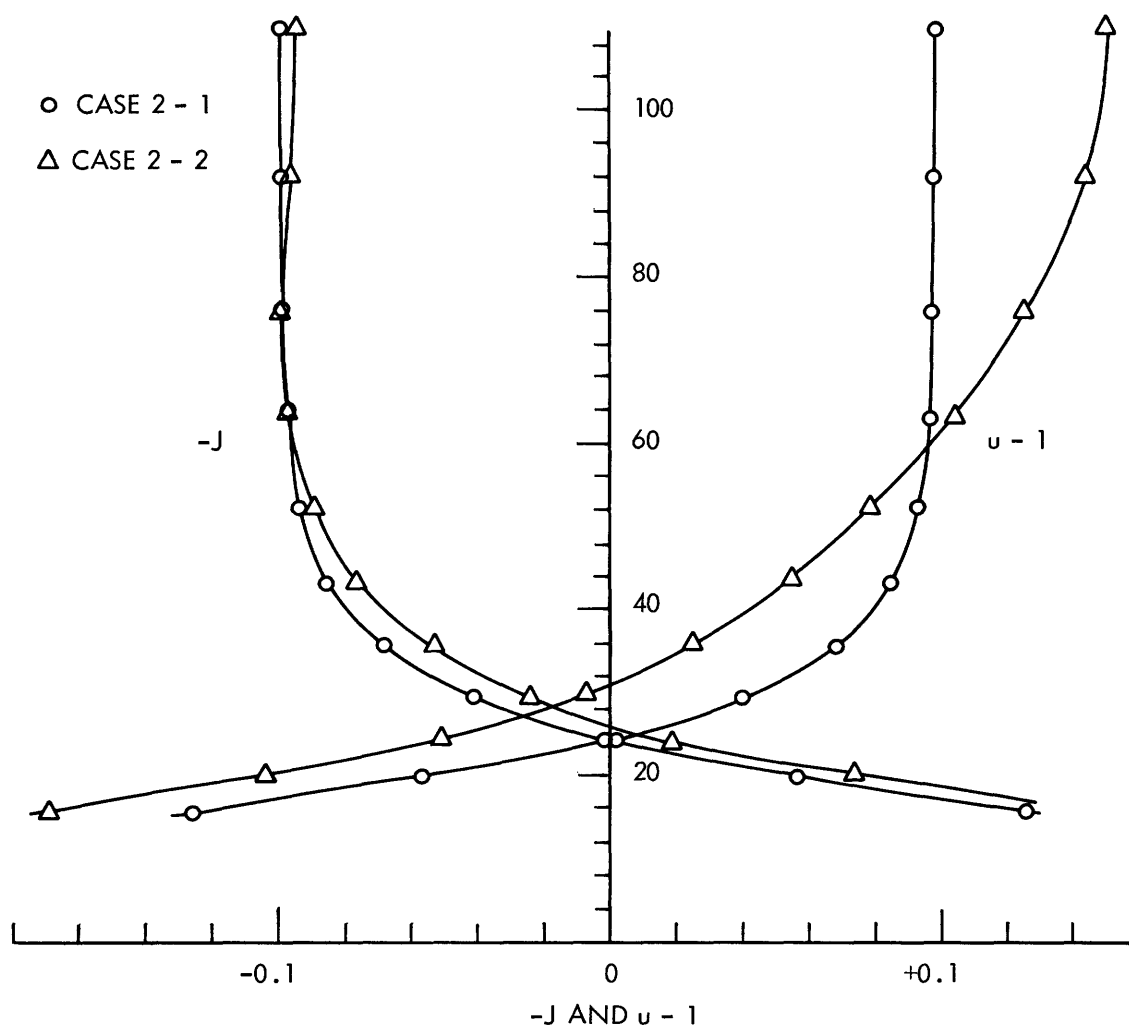


Fig. 37. Current-density and velocity profiles, Cases 2-1 and 2-2, $x=190$.

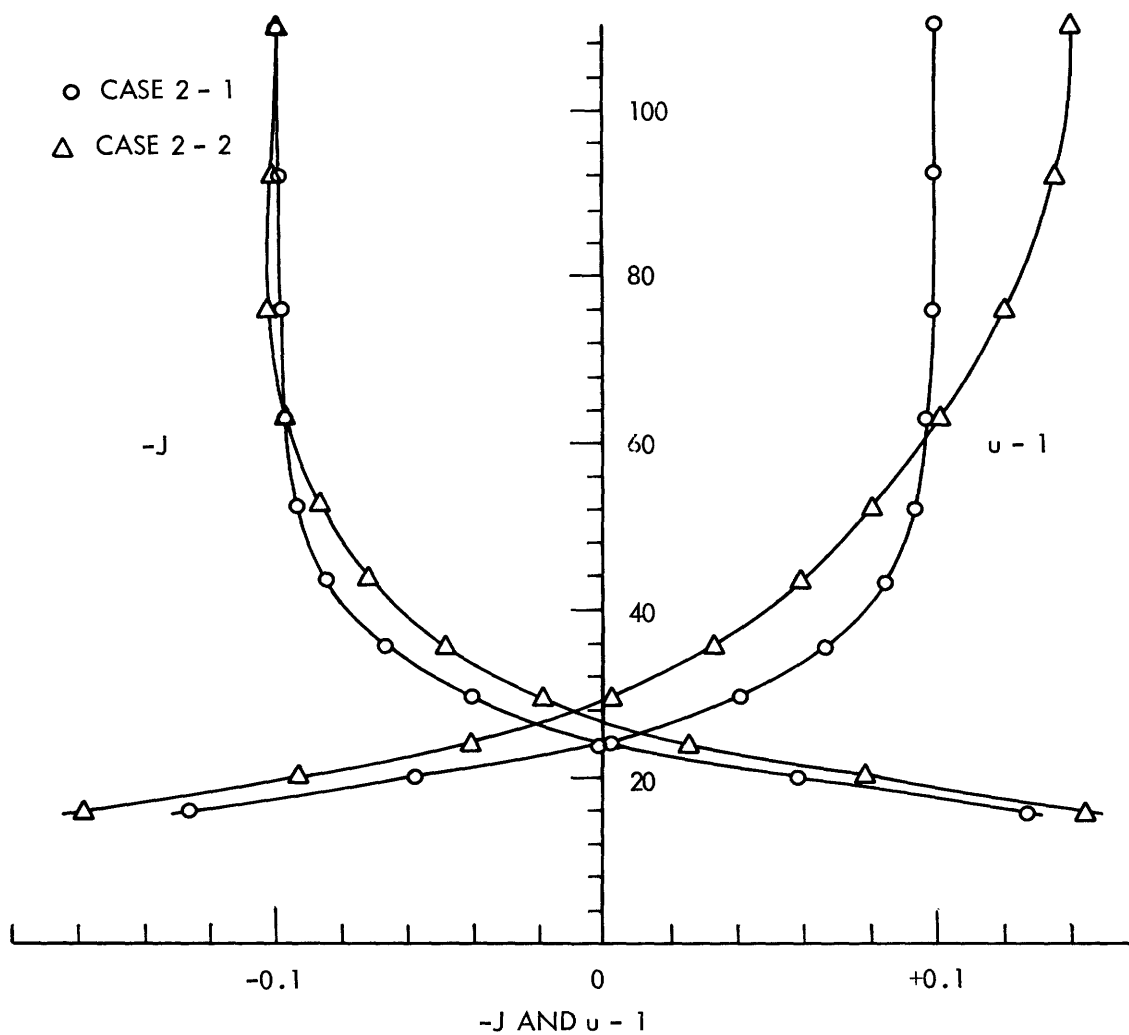


Fig. 38. Current-density and velocity profiles, Cases 2-1 and 2-2, $x=224$.

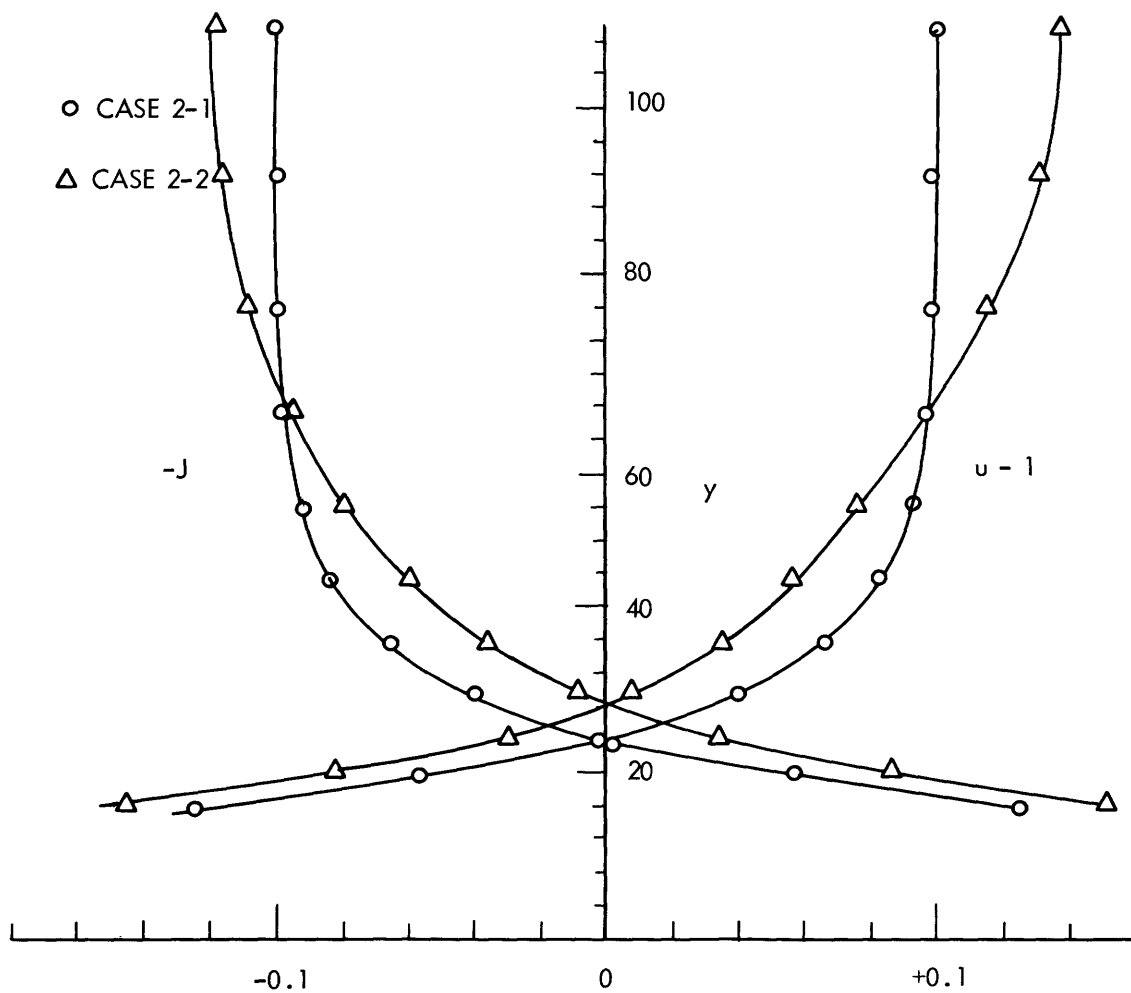


Fig. 39. Current-density and velocity profiles, Cases 2-1 and 2-2, $x=261$.

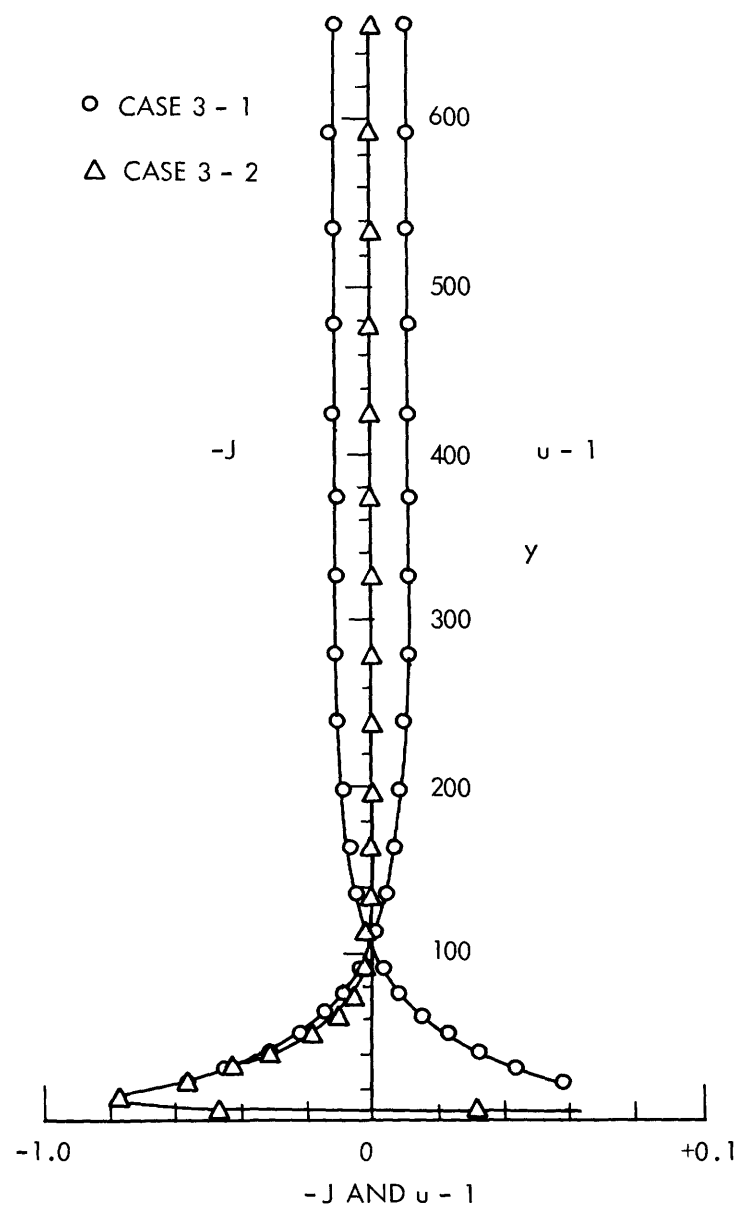


Fig. 40. Current-density and velocity profiles, Cases 3-1 and 3-2, $x=0$. (Velocity profile for Case 3-2 is not shown.)

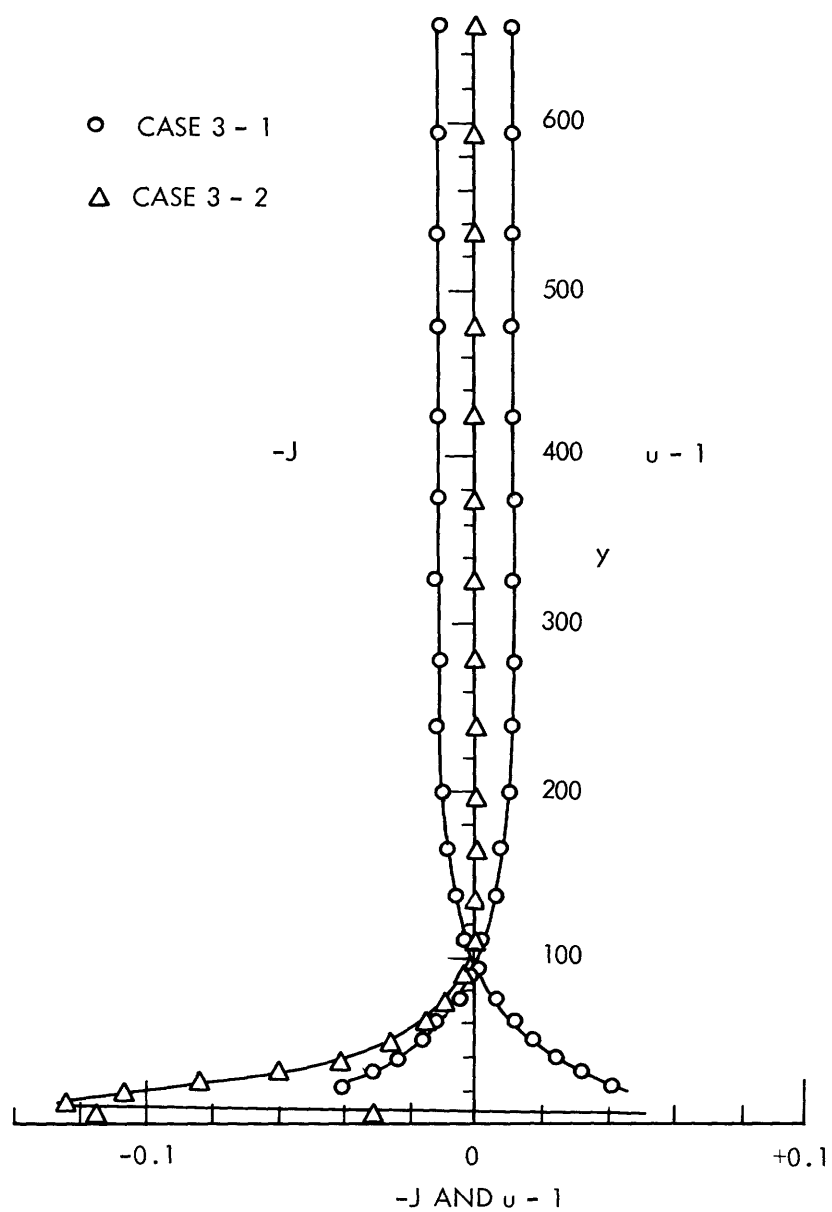


Fig. 41. Current-density and velocity profiles, Cases 3-1 and 3-2, $x=6$. (Velocity profile for Case 3-2 is not shown.)

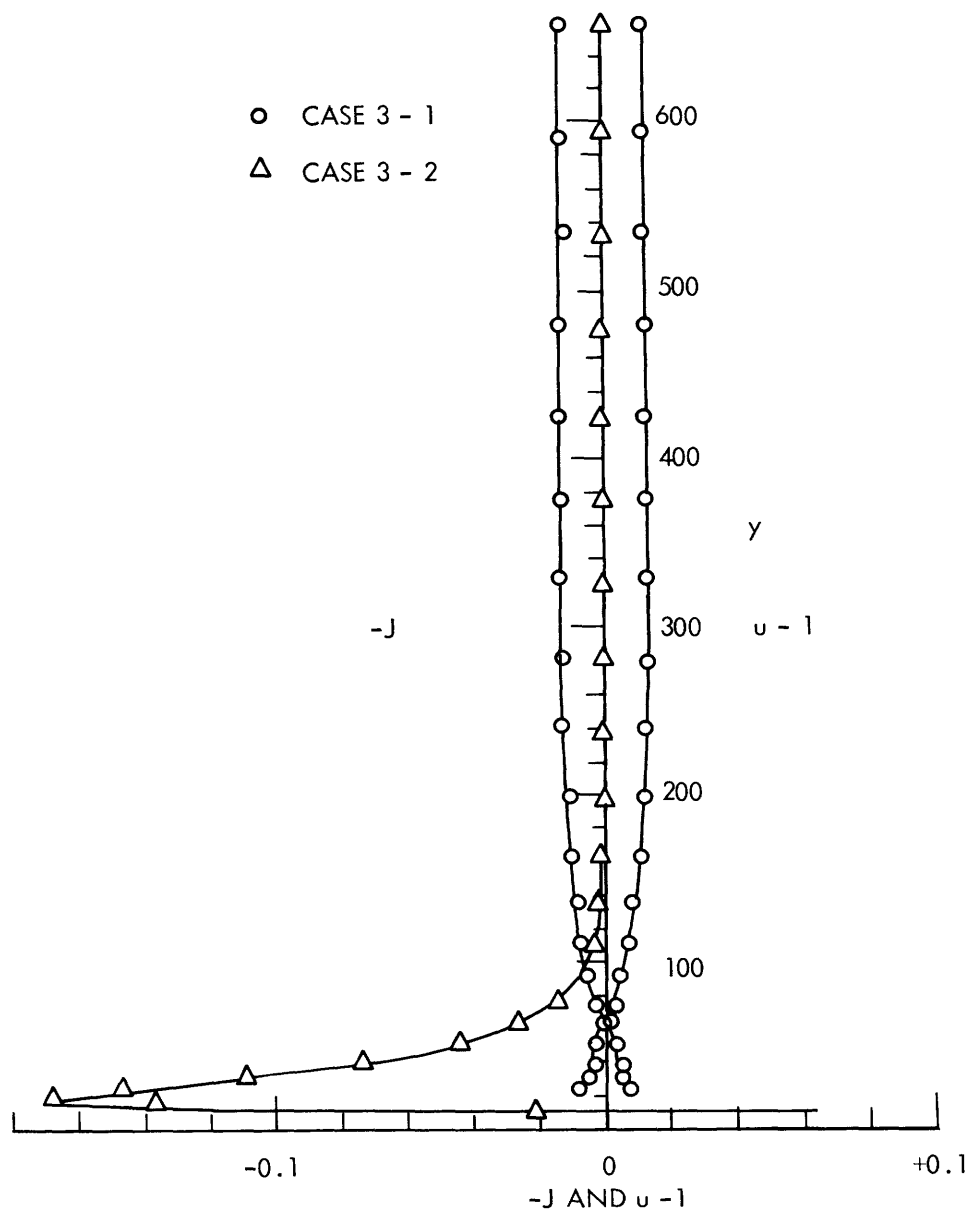


Fig. 42. Current-density and velocity profiles, Cases 3-1 and 3-2, $x=19$. (Velocity profile for Case 3-2 is not shown.)

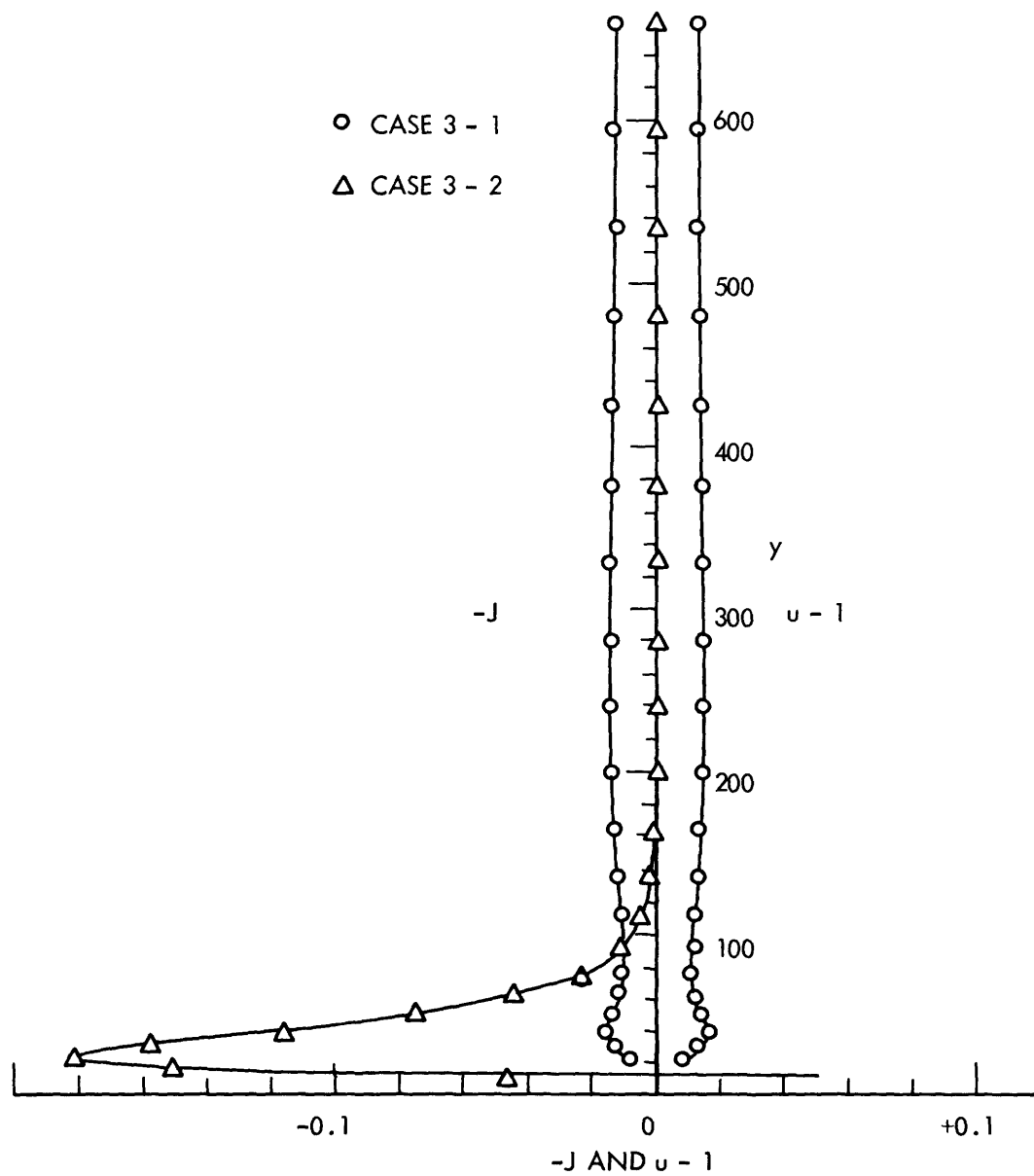


Fig. 43. Current-density and velocity profiles, Cases 3-1 and 3-2, $x=34$. (Velocity profile for Case 3-2 is not shown.)

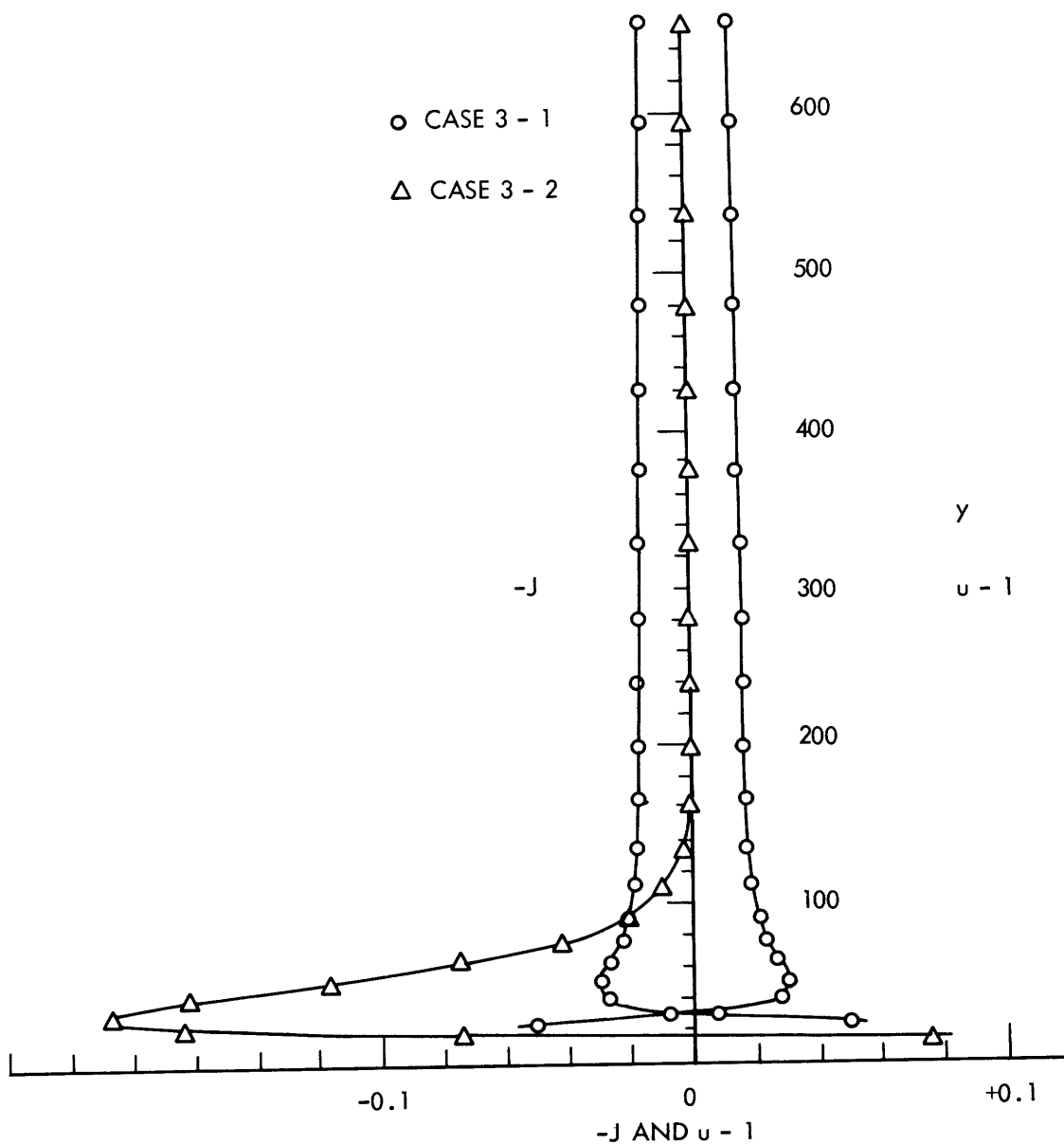


Fig. 44. Current-density and velocity profiles, Cases 3-1 and 3-2, $x=55.1$. (Velocity profile for Case 3-2 is not shown.)

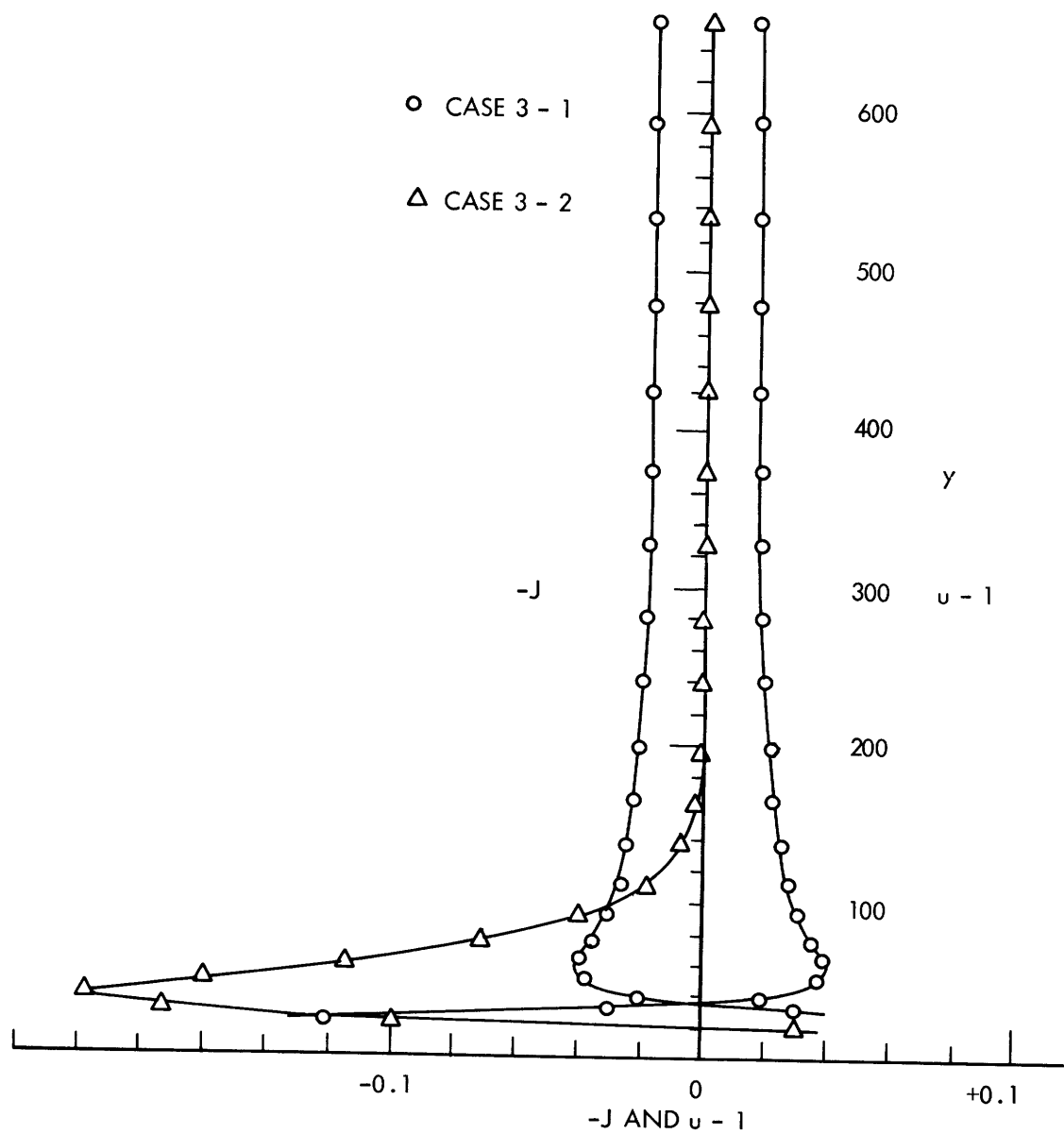


Fig. 45. Current-density and velocity profiles, Cases 3-1 and 3-2, $x=83.9$. (Velocity profile for Case 3-2 is not shown.)

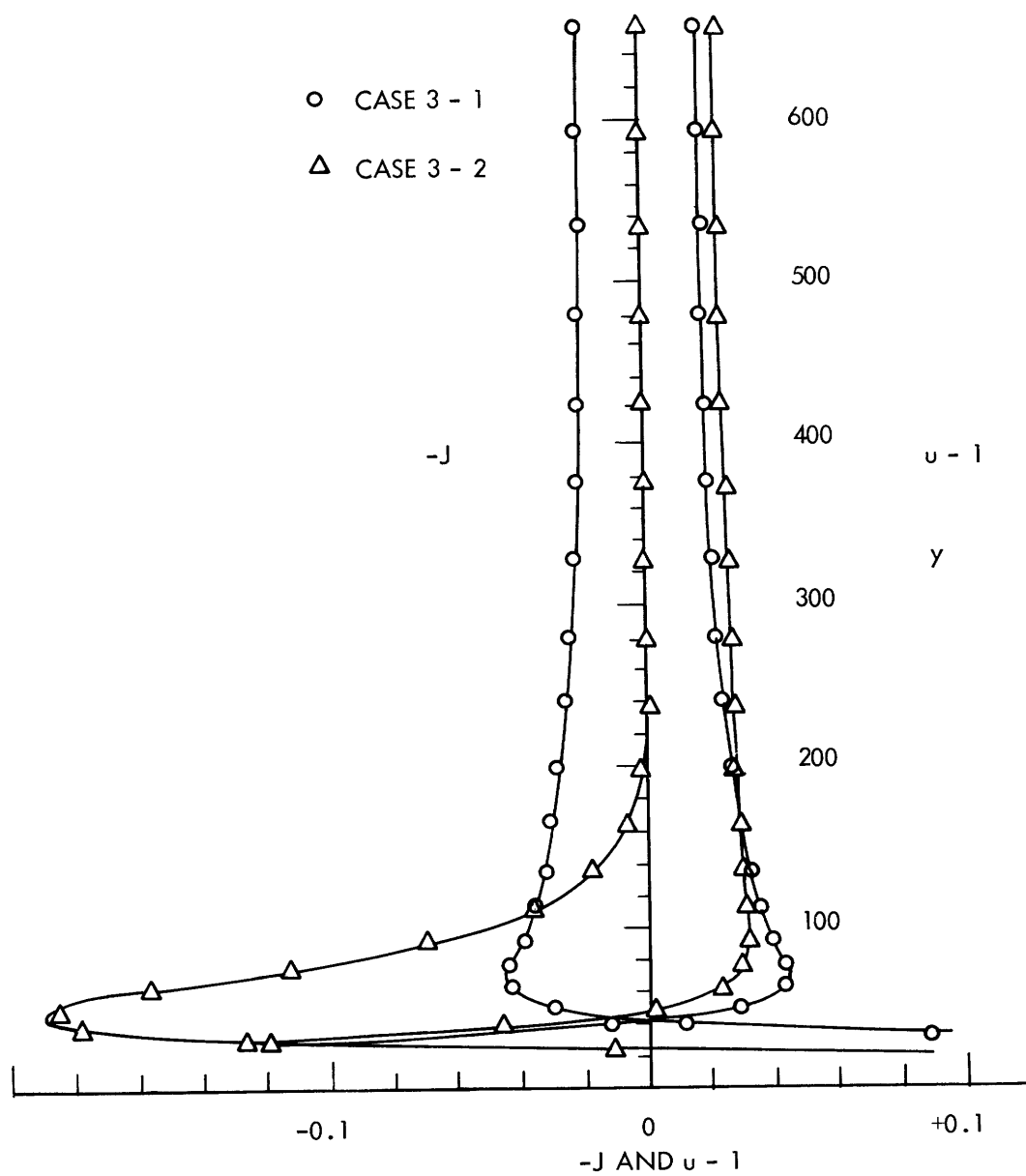


Fig. 46. Current-density and velocity profiles, Cases 3-1 and 3-2, $x=123.5$.

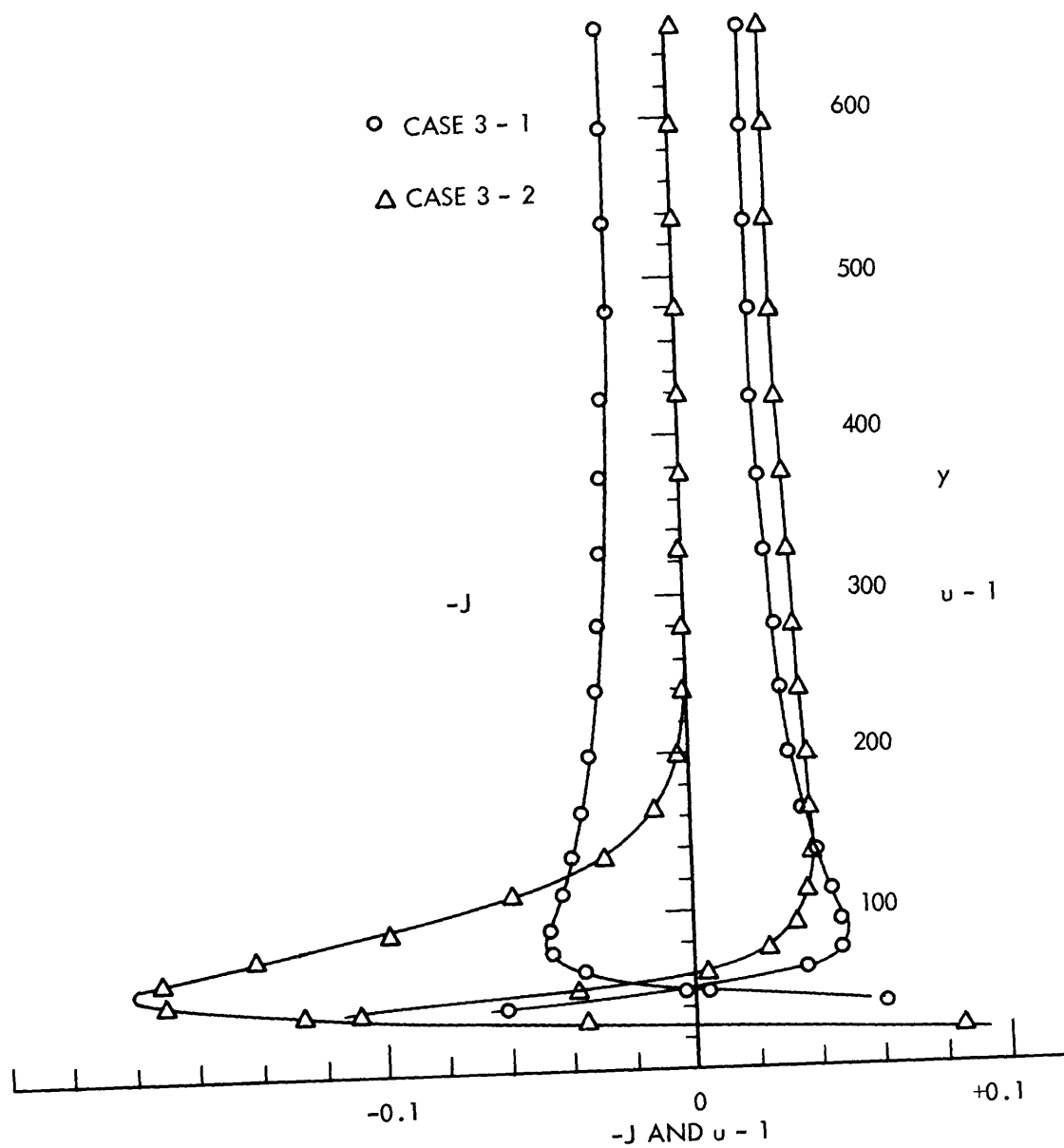


Fig. 47. Current-density and velocity profiles, Cases 3-1 and 3-2, $x=178$.

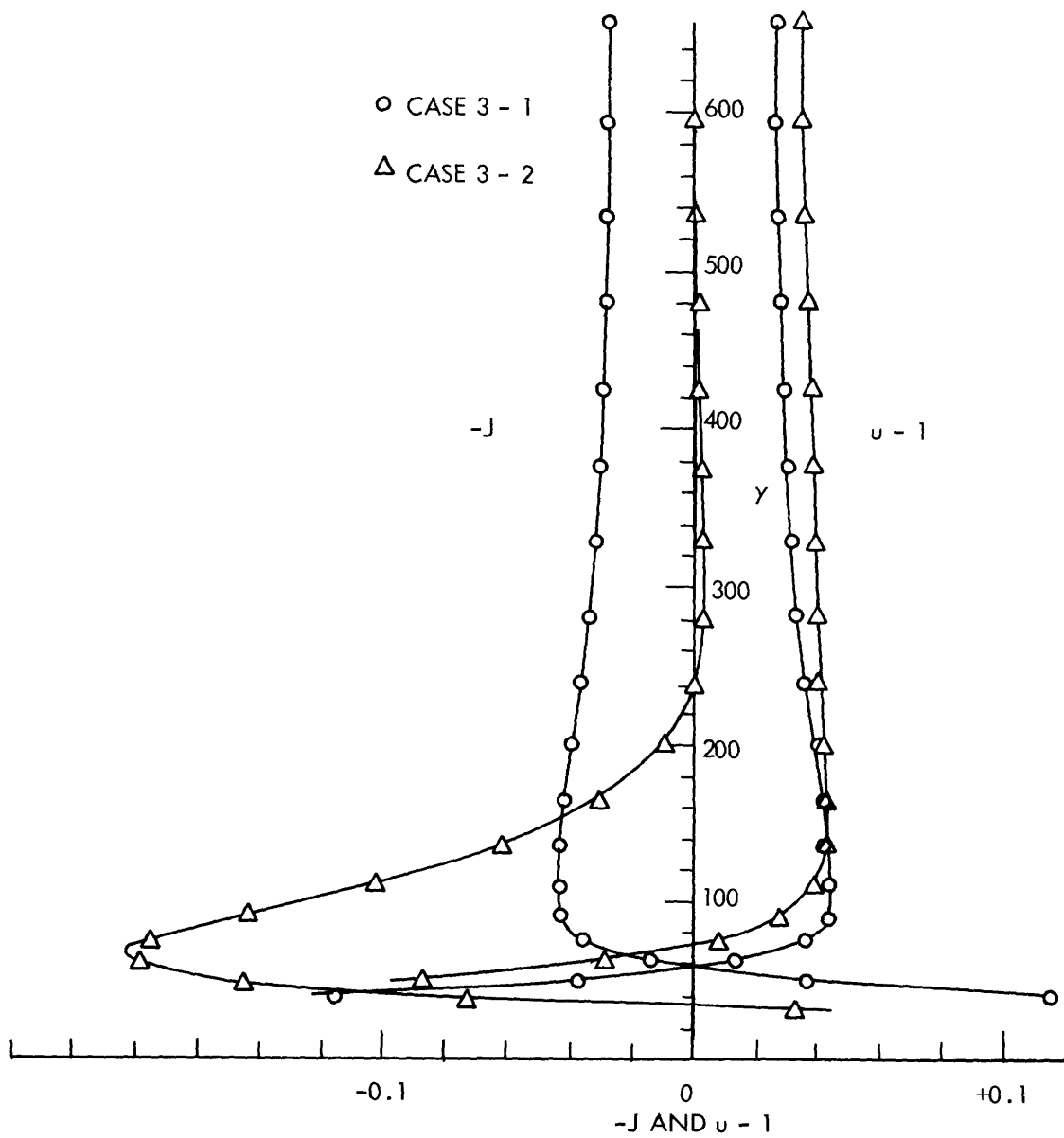


Fig. 48. Current-density and velocity profiles, Cases 3-1 and 3-2, $x=253$.

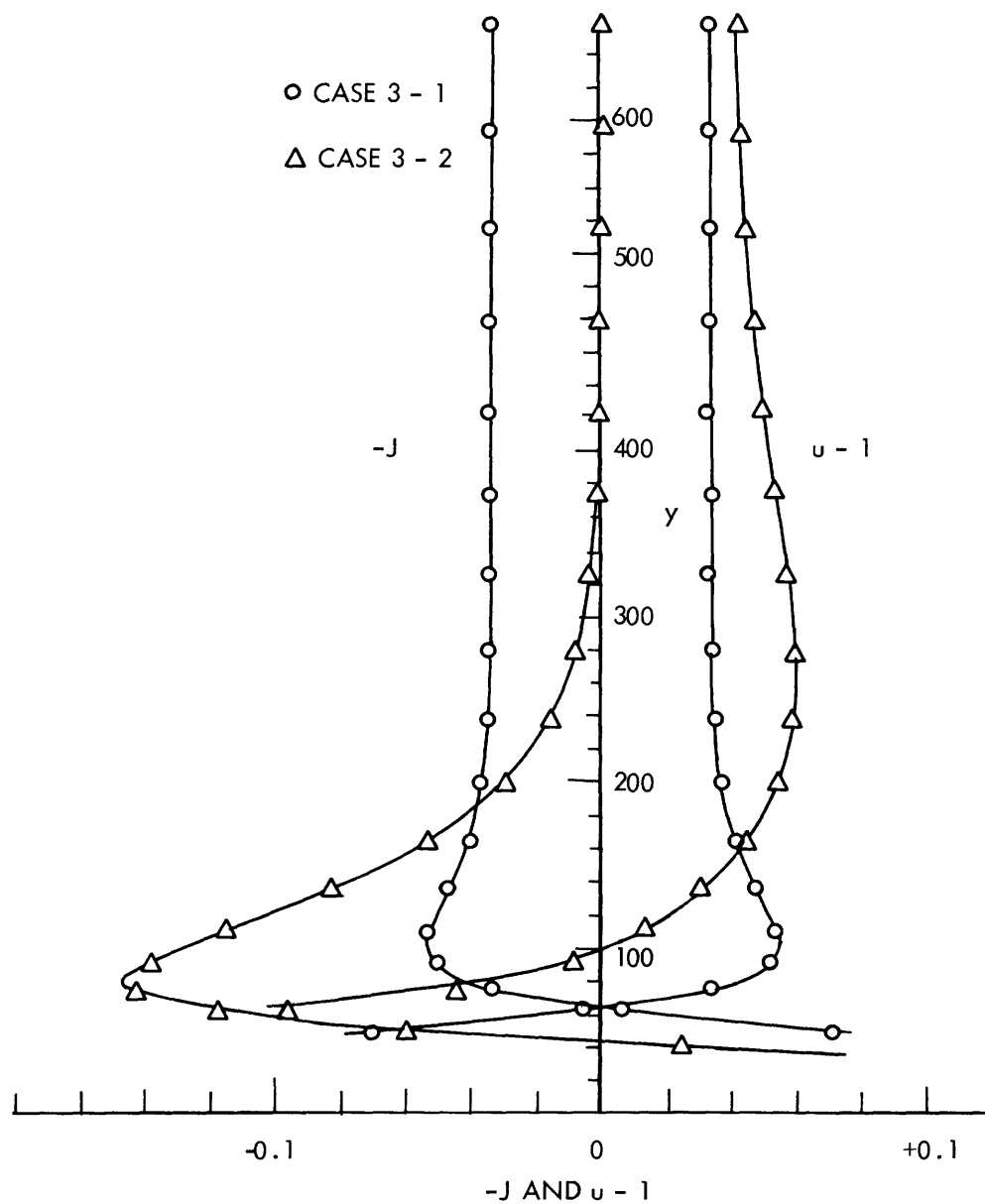


Fig. 49. Current-density and velocity profiles, Cases 3-1 and 3-2, $x=357$. (Note potential flow characteristics of velocity profile for Case 3-2.)

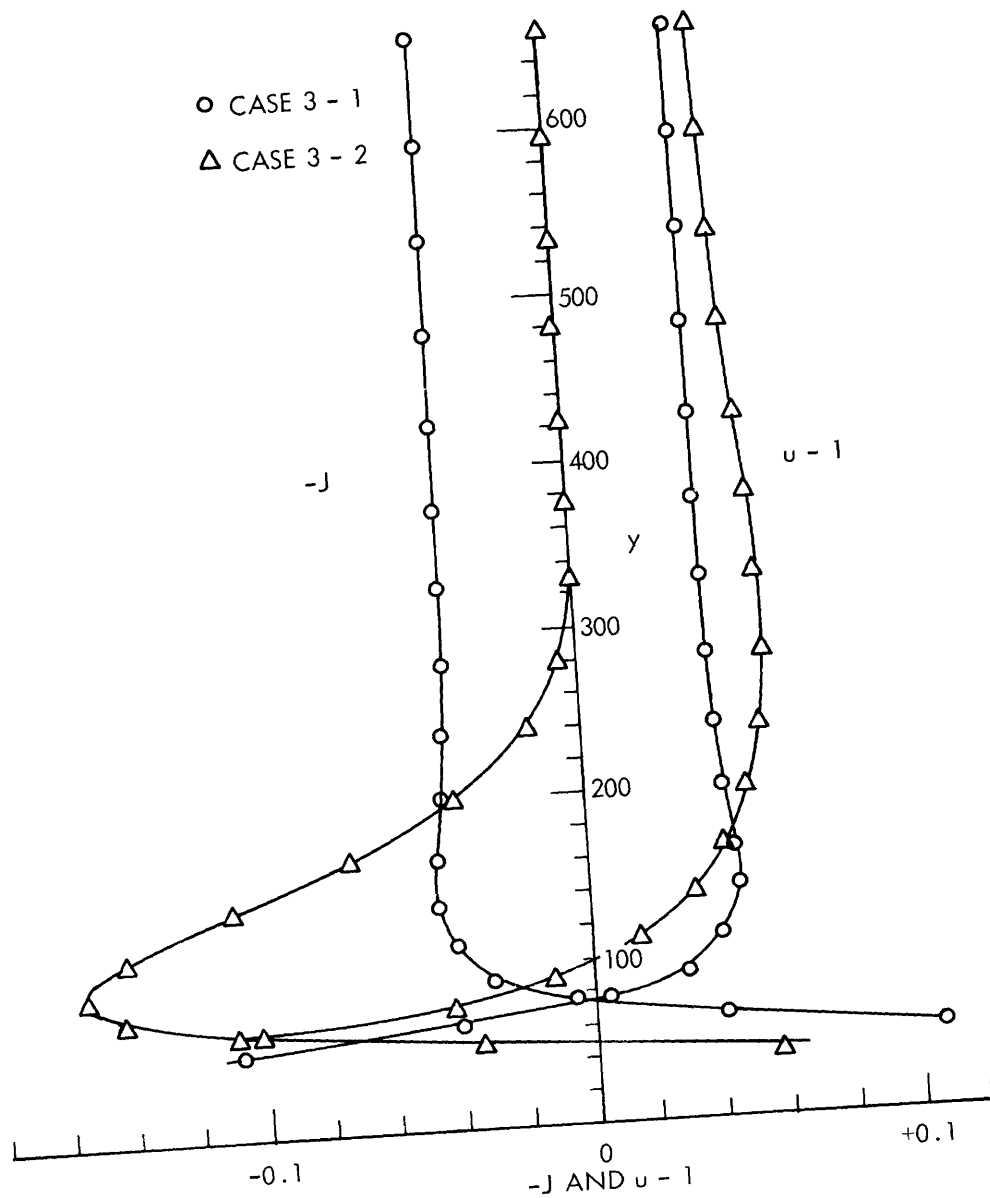


Fig. 50. Current-density and velocity profiles, Cases 3-1 and 3-2, $x=454$.

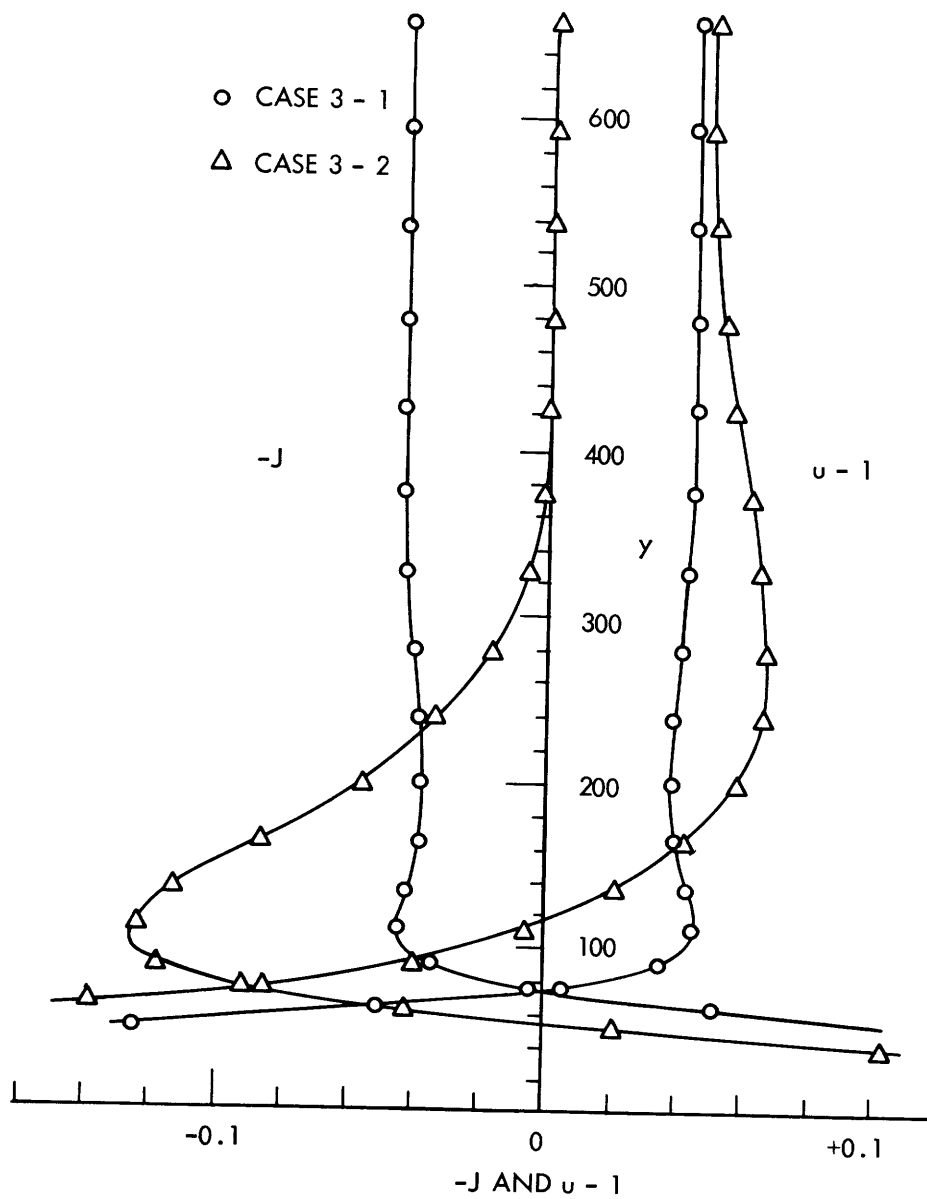


Fig. 51. Current-density and velocity profiles, Cases 3-1 and 3-2, $x=552$.

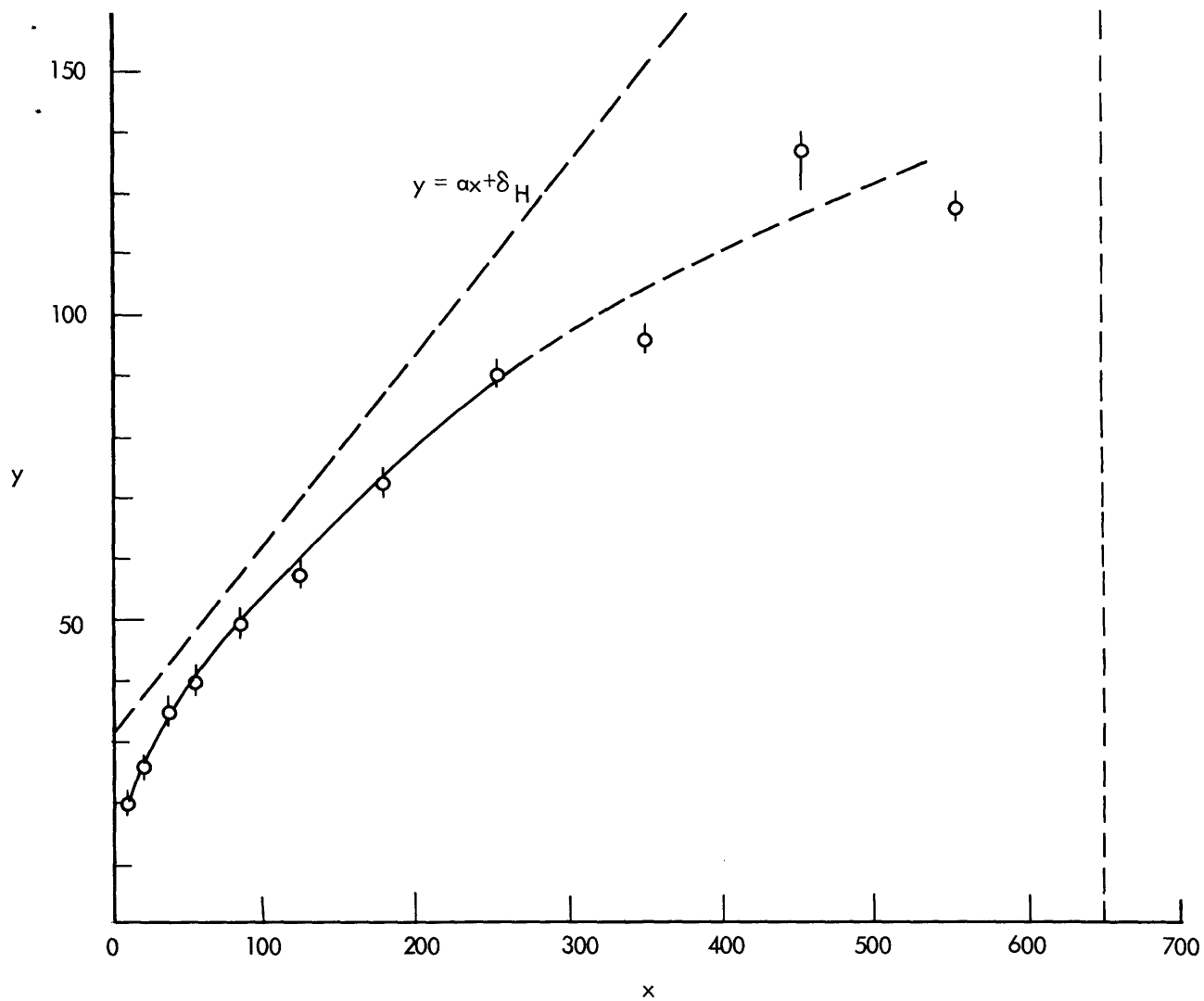


Fig. 52. Location of maximum positive current, Case 1-3.
(Vertical lines at points are estimated uncertainty
in location. Broken line on right indicates down-
stream boundary position.)

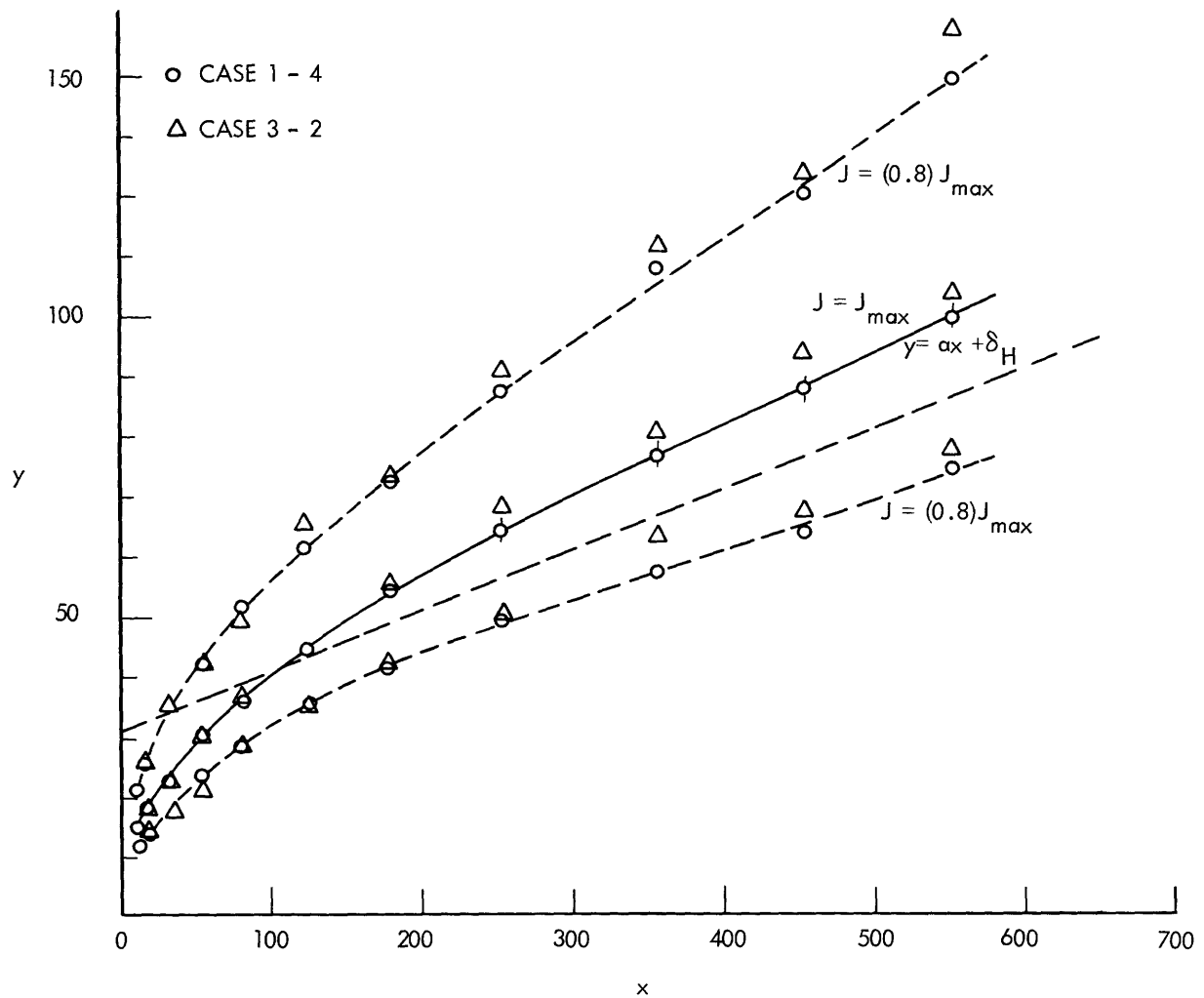


Fig. 53. Location of maximum positive current, Cases 1-4 and 3-2. (Vertical lines at points for Case 1-4 are estimated uncertainty in location of maxima. Downstream boundary position is at far right.)

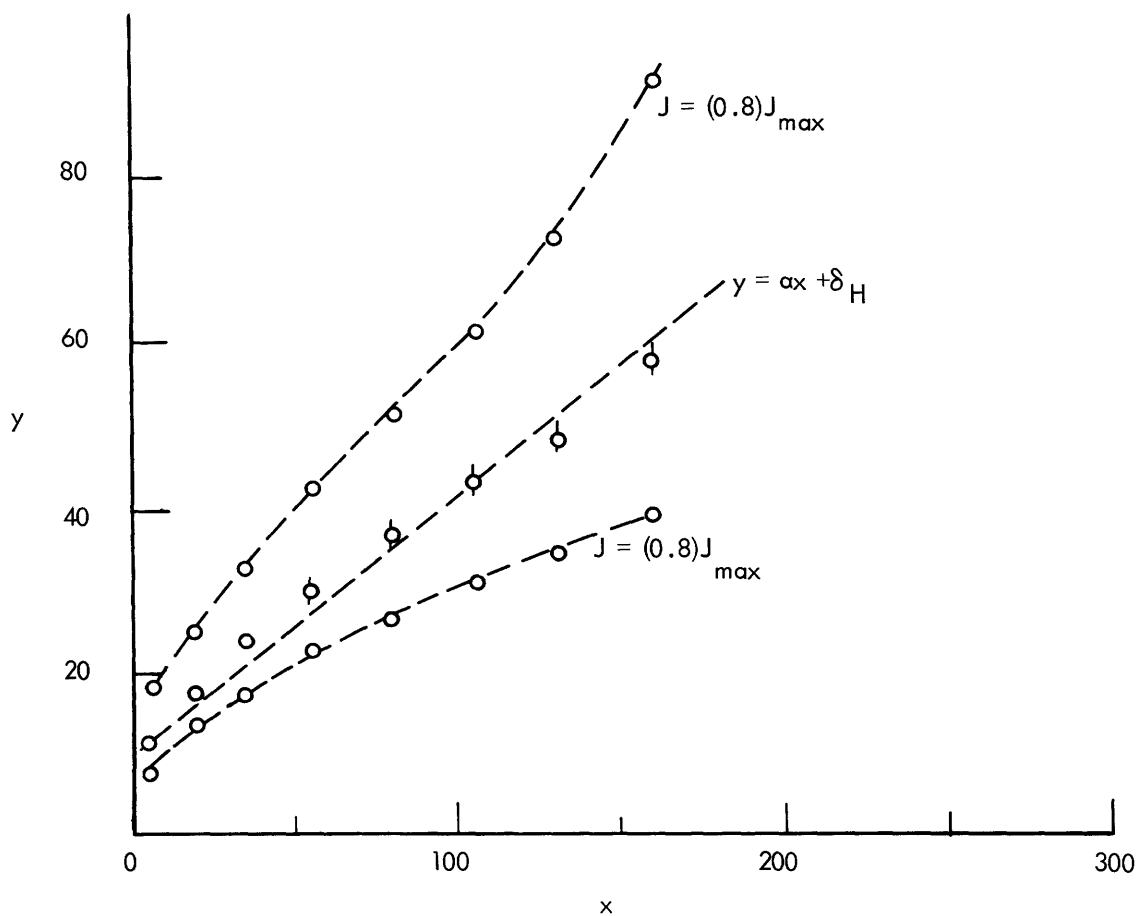


Fig. 54. Location of maximum positive current, Case 2-1. (Vertical lines at points are estimated uncertainty in location of maxima. Downstream boundary is at far right.)

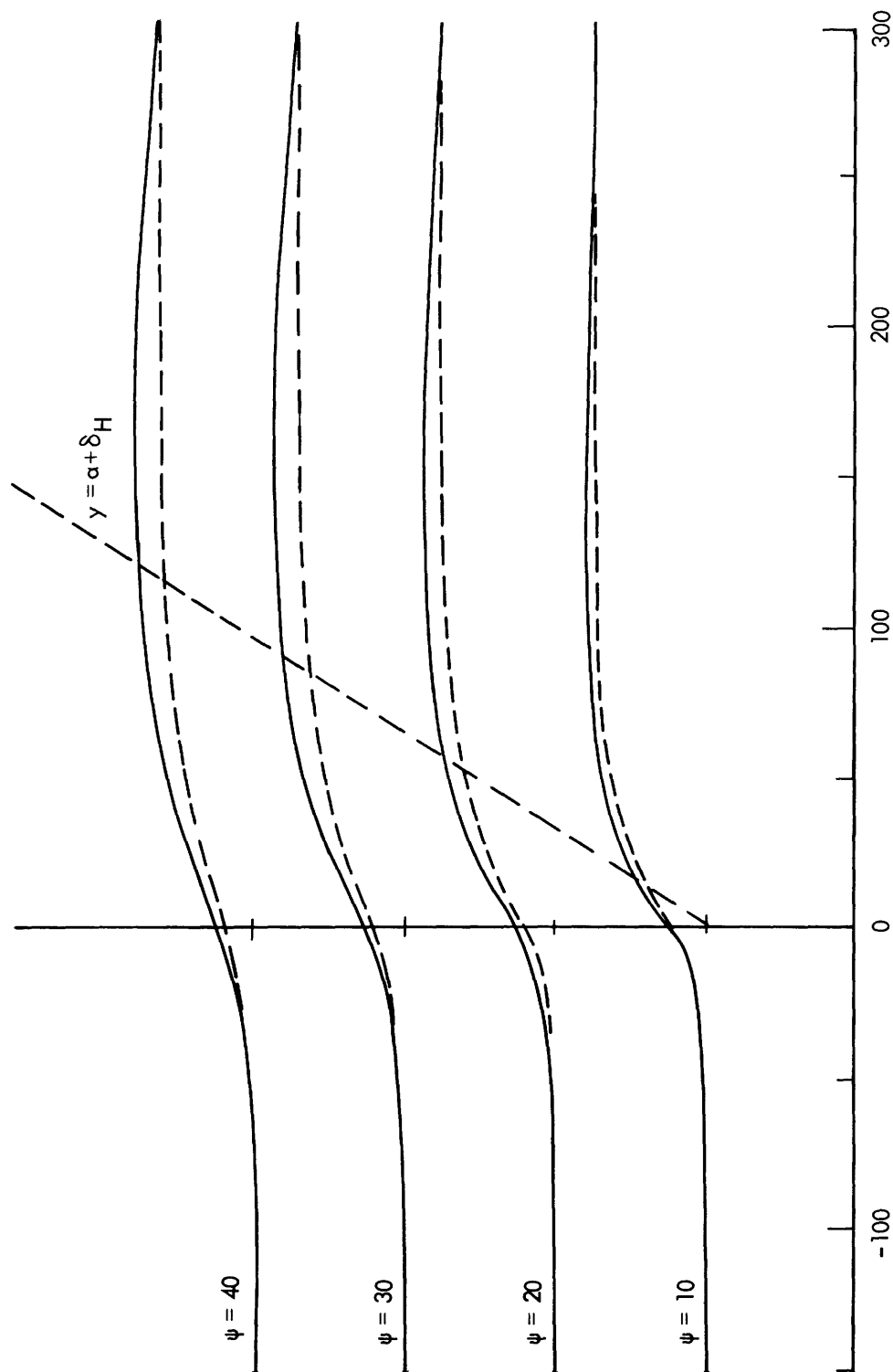


Fig. 55. Location of streamlines, Cases 2-1 and 2-2. (Broken lines are location of streamlines for Case 2-1 (Hartmann flow). Downstream boundary is at far right.)

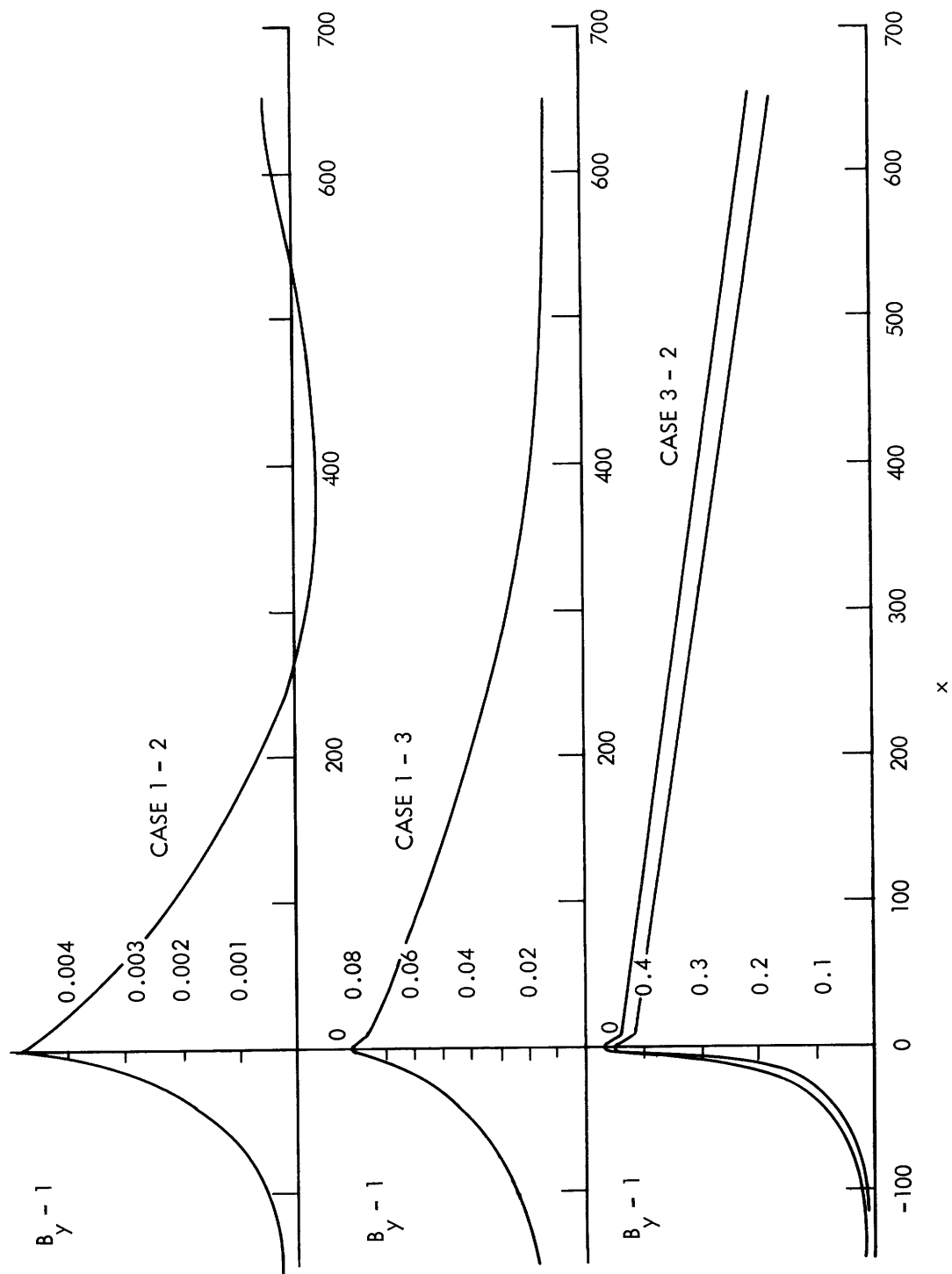


Fig. 56. Normal component of magnetic field at plate, Cases 1-2, 1-3, 1-4, and 3-2.

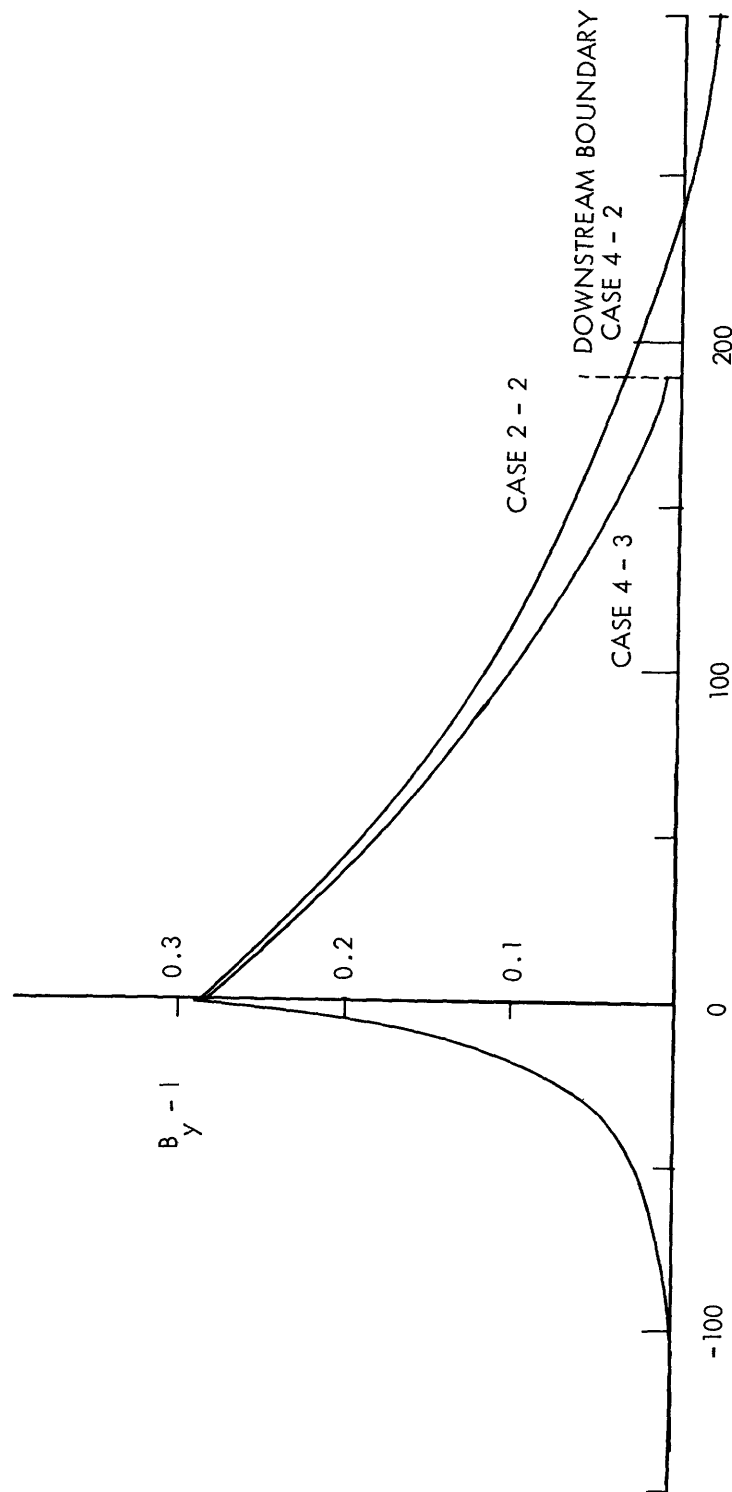


Fig. 57. Magnetic field at plate, Cases 2-2 and 4-2. (Downstream boundary for Case 2-2 is located at $x=300$.)

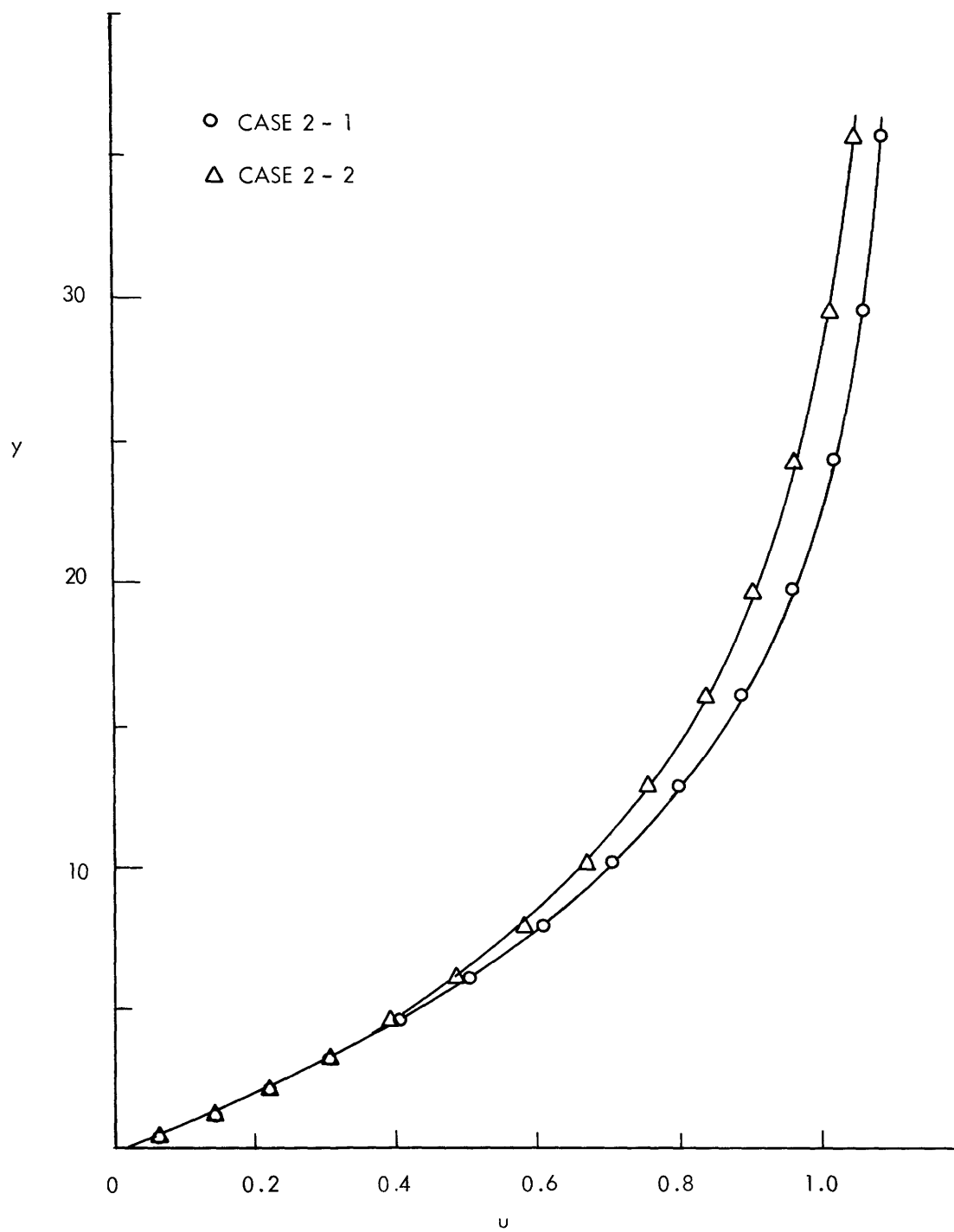


Fig. 58. Velocity profiles at plate, Cases 2-1, 2-2, $x=105$.

V. DISCUSSION OF RESULTS

5.1 DISCUSSION AND SUMMARY

a. Hartmann Flow

It is of interest to compare the skin friction obtained for the Hartmann type of flows (Cases 1-1, 2-1, 3-1, and 4-1) with that obtained from the linearized solution of Section III. To accomplish a meaningful comparison it is necessary to eliminate as much as possible the effects of the transverse boundary on the numerical results, and also to select an appropriate value of the average longitudinal component of velocity to be used in the linearized solution (the factor K in Eq. 85).

Channeling effects were approximately eliminated by dividing the actual skin friction obtained at a given x -position by the dimensionless velocity at the transverse boundary at the same x -position. This, of course, is not an exact procedure, since the equations are nonlinear, but the error so introduced must be much smaller than the increase in skin friction resulting from channeling effects, which never exceeds 10 per cent in the cases investigated here.

The selection of the average longitudinal component of velocity to be used in the linearized solution was made on the basis of a reasonable correlation with the numerical results and is therefore somewhat arbitrary. The results are shown in Fig. 15 in the form of the ratio of the skin friction to that of a fully developed Hartmann layer versus the dimensionless x -coordinate $x_H = \epsilon a^2 x$ divided by the factor K . There are two significant features of these results. First, it is evident that the functional form of the linearized solution is not exactly correct because a single value of K for any given case does not yield exact correlation. However, the correlation obtained is relatively good. Second, as the value of the interaction parameter, ϵa^2 , is increased, the best value of the factor K increases. This can be interpreted on physical grounds, for as the interaction parameter increases the viscous layer becomes thinner, and hence one can expect that the appropriate average velocity employed in the linearized solution would increase.

We conclude, furthermore, that since a reasonable correlation can be obtained, the accuracy of the numerical computations is sufficient for the purposes of this report. Of course, this accuracy could be estimated by merely reducing the net spacing and recalculating the solution for a given case, but we feel that this more accurate appraisal is not commensurate with the extremely large computational time involved.

Finally, it is necessary to evaluate the effect of the boundaries imposed on these solutions. The effect of the transverse boundary on the skin friction can be seen to be easily predictable on the basis of the increase in velocity above the free-stream value at this boundary by comparing the results of Cases 1-1 and 3-1 in Fig. 15 in which this effect has been eliminated. The location of the downstream boundary has no appreciable effect (less than 0.5 per cent) in the results of Cases 2-1 and 4-1, in spite of the fact that the position of the downstream boundary in the latter case is $l/x_g = 1.9$, as compared

with $\ell/x_g = 3.0$ in the former case. In Cases 1-1 and 3-1, the location of the downstream boundary is $\ell/x_g = 0.65$, and it is expected that the boundary effect is more appreciable than in the preceding cases, but is still not significant. Considerations of these boundary effects when the magnetic field distortion is appreciable is somewhat more complex, and hence the discussion is now deferred.

The primary usefulness of the above-mentioned results, in addition to yielding insight into the general behavior of the flow and the significant parameter involved, lies in their verification of other boundary-layer calculations. For example, Moffatt,²⁶ employing the usual integral methods with similar velocity profiles, obtains the following result for the skin friction:

$$\psi_{yy} = \frac{.817 \sqrt{\epsilon a^2}}{(1 - \epsilon^{-5x_H})^{1/2}}.$$

This relation is also plotted in Fig. 15. It is seen that the correlation with the numerical results obtained becomes poorer as the parameter ϵa^2 is increased. This indicates that the assumption of similar velocity profiles needs modification if the accuracy of the method is to be improved.

b. Significant Features of the Numerical Results for the Complete Flow

There are two basic categories for the significant features of the numerical results: those features that represent the actual physical character of flow past a flat plate, and the effect of these features caused by the imposed boundaries. We shall deal with these features in order.

Current-Density Distribution

From the current-density profiles presented for the various cases in Figs. 16-27, Figs. 28-39, and Figs. 40-51, it can be seen that as the parameter ϵ is increased (while the parameter ϵa^2 remains fixed), the current density outside the viscous layer becomes more concentrated in specific regions and results in maxima in the profiles. The maximum magnitudes of this effect are summarized in tabular form:

| Case | x | $-J_{\text{Max}}/J_{y=0}$ (per cent) | $-J_H/J_{y=0}$ (per cent) |
|------|------|---|------------------------------|
| 1-3 | 83.9 | 8.4 | 5.0 |
| 1-4 | 83.9 | 18.8 | 2.0 |
| 3-2 | 83.9 | 20.0 | 2.0 |
| 2-2 | 19 | 14.0 | 5.5 |

Here, $-J_{\text{Max}}/J_{y=0}$ denotes the value of the current density at the maximum of the profile

expressed as a percentage of the value at the plate; similarly, $-J_H/J_{y=0}$ denotes the value of the current density in the relevant Hartmann flow at the same location.

When the location of the resultant maxima of these current-density profiles is plotted as in Figs. 52, 53, and 54, it appears to correlate somewhat with the corresponding Alfvén line originating at the x-coordinate of the leading edge and at a y-coordinate equal to the displacement thickness of the viscous layer. This is particularly true for the maximum value of $\epsilon = 0.1$ employed (Figs. 53 and 54). In Fig. 52, for Case 1-3, the correlation is very poor indeed, and is attributed to the fact that the interaction between magnetic field and fluid field is not sufficient to overcome the potential flow effects created by the displacement of the flow caused by the viscous layer. This conclusion is supported by the velocity profiles shown in Figs. 22-27 for Case 1-3. Also plotted in

Table V. Correlation of width of Alfvén line with \sqrt{x} .

| Case 1-4 | | Case 2-2 | |
|----------|---------------------|----------|---------------------|
| x | $\Delta y/\sqrt{x}$ | x | $\Delta y/\sqrt{x}$ |
| 19 | 5.51 | 19 | 2.57 |
| 55.1 | 4.97 | 34 | 2.68 |
| 83.9 | 4.91 | 55.1 | 2.69 |
| 123.5 | 4.85 | 80 | 2.77 |
| 178 | 4.80 | 105 | 2.96 |
| 253 | 4.83 | 131 | 3.32 |
| 357 | 4.97 | 159 | 4.15 |
| 454 | 5.24 | | |

Figs. 53 and 54 are lines showing where the current density outside the viscous layer becomes 80 per cent of the maximum value and thereby provides a measure of the width of the band of concentrated current density. Table V shows the relatively good correlation between the width of this band and \sqrt{x} for Cases 1-4 and 2-2. Order-of-magnitude considerations show that the ratio of the width of an Alfvén line to the distance from point of origin is $1/\sqrt{\epsilon}$; this compares favorably with the ratios listed in Table V.

Velocity Profiles

The longitudinal velocity profiles for the cases investigated are also plotted in Figs. 22-27, Figs. 28-39, and Figs. 40-51. From these figures it is noted that as the parameter ϵ is increased the velocity between the maximum of the current density and the plate decreases, with a corresponding increase in velocity between the current-density maximum and the transverse boundary. The maximum magnitudes of this effect for the cases investigated are summarized in tabular form:

| Case | x | Decrease (per cent) | Increase (per cent) |
|------|-----|------------------------|------------------------|
| 1-3 | 357 | 1.4 | 1.0 |
| 1-4 | 357 | 8.4 | 3.9 |
| 2-2 | 131 | 5.8 | 4.9 |
| 3-2 | 357 | 9.2 | 2.5 |
| 4-2 | 131 | 4.6 | 3.7 |

The percentage changes are the changes in velocity from the corresponding Hartmann flow values referred to the free-stream velocity. It is seen that this effect does not become appreciable until the parameter $\epsilon = 10^{-2}$ is reached and, in the cases investigated, the maximum effect is a 9.2 per cent decrease in (from the Hartmann flow values) velocity near the plate and a 2.5 per cent increase in velocity near the transverse boundary (Case 3-2). The transverse velocity component, which is not shown, tends to increase upstream of the line of maximum current density and decreases downstream of this line. Both of these effects are demonstrated by the change in location of the streamlines in Cases 2-1 and 2-2, shown in Fig. 55.

Note that the potential-flow effect indicated by the maxima in velocity profiles in Case 1-1 (Hartmann flow) completely disappears in Case 1-4 (Figs. 22-27). However, in Case 3-2 (Figs. 46-51), which is identical with Case 1-4 with the exception of the position of the transverse boundary, the maxima reappear, indicating that the potential-flow effect is at a much greater distance from the plate (on the free-stream side of the current-density maxima).

Magnetic Field

The normal component of the magnetic field at the plate is plotted in Figs. 56 and 57. It is seen that the changes in this component do not become appreciable until $\epsilon = 10^{-2}$ is reached, and the maximum amount is found in Case 3-2 (Fig. 56). The normal component at the transverse boundary (not shown) tends to decrease from the applied value; the maximum amounts of this decrease are summarized in tabular form:

| Case | Decrease (per cent) |
|------|------------------------|
| 1-2 | 0.6 |
| 1-3 | 2.5 |
| 1-4 | 10.6 |
| 2-2 | 8.2 |
| 3-2 | 4.8 |
| 4-2 | 8.0 |

It is also of interest to compare the change in the normal component of the magnetic field at the plate with that predicted by the linearized solution (Eq. 86). The comparison of the maximum change is illustrated in tabular form:

| $(B_y - 1)/\epsilon^{1/2}$ | | |
|----------------------------|-----------|--------|
| Case | Numerical | Eq. 86 |
| 1-2 | 0.150 | 0.87 |
| 1-3 | 0.794 | 1.195 |
| 2-2 | 0.920 | 0.995 |

The correlation is seen to be poor, in general, although the general character and order of magnitudes of the two results compare favorably. Furthermore, the rate of decay of this change is more rapid in the numerical results obtained than that predicted by the linearized solution.

Skin Friction

The skin friction at the plate is tabulated in Table IV for the cases investigated. It is seen that as the parameter ϵ is decreased, the skin friction tends to decrease very slightly. The maximum magnitude of this decrease is slightly more than 3 per cent for Case 2-2.

Boundary Effects

We turn now to the effect of the position of the downstream and transverse boundaries on the significant features of the flow just described. By comparing the current-density profiles for Case 1-4 (Figs. 16-27) with those for Case 3-2 (Figs. 40-51), we see that the general character of these profiles is unaltered by the position of the transverse boundary. The maximum change in current density from the Hartmann value is slightly greater for Case 3-2 than for Case 1-4, as we have already shown. The location of these maxima and the width of the band of concentrated current density are affected only slightly by the position of this boundary, as shown in Fig. 53. Similarly, the effect of the downstream boundary is portrayed in Cases 2-2 and 4-2. As shown in Figs. 32-39, the effect of placing the downstream boundary closer to the leading edge makes the changes in current-density profiles less pronounced, but only very slightly.

Examination of the longitudinal velocity profiles for Case 1-4 (Figs. 22-27) and Case 3-2 (Figs. 40-51) indicates again that the basic character of the flow is not changed by the position of the transverse boundary. We have seen that the change in velocity near the plate from the Hartmann value is increased and the change in velocity away from the plate is decreased when the transverse boundary is at a greater distance from the plate. Furthermore, it appears that in Cases 1-4 and 2-2, the channeling effects are obscuring

the potential-flow effects that are evident in the profiles for Case 3-2. As shown in Figs. 32-39 for Cases 2-2 and 4-2 and as indicated in tabular form, placing the downstream boundary closer to the leading edge does not alter the character of the flow, although the changes from Hartmann flow are less pronounced.

Figure 56 shows that placing the transverse boundary farther from the plate increases the change in the normal component of magnetic field at the plate (Cases 1-4 and 3-2), although the form of the disturbance is unchanged. We have shown that the decrease in magnetic field from the applied value at the transverse boundary decreases as the boundary is placed farther from the plate. Figure 57 indicates that the effect of placing the downstream boundary farther from the leading edge increases the magnetic field distortion at the plate and decreases the rate of decay.

It is evident from the preceding discussion that the effect of the finite position of the boundaries does not alter the basic character of the flow, but does slightly decrease the magnitudes of the effects encountered as the parameter ϵ is increased.

c. Summary of Results

From the numerical results presented, it is concluded that the presence of a nonconducting flat plate in an initially uniform, current-free flow of a conducting fluid in the presence of an applied transverse magnetic field, in addition to causing the formation of a thin viscous layer adjacent to the plate, excites an Alfvén type of disturbance which propagates into the free stream. This disturbance is readily identified as a region of high current density; henceforth we shall refer to it as an Alfvén line. The line, of course, has a finite width, which increases as \sqrt{x} because of diffusive effects. In addition to being a region of high current density, the line tends to decrease the longitudinal component of velocity of the fluid as the fluid crosses it; the net result is the creation of a sizeable disturbance to the uniform flow. The position of the line is a strong function of the ratio of the Alfvén speed to the free-stream velocity (our parameter α), while the magnitude of the disturbance created is a strong function of the ratio of the two diffusivities ($\epsilon = \sigma \mu_0 \nu$) and does not appear to become appreciable until $\epsilon \geq 10^{-2}$ is reached. This disturbance resulting from the Alfvén line is in marked contrast to the disturbance caused by a flat plate in the pure fluid mechanics case; it indicates that in flows of high electrical conductivity the effects of viscosity are no longer confined to a thin layer near the plate.

d. Interpretation of the General Character of the Numerical Results

Still to be interpreted are the significant features of the numerical results presented in the preceding section. We shall employ as a basis the fundamental concepts of Alfvén lines and viscous layers. The logical starting point for such a discussion is the analogy between the relevant Rayleigh problem and the present one, as discussed briefly in

Section II. Certainly, the general character of the numerical results (e.g., the changes in current density distribution and velocity profiles caused by the induced magnetic field) suggests a flow field of the type shown in Fig. 7, which was constructed by analogy with the Rayleigh problem. Of particular interest is the analogy of the ultimate state of the Rayleigh problem to some corresponding state, if there is any, in the present problem.

An examination of the differences in basic mathematical character of the two sets of equations governing the two problems is quite useful. The first major difference between these sets of equations is that the set governing the Rayleigh problem (Eqs. 7 and 8) is linear, while the set governing the semi-infinite plate problem (Eqs. 35 and 36) is nonlinear. If this were the sole difference between the two sets of equations, then it would be expected that the only major difference in the flow fields would be due to the fact that in the semi-infinite plate problem the slope of the Alfvén line would be determined by the local conditions rather than by the free stream conditions.

The second major difference between the two sets of equations is that while the set governing the Rayleigh problem exhibits only damped-wave characteristics in u and B , the linearized version (Eqs. 40 and 41) of the set governing the semi-infinite plate problem exhibits only damped-wave characteristics in ξ and J (see Sears and Resler,²³ for example). In the latter case this yields solutions for \underline{V} and \underline{B} which are the superposition of damped-wave solutions and potential solutions. This indicates that in the solutions for \underline{V} and \underline{B} the wave character may be considerably less pronounced than in the Rayleigh problem. Also, the existence of potential solutions coupled with the nonlinearity of the problem may change the location of the Alfvén line considerably from that expected on the basis of free-stream conditions.

The third major difference between the two sets of equations is that the relationship of the current density to the other field quantities is not analogous. This is due to the fact that in the Rayleigh problem, the electric field is related to $\partial \underline{B} / \partial t$ by Faraday's law, while in the semi-infinite plate problem the electric field is constant. This is emphasized by the fact that the quantity J^* / σ at the plate in the latter problem is not dependent upon the value of σ ; hence, as will be seen, this difference is of particular importance in the lack of analogy between the viscous layers of the two problems.

The fourth difference between the Rayleigh problem studied in Section II and the semi-infinite plate problem studied in Section IV is the presence of boundaries in the second problem.

With the basic character of the two problems in mind, we now turn our attention to the basic features of the flow in the semi-infinite plate problem. The model adopted here is that shown in Fig. 7, which is suggested both by analogy with the Rayleigh problem and the character of the numerical results previously obtained. For reasons that will become clear, we shall admit the possibility of velocity and magnetic field components v_1 and B_{x1} upstream of the Alfvén line. It is emphasized that this model cannot be accepted a priori, and its use here is as a base from which a more accurate picture of the flow can be synthesized, if necessary.

By applying dimensional arguments similar to those employed in Section II, the ultimate state of the semi-infinite plate problem (defined as the state in which the viscous layer is fully developed and the Alfvén line is clearly separated from it), if it exists, will be reached at a distance downstream from the leading edge so that

$$x^* > \frac{\mu_0 \rho U_\infty^2}{B_\infty^2} \frac{D}{\nu},$$

where D represents the larger of the two diffusivities ν or $1/\mu_0 \sigma$. In the dimensionless form, this becomes

$$x > \frac{D}{\nu a^2} \quad (108)$$

or

$$x > \frac{1}{\epsilon a^2} \quad (\epsilon < 1)$$

$$x > \frac{1}{a^2} \quad (\epsilon > 1).$$

The relationships governing the change of quantities across the Alfvén line are given (in dimensionless form) by

$$u_2 B_{y2} - v_2 B_{x2} = 1 - v_1 B_{x1}$$

$$\tan \theta - v_1 = u_2 \tan \theta - v_2 = a(1 - B_{x1} \tan \theta) \quad (109a-c)$$

$$B_{y2} = 1 + B_{x2} \tan \theta - B_{x1} \tan \theta$$

and the change in the longitudinal component magnetic field across the fully developed viscous layer is given by

$$B_{x2} = \frac{\sqrt{\epsilon}}{a} u_2. \quad (110)$$

The solution of these equations for the quantities of interest is indicated by

$$u_2 = \frac{1 + a B_{x1}}{1 + \sqrt{\epsilon}}$$

$$B_{x2} = \frac{\sqrt{\epsilon}}{1 + \sqrt{\epsilon}} \frac{(1 + a B_{x1})}{a} \quad (111a-e)$$

$$v_2 = \frac{(1 + 2a B_{x1} + \sqrt{\epsilon} a B_{x1}) v_1 + a^2 B_{x1} - \sqrt{\epsilon} a}{(1 + \sqrt{\epsilon})(1 + a B_{x1})}$$

$$\tan \theta = \frac{a + v_1}{1 + aB_{x1}} = \frac{(a+v_2)(1+\sqrt{\epsilon})}{1 + 2aB_{x1} + \sqrt{\epsilon}aB_{x1}}$$

$$B_{y2} = 1 + \left[\frac{\sqrt{\epsilon} - aB_{x1}}{a(1+\sqrt{\epsilon})} \right] \left[\frac{a + v_1}{1 + aB_{x1}} \right] = 1$$

$$+ \left[\frac{\sqrt{\epsilon} - aB_{x1}}{a} \right] \left[\frac{a + v_2}{1 + 2aB_{x1} + \sqrt{\epsilon}aB_{x1}} \right].$$

If it is now assumed that conditions upstream of the Alfvén line are the free stream conditions, then $v_1 = B_{x1} = 0$ and these solutions reduce to:

$$u_2 = \frac{1}{1 + \sqrt{\epsilon}}$$

$$B_{x2} = \frac{\sqrt{\epsilon}}{a(1+\sqrt{\epsilon})} \quad (112a-b)$$

$$v_2 = - \frac{\sqrt{\epsilon}a}{1 + \sqrt{\epsilon}}$$

$$\tan \theta = a \quad (112c-e)$$

$$B_{y2} = \frac{1 + 2\sqrt{\epsilon}}{1 + \sqrt{\epsilon}}.$$

It is evident that the results for u_2 , B_{x2} , and $\tan \theta$ are analogous to those obtained from the Rayleigh problem. However, the fact that v_2 does not vanish prevents this solution from being entirely satisfactory.

An alternative possibility is to require $v_2 = B_{x1} = 0$. This yields:

$$u_2 = \frac{1}{1 + \sqrt{\epsilon}}$$

$$B_{x2} = \frac{\sqrt{\epsilon}}{a(1+\sqrt{\epsilon})}$$

$$v_1 = \sqrt{\epsilon}a \quad (113a-e)$$

$$\tan \theta = a(1+\sqrt{\epsilon})$$

$$B_{y2} = 1 + \sqrt{\epsilon}.$$

Here again, the fact that v_1 does not vanish makes this solution unsatisfactory.

To reconcile either of these solutions with the problem at hand, it is necessary to return to the basic mathematical character of the equations; specifically, to the fact that potential solutions for the velocity field are admissible. In a qualitative way, then, the complete solution will consist of a wave solution of the general type of either of the preceding ones, plus a potential solution in \underline{V} and, if necessary, \underline{B} , in order that the boundary conditions may be satisfied. Furthermore, it is not difficult to see that this potential flow must resemble the perturbation from uniform flow caused by a wedge of included half-angle $\beta = \tan^{-1}(\sqrt{\epsilon}a)$. This potential flow effect is evident in the velocity profiles of Case 3-2 (Figs. 46-51). This fact at once makes the existence of some ultimate state extremely problematical, and at the same time permits amplification of the general conclusions regarding the nature of the flow.

These amplifications are limited in scope to that region of the flow where the superposition of the wave solution and the potential solution is valid; that is, the inequality (108) must be satisfied and, in addition, the parameter ϵa^2 must be small in order that the transverse component of velocity induced by the Alfvén line is not large, and, also, x must be limited in such a way that the potential solution does not become dominant. With these restrictions, it may be concluded, first, that the slope of the Alfvén line is not constant and is somewhat greater than a based on the free-stream conditions at every point. This is evident from the fact that the wave solution must lie between the two presented previously. This conclusion is also supported by the character of the Alfvén line near the leading edge of the plate in the numerical results presented (Figs. 53 and 54), since the potential solution around the leading edge excited by viscous layer development is similar to the potential solution excited by the Alfvén line. Second, it may be concluded that the change in the longitudinal component of velocity across the Alfvén line is not as great as expected from the idealized wave solution because of the potential-flow effect. These conclusions are certainly supported by the numerical results presented, although some consideration must be given to boundary effects (discussed below) and the fact that Cases 1-1 through 1-4 and Cases 3-1 and 3-2 allow only marginal separation of the Alfvén line and viscous layer. Of course, for regions that do not satisfy the restrictions previously imposed (i. e., that superposition of wave and potential solutions is valid), the flow pattern is more difficult to deduce and no attempt will be made to do so now.

Turning our attention to the viscous layer, we can see a fundamental difference between the semi-infinite plate problem and the Rayleigh problem. It may be readily verified that for a fully developed layer in the former problem the skin friction at the plate is given by $(\partial u / \partial y)_{y=0} = a\sqrt{\epsilon} u_2 B_{y2}$. Neglecting potential flow effects, from Eqs. 111a-e we have

$$u_2 B_{y2} = \frac{a(1+2\sqrt{\epsilon}) + v_1\sqrt{\epsilon} + aB_{x1}(a\sqrt{\epsilon} - v_1B_{x1})}{a(1+\sqrt{\epsilon})^2} \quad (114)$$

In the two extreme cases considered, namely $v_1 = B_{x1} = 0$ and $v_2 = B_{x1} = 0$, we have,

respectively,

$$u_2 B_{y2} = \frac{1 + 2\sqrt{\epsilon}}{(1 + \sqrt{\epsilon})^2}$$

and

$$u_2 B_{y2} = 1.$$

Hence it would be expected that the skin friction is relatively insensitive to the value of ϵ alone, but, of course, is sensitive to the combination ϵa^2 . This is expected from the physical fact that the current density at the plate is likewise insensitive to the value of ϵ alone, but sensitive to the value of ϵa^2 . This conclusion is supported by the numerical results presented in Table IV, in which it is seen that the skin-friction change that is due to a change in ϵ , with ϵa^2 fixed, is small. The change in a typical velocity profile caused by a change in ϵ , with ϵa^2 fixed, is shown in Fig. 58; thus we conclude that the velocity profile in the region very near the plate is insensitive to the change in ϵ .

e. Interpretation of Boundary Effects

To complete the interpretation of the numerical results, it is necessary to interpret the boundary effects. Of the three boundaries placed on the flow field, the effects of the transverse (y) boundary and the downstream (x) boundary are the most important. The upstream x-boundary represents a constraint to the flow, of course, but from the manner in which the various quantities approach their respective boundary values (e.g., the normal component of magnetic field plotted in Figs. 56 and 57 and the streamlines

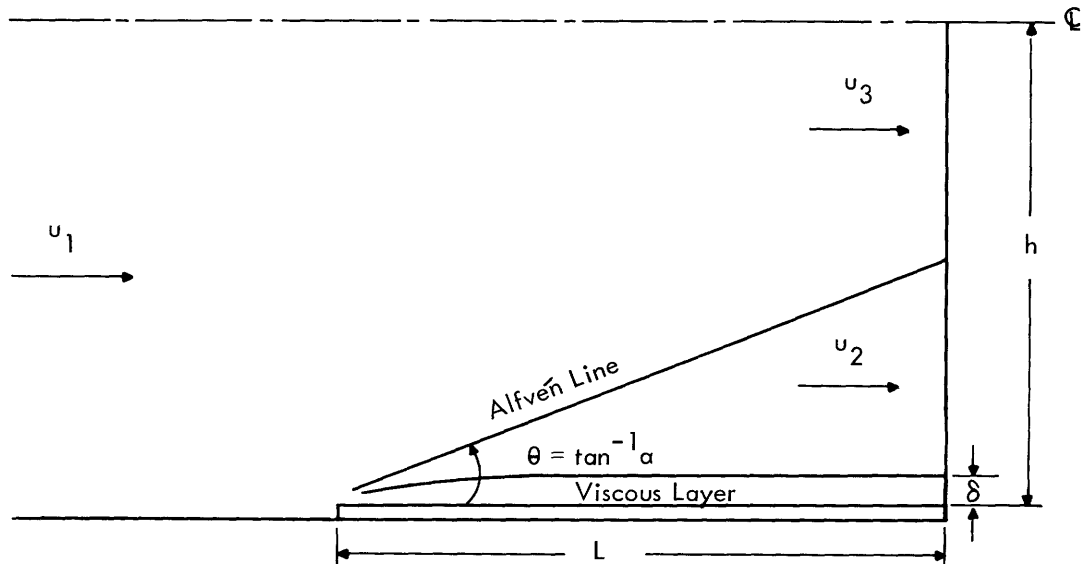


Fig. 59. Idealized channel flow.

shown in Fig. 55), we see that this effect is small.

The transverse boundary, representing the center line of a channel, further constrains the flow. This can be deduced by considering the highly idealized channel flow shown in Fig. 59. As we have seen, as the fluid crosses the Alfvén line its velocity is decreased. As a result of this decrease, elementary continuity considerations dictate that the velocity outside the Alfvén line must increase. This implies that as the fluid with increased velocity crosses the Alfvén line, although the decrease in velocity is the same as before, the net deficit behind the line from the original free-stream value is decreased. Hence this channeling effect decreases the velocity defect behind the Alfvén line from that expected from the elementary considerations already discussed [i. e., $u_2 = u_1/(1+\sqrt{\epsilon})$]. It is evident that the significant parameter in determining the magnitude of this effect is the ratio aL/h . For Cases 1-4 and 3-2, respectively, this ratio is 0.187 and 0.099; it is therefore to be expected that the magnitudes of the effects resulting from increasing the parameter ϵ are less and the channeling effects greater for the former case. This conclusion is supported by the numerical evidence also shown in tabular form. Note that the potential-flow effect caused by the disturbance, which we have discussed, is of the same qualitative nature as this channeling effect, and hence tends to decrease the velocity defect from that expected by elementary considerations.

The channeling effect attributable to the transverse boundary also affects the magnetic field distribution. The increased velocity tends to increase the current flow in the positive z -direction, which in turn tends to decrease the normal component of magnetic field. This effect is readily seen in the numerical results presented in tabular form and in Figs. 56-57 for the normal component at the transverse boundary and at the plate, respectively. Also, this effect undoubtedly plays an important part in the lack of correlation between the magnitudes of the distortion of magnetic field at the plate obtained numerically and those obtained from the linearized solution. For, at low values of ϵ ($<10^{-2}$), the magnetic field distortion is small, and the effect of channeling caused by the viscous layer on this distortion is comparable in magnitude to the distortion. Hence good correlation at these low values cannot be expected, and it may also be expected that the numerical results obtained will reflect less distortion of the normal component at the plate than was predicted by the linearized solution. The more rapid rate of decay of the numerical result is also attributed to the channeling effect.

As we have shown, the downstream boundary serves to reduce the magnitudes of the effects encountered as a result of increasing the parameter ϵ , and merits no further comment.

5.2 CONCLUSIONS AND RECOMMENDATIONS

a. Conclusions

Our primary conclusion is that in flows of high electrical conductivity about slender nonconducting obstacles in the presence of transverse magnetic fields, the effects of

viscosity are not confined solely to a thin viscous layer about the body, in contrast to the pure fluid-mechanic case. In addition to a thin viscous layer, an Alfvén type of disturbance is excited which propagates into the free stream; this character of the flow is forecast by the relevant Rayleigh problem. The magnitude of the disturbance does not appear to become appreciable until the ratio of the viscous-to-magnetic diffusivities, ϵ , becomes greater than 10^{-2} . This Alfvén type of disturbance in turn excites a potential-flow type of disturbance which increases in significance as the parameters ϵ and α are increased. This type of flow is relevant to the flow about obstacles placed in magneto-hydrodynamic shock tubes, and the flow at the walls of certain types of these devices.

We conclude that for flows of low electrical conductivity ($\epsilon < 10^{-2}$), the skin friction and magnetic field distortion at the surface of a flat plate can be reasonably estimated by utilizing the results of the linearized analysis, provided that care is taken in selecting the appropriate average values for linearization. In addition, the numerical results obtained for these low-conductivity flows are useful for purposes of comparison with the results of conventional boundary-layer techniques.

b. Recommendations

It would be of interest to examine the effects portrayed by the numerical results obtained herein on an experimental basis. At present, the high-speed, magnetically driven annular shock tube offers the most promise from the aspect of obtaining the necessary high values of the parameter ϵ .

From an analytical point of view, a simplified method of analysis is greatly to be desired, since the numerical solution of the complete set of equations for extended flow regions is neither practical nor desirable. Presumably, a method based on the separation of the various effects, as performed very crudely in section 5.1d, would offer some promise. If such a method could be devised, it would then be possible to extend the analysis to the more interesting and practical case of compressible flow.

APPENDIX I

INVERSION OF THE FOURIER TRANSFORM OF Eq. 78

We desire to obtain the inverse transform for positive x of the second term on the right-hand side of Eq. 78 (denoted here by $(\bar{A}_x)_{II}$).

$$(\bar{A}_x)_{II} = \frac{-i^{1/2} \epsilon (p - i\epsilon a^2)^{1/2}}{(ip + \epsilon a^2)(p - ik)^{1/2} [(p + ik)^{1/2} + (p + i\epsilon)^{1/2}]} \quad (A-1)$$

This can be rearranged to yield

$$(\bar{A}_x)_{II} = \frac{-i^{1/2} (p + ik)^{1/2}}{(p - i\epsilon a^2)^{1/2} (p - ik)^{1/2}} + \frac{i^{1/2} (p + i\epsilon)^{1/2}}{(p - i\epsilon a^2)^{1/2} (p - ik)^{1/2}} \quad (A-2)$$

Hence, from Eq. 47, the integral to be evaluated is

$$\begin{aligned} (A_x)_{II} = & -\frac{1}{2\pi} \int_{-\infty}^{\infty} \frac{i^{1/2} (p + ik)^{1/2} e^{ipx}}{(p - i\epsilon a^2)^{1/2} (p - ik)^{1/2}} dp \\ & + \frac{1}{2\pi} \int_{-\infty}^{\infty} \frac{i^{1/2} (p + i\epsilon)^{1/2}}{(p - i\epsilon a^2)^{1/2} (p - ik)^{1/2}} dp, \end{aligned} \quad (A-3)$$

where k goes to zero in the limit. We shall denote the two terms in this equation by $(A_x)_{II-1}$ and $(A_x)_{II-2}$, respectively, and perform the integrations separately.

The integrand of $(A_x)_{II-1}$ possesses branch points at $p = \pm ik$ and $p = i\epsilon a^2$. The contour for integration is sketched in Fig. 60. The contribution of the two arcs BC and JA is zero. We now replace the terms involving the two branch points in question as follows. The substitution involved is $p = r e^{i\pi/2}$ on the imaginary axis; also $i^{1/2} = e^{i\pi/4}$

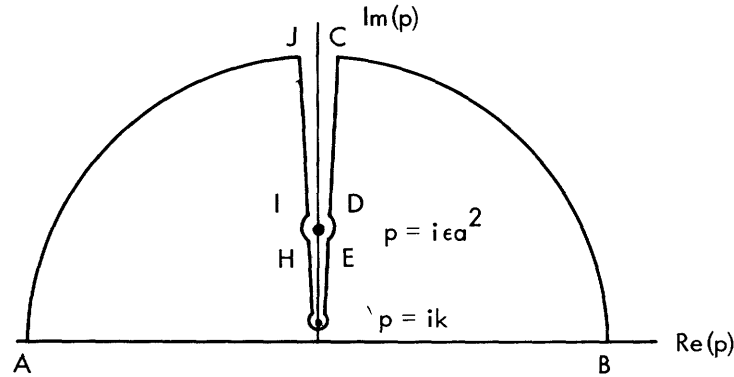


Fig. 60. Integration contour.

and $db = e^{i\pi/2} dr$.

$$\begin{aligned}
(p-i\epsilon a^2)^{1/2} &= |r-\epsilon a^2| e^{i\pi/2} && \text{on CD} \\
&= |\epsilon a^2-r| e^{-i\pi/2} && \text{on EF and GH} \\
&= |r-\epsilon a^2| e^{-i3\pi/2} && \text{on IJ} \\
(p-ik)^{1/2} &= |r-k| e^{+i\pi/2} && \text{on CD and EF} \\
&= |r-k| e^{-i3\pi/2} && \text{on GH and IJ.}
\end{aligned}$$

It is also evident from the form of (A-3) that the integrals around the arcs DE, FG, and HI are zero as the radius there approaches zero. Hence the integral becomes

$$\begin{aligned}
(A_x)_{II-1} &= \lim_{\substack{\rho \rightarrow 0 \\ k \rightarrow 0}} \left\{ \frac{1}{2\pi} \left[\int_{\epsilon a^2-\rho}^{k+\rho} \frac{e^{i\pi/4} (r+k)^{1/2} e^{i\pi/4} e^{-rx} e^{i\pi/2} dr}{(\epsilon a^2-r)^{1/2} e^{-i\pi/4} (r-k)^{1/2} e^{i\pi/4}} \right. \right. \\
&\quad \left. \left. + \int_{k+\rho}^{\epsilon a^2-\rho} \frac{e^{i\pi/4} e^{i\pi/4} (r+k)^{1/2} e^{-rx} e^{i\pi/2} dr}{(\epsilon a^2-r)^{1/2} e^{-\pi/4} (r-k)^{1/2} e^{-i3\pi/4}} \right] \right\}. \tag{A-3a}
\end{aligned}$$

These terms may be combined to yield

$$(A_x)_{II-1} = \frac{1}{\pi} \int_0^{\epsilon a^2} \frac{\epsilon^{-rx} dr}{(\epsilon a^2-r)^{1/2}}. \tag{A-4}$$

The second term, $(A_x)_{II-2}$, is similar to the first in its essential features, so that by analogy

$$(A_x)_{II-2} = -\frac{1}{\pi} \int_0^{\epsilon a^2} \frac{(r+\epsilon)^{1/2} e^{-rx} dr}{(\epsilon a^2-r)^{1/2} r^{1/2}}. \tag{A-5}$$

Hence the result becomes

$$(A_x)_{II}(y=0, x>0) = -\frac{1}{\pi} \int_0^{\epsilon a^2} \frac{(r+\epsilon)^{1/2} - r^{1/2}}{(\epsilon a^2-r)^{1/2} r^{1/2}} e^{-rx} dr. \tag{A-6}$$

APPENDIX II

PERTURBATION SOLUTION OF Eq. 43

We assume a perturbation series of ψ in the parameter ϵa^2 :

$$\psi = \psi^{(0)} + \epsilon a^2 \psi^{(1)} + (\epsilon a^2)^2 \psi^{(2)} + \dots \quad (\text{A-7})$$

Substitution of this expansion in Eq. 43 and equating terms of equal order in ϵa^2 yields the following set of equations:

$$\begin{aligned} \nabla^4 \psi^{(0)} + \nabla^2 \psi_x^{(0)} &= 0 \\ \nabla^4 \psi^{(n)} + \nabla^2 \psi_x^{(n)} &= \psi_{yy}^{(n-1)} \quad n \geq 1. \end{aligned} \quad (\text{A-8})$$

The corresponding boundary conditions are:

$$\begin{aligned} \psi_x^{(n)} = \psi_y^{(n)} &= 0 \text{ as } x \rightarrow -\infty, \quad n \geq 0 \\ \left. \begin{aligned} \psi_x^{(0)} &= 0, \quad \psi_x^{(n)} = 0 \\ \psi_1^{(0)} &= -1, \quad \psi_y^{(n)} = 0 \\ \psi^{(n)} &= 0 \end{aligned} \right\} & \text{at } y = 0, \quad x > 0; \quad n \geq 0 \\ \psi_{yy}^{(n)} &\text{ discontinuous} \end{aligned}$$

The solutions for all sets of these equations can be obtained in a manner completely analogous to the Fourier-transform, Weiner-Hopf technique employed in section 3.3. We shall deal with only the first two orders here. The zero-order solution is merely that for the classical fluid-mechanics problem, which has been obtained by Lewis and Carrier.¹³ The results that we need here are:

$$\bar{\psi}^{(0)} = \frac{i r \bar{f}^{(0)}}{(r^2 - p^2)(r^2 + p^2 + ip)}, \quad (\text{A-9})$$

in which we have utilized the Fourier transforms as defined in (45) and (46), and $f^{(n)} = \psi_{yy}^{(n)}(0+) - \psi_{yy}^{(n)}(0-)$. The solution for \bar{f} is

$$\bar{f}^{(0)} = \frac{2}{(ip + \delta)^{1/2}} \quad (\text{A-10})$$

and hence

$$\psi_{yy}^{(0)}(0+) = \frac{1}{\sqrt{\pi x}}. \quad (\text{A-11})$$

Transforming the first-order set of equations yields

$$\bar{\psi}^{(1)} = \frac{ir\bar{f}^{(1)}}{(r^2+p^2)(r^2+N_3^2)} - \frac{r^2\bar{\psi}^{(0)}}{(r^2+p^2)(r^2+N_3^2)}. \quad (\text{A-12})$$

Here, we have defined

$$N_3^2 = p^2 + ip. \quad (\text{A-13})$$

If we employ (A-9), (A-12) becomes

$$\bar{\psi}^{(1)} = \frac{ir\bar{f}^{(1)}}{(r^2+p^2)(r^2+N_3^2)} - \frac{ir^3\bar{f}^{(0)}}{[(r^2+p^2)(r^2+N_3^2)]^2}. \quad (\text{A-14})$$

Inverting (A-14) with respect to r yields

$$\begin{aligned} \frac{y}{|y|} \bar{\psi}^{(1)} &= -\frac{\bar{f}^{(1)}}{2} \left[\frac{e^{-|p||y|} - e^{-|N_3||y|}}{N_3^2 - p^2} \right] + \frac{\bar{f}^{(0)}}{2} \left[\frac{N_3^2 + p^2}{(N_3^2 - p^2)^2} \right] \\ &\times \left[\frac{e^{-|p||y|} - e^{-|N_3||y|}}{N_3^2 - p^2} \right] - \frac{\bar{f}^{(0)}}{4} \frac{y}{(N_3^2 - p^2)^2} \\ &\times \left[|p| e^{-|p||y|} + |N_3| e^{-|N_3||y|} \right]. \end{aligned} \quad (\text{A-15})$$

Again, the branches are selected so that the exponentials decay. Now at $y = 0$, $\psi_y = u^{(1)}$, with

$$\begin{aligned} u^{(1)} &= u \quad (x < 0) \\ &= 0 \quad (x > 0). \end{aligned}$$

Hence applying this condition to (A-15) yields

$$\begin{aligned} \bar{u}^{(1)} &= -\frac{\bar{f}^{(1)}}{2} \left[\frac{1}{|N_3| + |p|} \right] + \frac{\bar{f}^{(0)}}{2} \left[\frac{N_3^2 + p^2}{(N_3^2 - p^2)^2} \right] \left[\frac{1}{|N_3| + |p|} \right] \\ &- \frac{\bar{f}^{(0)}}{4} \left[\frac{1}{(N_3^2 - p^2)} \right] \left[\frac{1}{|N_3| - |p|} \right]. \end{aligned} \quad (\text{A-16})$$

Again, we replace $|p|$ by $\lim_{k \rightarrow 0} (p^2 - k^2)^{1/2}$, and some manipulation yields

$$\begin{aligned}
(p-ik) \bar{u}_{\oplus}^{(1)} [(p+i)^{1/2} + (p+ik)^{1/2}]_{\oplus} = & -\frac{\bar{f}_{\theta}^{(1)}}{2} (p-ik)^{1/2} - \frac{2(p+i/2)}{i^{1/2}(p-ik)} \\
& - \frac{1}{2i^{3/2}(p-ik)} - \frac{1}{2i^{3/2}(p-ik)} \\
& \times \left[\frac{(p+i)^{1/2} + (p+ik)^{1/2}}{(p+i)^{1/2} - (p+ik)^{1/2}} - 1 \right]. \quad (A-17)
\end{aligned}$$

The left-hand and right-hand sides are analytic in the upper and lower half-planes, respectively, with a region of overlap at the real axis, so that

$$\frac{\bar{f}^{(1)}}{2} = - \frac{2(p+i/2)}{i^{1/2}(p-ik)^{3/2}} - \frac{1}{2i^{3/2}(p-ik)^{3/2}}. \quad (A-18)$$

This can be readily inverted to yield

$$\bar{f}^{(1)} = - \frac{2}{\sqrt{\pi x}} + \sqrt{\frac{x}{\pi}}. \quad (A-19)$$

Hence the solution for the skin friction for the first two orders yields

$$\psi_{yy}(y=0+) = \frac{1}{\sqrt{\pi x}} (1 + \epsilon a^2 x - 2\epsilon a^2). \quad (A-20)$$

Acknowledgement

The author wishes to acknowledge the assistance of Professor A. H. Shapiro, his thesis supervisor, who contributed many helpful suggestions that aided significantly the completion of this work. Professor J. A. Fay and Professor L. Trilling also contributed many suggestions that served to clarify the results presented in this report. Thanks are due to Professor J. A. Shercliff for his interest in the problem studied here, and for his contribution to the ideas resulting therefrom.

The author also wishes to express his gratitude to the Research Laboratory of Electronics and its associated supporters, particularly the National Science Foundation, for financial assistance, and to the Computation Center, M.I.T., whose facilities were employed for the extensive digital computations that were required.

References

1. W. B. Bush, Compressible flat plate boundary layer flow with an applied magnetic field, *J. Aero/Space Sci.*, 27, 49 (1960); see especially Table 549.
2. G. A. Campbell and R. M. Foster, Fourier Integrals for Practical Applications (D. Van Nostrand Company, Inc., New York, 1948).
3. G. F. Carrier, Useful approximations in Weiner-Hopf problems, *J. Appl. Phys.* 30, 1769 (1959).
4. G. F. Carrier and H. P. Greenspan, The time dependent magnetohydrodynamic flow past a flat plate, *J. Fluid Mech.* 7, 22 (1960).
5. G. C. Chang and J. T. Yen, Rayleigh's problem in magnetohydrodynamics, *Phys. Fluids* 2, 393 (1959).
6. W. Chester, The effect of a magnetic field on Stokes flow in a conducting fluid, *J. Fluid Mech.* 3, 304 (1957).
7. S. H. Crandall, Engineering Analysis (McGraw-Hill Book Company, New York, 1956).
8. H. P. Greenspan and G. F. Carrier, Magnetohydrodynamic flow past a flat plate, *J. Fluid Mech.* 6, 77 (1959).
9. H. P. Greenspan, On the Flow of a Viscous, Electrically Conducting Fluid, AVCO Research Report No. 73, Everett, Massachusetts, October 1959.
10. R. V. Hess, Some Basic Aspects of Magnetohydrodynamic Boundary Layer Flows, NASA Memorandum 4-9-591, 1959.
11. N. H. Kemp, On Hypersonic Blunt Body Flow with a Magnetic Field, AVCO Research Report No. 19, Everett, Massachusetts, February 1958.
12. W. S. Lewellen, An Inviscid Boundary Layer of Magnetohydrodynamics, AFOSR-TN-59-927, September 1959.
13. J. H. Lewis and G. F. Carrier, Some remarks on the flat plate boundary layer, *Quart. Appl. Math.* 7, 228 (1949).
14. G. S. S. Ludford, Rayleigh's problem in hydromagnetics: The impulsive motion of a pole piece, *Arch. Ratl. Mech. Anal.* 13, 14 (1959).
15. P. S. Lykoudis, On a Class of Magnetic Laminar Boundary Layers, IX International Astronautical Congress, October 1958.
16. J. L. Neuringer and W. McIlroy, Incompressible two-dimensional stagnation point flow of an electrically conducting viscous fluid in the presence of a magnetic field, *J. Aero/Space Sci.* 25, 194 (1958).
17. B. Noble, Methods Based on the Weiner-Hopf Technique for the Solution of Partial Differential Equations (Pergamon Press, New York, 1958).
18. E. L. Resler and J. E. McCune, Electromagnetic interactions with aerodynamic flows, The Magnetohydrodynamics of Conducting Fluids, edited by D. Bershader (Stanford University Press, Stanford, Calif., 1959).
19. V. J. Rossow, On Flow of Electrically Conducting Fluids over a Flat Plate in the Presence of Transverse Magnetic Fields, NACA TN 3971, 1957.
20. V. J. Rossow and M. Field, On magneto-aerodynamic boundary layers, *J. Appl. Math. Phys.* 9b, 519-527 (1958).
21. V. J. Rossow, On Rayleigh's problem in magnetohydrodynamics, *Phys. Fluids* 3, 395 (1960).
22. W. R. Sears, Some Solutions of the Macroscopic Equations of Magnetohydrodynamics, American Rocket Society Preprint 899-59, August 1959.
23. W. R. Sears and E. L. Resler, Theory of thin airfoils in fluids of high electrical conductivity, *J. Fluid Mech.* 5, 257 (1959).

24. Z. J. J. Stekly, Magnetohydrodynamic Waves in a Transverse Magnetic Field, Sc.D. Thesis, M.I.T., September 1959.
25. C. C. Lin and G. F. Carrier, On the nature of the boundary layer near the leading edge of a flat plate, Quart. Appl. Math. 6, 63 (1948).
26. W. C. Moffatt, Boundary Layer Effects in Magnetohydrodynamic Flows, Report 61-4, Magnetogasdynamics Laboratory, M.I.T., May 1961.